GKSS
FORSCHUNGSZENTRUM
in der HELMHOLTZ-GEMEINSCHAFT

# The role of different forcings on the historical climate variability, with special consideration of the Dalton Minimum (1790–1830): A model study

**(Vom Fachbereich Geowissenschaften der Universität Hamburg als Dissertation angenommene Arbeit)**

**Author:**

***S. Wagner***

**GKSS 2004/13**

GKSS 2004/13

# The role of different forcings on the historical climate variability, with special consideration of the Dalton Minimum (1790–1830): A model study

**(Vom Fachbereich Geowissenschaften der Universität Hamburg als Dissertation angenommene Arbeit)**

**Author:**

***S. Wagner***

**(Institute for Coastal Research)**

**GKSS-Forschungszentrum Geesthacht GmbH • Geesthacht • 2004**

Die Berichte der GKSS werden kostenlos abgegeben.
The delivery of the GKSS reports is free of charge.

*Anforderungen/Requests:*

GKSS-Forschungszentrum Geesthacht GmbH
Bibliothek/Library
Postfach 11 60
D-21494 Geesthacht
Germany
Fax.: (49) 04152/871717



ISSN 0344-9629

GKSS-Forschungszentrum Geesthacht GmbH · Telefon (04152)87-0
Max-Planck-Straße · D-21502 Geesthacht / Postfach 11 60 · D-21494 Geesthacht

GKSS 2004/13

# The role of different forcings on the historical climate variability, with special consideration of the Dalton Minimum (1790–1830): A model study

*(Vom Fachbereich Geowissenschaften der Universität Hamburg als Dissertation angenommene Arbeit)*

Sebastian Wagner

*117 pages 50 figures and 14 tables*


## Abstract

The main goal of this study is to assess the modelled influence of different external forcings on the climate during the Dalton Minimum (DM, 1790–1830) concerning the role of the solar insolation, the volcanic activity and the influence of the rising $CO_2$-concentrations.

To investigate those phenomena, different ensemble simulations with the global climate model ECHO-G were carried out. Within the different experiments the different forcings were held constant or they changed according to their temporal varying reconstruction. The reference simulation, from which different initial conditions were derived, is a 1000 year integration, forced with variable solar and volcanic output and a variable amount of selected greenhouse gases ($CO_2$, $CH_4$).

Without any volcanic influence there is no pronounced reduction within the global mean nearsurface air-temperatures during the DM with respect to the reference simulation including the volcanic activity. The reduction within the solar insolation seems to be of minor importance compared to the volcanic activity. However, on the extratropical regional scales there is little evidence for a pronounced volcanic signal. This result is also supported by the comparison with reconstructed data. Furthermore, the strong $CO_2$-increase in the course of the DM seems tohave no significant impact on the temperatures of the DM.


# Die Bedeutung verschiedener Antriebsfaktoren für die historische Klimavariabilität unter besonderer Berücksichtigung des Dalton Minimum (1790–1830): Eine Modellstudie


## Zusammenfassung

Ziel dieser Studie ist die Abschätzung des modellierten Einflusses verschiedener äußerer Antriebsfaktoren auf das Klima während des Dalton Minimum (DM, 1790–1830) in bezug auf die solare Einstrahlung, die vulkanische Aktivität und den Einsfluss steigender $CO_2$-Konzentrationen.

Um diese Einflüsse auf das Klima genauer zu untersuchen, wurden verschiedene Ensemble-Simulationen mit dem globalen Klimamodell ECHO-G durchgeführt, wobei innerhalb der verschiedenen Experimente die unterschiedlichen Antriebsfaktoren konstant gehalten wurden oder den zeitlich veränderlichen Rekonstruktionen entsprechen. Die verschiedenen Anfangsbedingungen wurden hierbei von einer 1000jährigen Referenzsimulation abgeleitet, welche mit variablem solarem

und vulkanischem Antrieb sowie variablen Konzentrationen ausgewählter Treibhausgase ($CO_2$, $CH_4$) durchgeführt wurde.

Ohne den vulkanischen Einfluss ist kein nennenswerter Rückgang der mittleren globalen bodennahen Lufttemperaturen während des DM im Vergleich zur Referenzsimulation mit vulkanischem Antrieb festzustellen. Die Reduktion innerhalb der solaren Einstrahlung zeigt im Vergleich zur vulkanischen Aktivität einen nur untergeordneten Einfluss auf die Temperaturen während des DM. Im Gegensatz zur globalen Skala finden sich auf der regionalen außertropischen Skala nur geringe Anzeichen des vulkanischen Einflusses. Dieses Ergebnis wird durch den Vergleich mit empirischen Rekonstruktionen gestützt. Darüber hinaus scheint der relativ starke Anstieg der $CO_2$-Konzentrationen im Laufe des DM ebenso nur einen insignigfikanten Einfluss auf die Temperaturentwicklung auszuüben.

*Manuscript received / Manuskripteingang in TDB: 29. Oktober 2004*

# Contents

# Chapter 1

# Introduction

In the climate of the past 500 years at least three major solar anomalous periods can be identified: The Spörer (1450–1550), the Maunder (1645–1715) and the Dalton Minima (1790–1830) (Lean and Rind 1999). As deduced from empirical evidence, the time prior to 1850 experienced lower Northern hemispheric temperatures with respect to the 20th century (Mann et al. 1999a). Thus, this period from 1450 to 1850 is known as the Little Ice Age (LIA). The term 'Little Ice Age' suggests that this period was a continuous 400 year long period with below normal temperatures. However, it also could be shown that periods with 'normal' climatic conditions, especially in Europe, occurred. As a consequence, it seems to be more appropriate to speak of so called Little Ice Age type events (e.g. Maunder Minimum), where the climate conditions really were colder and wetter than normal (Glaser 1995).

A lot of work has been done reconstructing the climate of the Maunder Minimum, especially its last part known as the Late Maunder Minimum (LMM) from 1675-1705 (Eddy 1976; Shindell et al. 2001a; Luterbacher et al. 2001; Müller 2003; Zorita et al. 2004). The peculiarity of this minimum lies in the long term lack of sunspots and the ensuing drop in at least Northern hemispheric and European temperatures which is evident in historical observations as well as within proxy data.

The Dalton Minimum (hereafter DM) is a period of reduced solar insolation at the turn of the 18th to the 19th century. It is also referred as the 'Little Maunder Minimum' or the 'Sabine' Minimum. The exact temporal onset varies within literature. Eddy (1976) defines the DM from 1790 until 1830. This definition will also be used here. The term

'Dalton Minimum' is related to an anomalous low solar insolation. However, a reduced solar insolation does not necessarily produce a negative climate anomaly, e.g. concerning below-average temperatures, especially on regional scales. For example, a change within the atmospheric circulation on the extratropical hemispheres due to a reduced insolation could result in an altered advection regime of air masses, which might not necessarily point in the same thermal direction as the external forcing suggests.

The major differences between the DM and the preceding Maunder Minimum pertain to the short duration and the increased volcanic influence of the DM (e.g. Tambora 1815), respectively. In general there are two major volcanic eruptions during the times of the DM. The huge eruption of the year 1809 is only evident in ice-cores. The eruption of the Tambora in 1815 is the largest of the modern era, more specifically within the last 500 years. A second major difference between the DM and the Maunder Minimum is the increase in greenhouse gases at the beginning of the 19th century. These increases are due to the beginning of industrialization and the related burning of fossil fuels. On the other hand the huge volcanic eruptions may also have contributed to this rapid initial increase in greenhouse gases.
Accordingly, there are three climate factors which changed quite markedly during the time of the DM including i) the reduction of solar insolation, ii) the increased volcanic activity during the second half of the DM and iii) the marked increase within $CO_2$ concentrations.

The reconstruction of past climates by means of historical and proxy-based data (Mann et al. 1999a; Glaser 2001; Luterbacher et al. 2002a; 2004) is one way to assess the natural climate variability. The shortcomings of such reconstructions are the uncertainty within the proxy data (e.g. tree-rings, ice cores, corals) and the spatially limited availability of historical data. The latter are in general restricted to the populated territories in the Northern Hemisphere. Nevertheless, these reconstructions are a vital source of information of the past climates. Proxy data are often the only possibility to reconstruct climatic conditions in unsettled parts of the world. For example, Jones and Widmann (2002) use information from tree rings in the Southern Hemisphere to reconstruct the Antarctic Oscillation, which describes the intensity of the westerlies in the extratropical Southern Hemisphere. Luterbacher et al. (2002a; 2004) reconstructed climate variables (near-surface temperatures and precipitation and Sea Level Pressure (SLP)) for the North-Atlantic European region by means of observational and proxy-based data. In terms of temperature and precipitation this work is unprecedented concerning the temporal (monthly) resolution and spatial gridding (0.5° x 0.5°). It offers the possibility to detect highly resolved climate anomalies within the European continent.

Complementary to the reconstruction methodology by means of proxy data, climate model experiments have been carried out in order to get a global coherent picture of past climates (Cubasch et al. 1997; Shindell et al. 2003; González-Rouco et al. 2003). To now, climate models, which are applied within paleoclimatic studies, seem to be able to capture only the global, hemispheric and continental characteristics of the past climate but not the small-scale characteristics. This is possibly due to the coarse resolution of several hundreds of kilometers within climate models in use for paleoclimate applications.
Besides the possibility to investigate the state of the atmosphere, coupled climate models also allow for the assessment of the oceanic influence. As the oceans possess a huge amount of internal heat capacity they possibly play a dominant role modifying the externally induced climate signals transmitted via the atmosphere. This modification is maintained by several interacting mechanisms concerning the ocean currents (e.g. Gulf Stream), which itself is part of the global conveyor belt driven by the thermohaline circulation (Broecker 1991).

The aim of the following thesis is to assess the influence of different external forcings on climate during the DM including the influence of the sun, the volcanoes, the $CO_2$ and different initial conditions. Several working hypothesis have been formulated, which are tested using a special experiment setup.
The most important question is whether the formation of a thermal DM is significantly influenced by the volcanic activity. In order to prove this hypothesis one experiment is forced only with the influence of the solar variability and the variable amount of selected greenhouse gas concentrations ($CO_2$, $CH_4$).
A second question is, how much does the variability of the solar constant influence the evolution of e.g. global or hemispheric temperatures. In order to investigate this issue, a second experiment was carried out, where the solar radiation was held constant. Here, only the volcanic activity and the greenhouse gas concentrations vary in time.
Another issue investigated is the strong increase of $CO_2$ concentrations during the DM. In order to prove whether this strong increase within the $CO_2$ concentration has an significant impact on the temperatures of the DM a third simulation is carried out, where the $CO_2$ concentrations are kept constant at a pre-industrial level. The reason for not keeping the $CH_4$ concentrations constant is also the fact that one can not distinguish anymore between $CO_2$ and $CH_4$ related effects on climate, when changing the evolution of both greenhouse gases at the same time.
The three experiments were carried out as ensemble simulations each consisting of three members. Accordingly, hereafter the expression 'experiment' is related to the setup in terms of the different external forcings, whereas the expression 'simulation' is related to a single realization within an experiment. The difference between the simulations within the same experiment is the initial state of the oceanic and atmospheric conditions. These

initial conditions might have pronounced impacts on the future evolution of the climate system, especially the oceanic ones due to the longer response time of the oceans. This point may also be formulated as a working hypothesis, namely how much do the different initial oceanic conditions influence the behavior of different, global, hemispheric or regional climate variables and processes.

The thesis is structured as follows:
In the first chapter the external forcings on Earth's climate will be described in terms of the solar and volcanic activity, especially during the period of the DM. Here also the reconstructions of the solar and volcanic forcings will be described. This item will be followed by a short characterization of the climate of the DM in terms of observational evidence, for both the Northern hemispheric as well as for the regional European perspective. The climate model ECHO-G used for the following analysis and the experimental design is described in detail in chapter 4.
The main part of the work encompasses the atmospheric and oceanic climate variability. In this chapter, selected atmospheric and oceanic processes concerning the mean of the ensemble-experiments, as well as selected single member simulations, are analyzed. The focus is mainly on the DM. However, in the course of the work interesting spin-offs emerged, which are not necessarily directly related to the DM. A selection of them will also be discussed.
The first part of chapter 5 analyses the evolution of temperatures as a response to the different external forcings on global, hemispheric and regional scales. Furthermore the temperature evolution of the different ensembles within an experiment will be shown and a comparison with observational and reconstructed data will be presented.
The second part of chapter 5 deals with the extratropical atmospheric circulation variability on the Northern and Southern Hemisphere, respectively. Considerable emphasis is given to the possible impacts of the external solar forcing on the evolution of the circulation in terms of the Arctic and Antarctic Oscillations. Additionally, circulation-temperature connections are established in order to explain some of the peculiarities within the evolution of the regional temperatures.
The last part of chapter 5 analyses the oceanic temperature evolution and circulation within the North Atlantic basin, respectively. A question also discussed here is the influence of the initial oceanic conditions on the future evolution of the oceanic northward heat transport.
In the conclusions the results of the main part are summarized with respect to the initially formulated working hypothesis.
Concerning the statistical methodology, there will be a brief outline of the statistical concept behind the analysis, the risks and limitations, and the suitability for the question under consideration.

# Chapter 2

# Solar and Volcanic forcing

In the following two sections a short introduction will be given to the solar and volcanic forcing possibly controlling parts of the global climate. The next section gives an overview of the role of the solar forcing, followed by a presentation of the volcanic impacts on climate. Additionally, a description of the reconstruction of the solar and volcanic forcing will be presented.

## 2.1 Solar Forcing

Lean and Rind (1999) evaluate the sun-climate relationship since the Little Ice Age. They emphasize that likely the solar variability had an important influence on the climate within the pre-industrial era. However, they state that the sun-climate relationship cannot account for the warming of the recent decades. A paper of Rozelot (2001) investigates links between the solar radius and global climate. His findings suggest that warmer and colder periods coincide with a smaller and wider apparent diameter of the sun, respectively. Beer et al. (2000) emphasize the fact that, besides the amount of radiation received by the earth, the spectral composition of the sun light also deserves attention. Additionally, feedback processes connected with water vapor, clouds, ice cover, atmospheric and oceanic transport are important factors masking the original solar forcing signal. Especially, the spectral composition of the sun light receives more and more interest as it influences the ozone chemistry within the stratosphere, which itself seems to have an influence on the extratropical atmospheric circulation (Shindell et al. 2001a; 2001b).
Friis-Christensen and Svensmark (1997) put forward the argument that cloud formation

processes are very effective mechanisms altering the radiation balance of the earth. The authors suggest that the cloud formation is influenced by the cosmic ray flux which is modulated by the variable solar output.
Within the observations a positive correlation has been found between the period length of the solar Schwabe cycle, with a mean period of 10.8 years, and the long-term surface temperature change within the observations (Mende and Stellmacher 2001). Lean and Rind (1999) also points to the fact that sun-climate relationships occur on longer, decadal to centennial time scales, whereas the short lived solar influence is possibly hidden within the noise of the climate system.
Accordingly, these studies support some evidence for an influence of the solar variable activity on the climate variability, especially during the pre-industrial time.
Concerning paleoclimatic modelling Cubasch et al. (1997) investigate the sun-climate relationship from the beginning of the 18th century using the ECHAM3/LSG-model with a resolution of T21 (approx. 5.6° lat x 5.6° lon) and a reconstruction of the solar irradiance by Hoyt and Schatten (1993) (HS93). They concluded that the near-surface temperatures are dominated by the long periodic solar fluctuations. Accordingly, the DM is present in the simulated global near-surface temperatures with a maximum temperature decrease of approximately 0.3 °C.

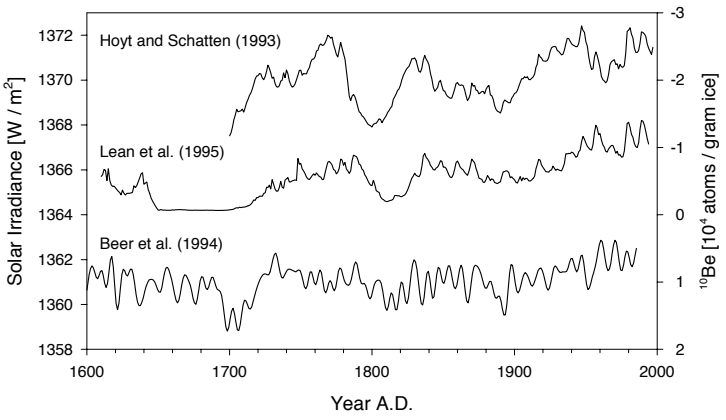


**Figure 2.1:** Comparison of different solar reconstructions by Hoyt and Schatten (1993) (HS93), Lean et al. (1995) (LBB95) and Beer et al. (1994) (based on $^{10}$Be). Note the discrepancies between HS93 and LBB95 for both, absolute values and temporal variability due to different reconstruction methodologies (after Oh et al. 2003).

A subsequent study carried out by Cubasch and Voss (2000) using the same climate model but with reconstructions of the solar radiation by Lean et al. (1995) (LBB95), shows a maximum temperature drop in the order of 0.2 °C. The timing of the maximum temperature depression is different, and also the external forcing of HS93 and LBB95 shows different

timing. The different solar reconstructions deviate markedly concerning both the absolute values within the solar irradiance and the temporal evolution. This discrepancies are due to the different reconstruction methodologies applied. Hence, the long-term component of the solar variability reconstruction of LBB95 is based on the average amplitude of the Schwabe cycle, whereas the long-term component within the HS93 reconstruction is based on the length of the Schwabe cycle. Fig. 2.1 shows the comparison between the HS93 and LBB95 solar reconstructions together with the evolution of $^{10}$Be which also serves as a proxy for the solar variability. The offset within the absolute values between the HS93 and LBB95 time series are due to different calibration with different instrumental satellite measurements of the solar irradiance. The uncertainties of present-day values of the solar irradiance are as high as $4W/m^2$ (Lean and Rind 1998). In this study the reconstruction of the solar irradiance by Crowley (2000) will be used.

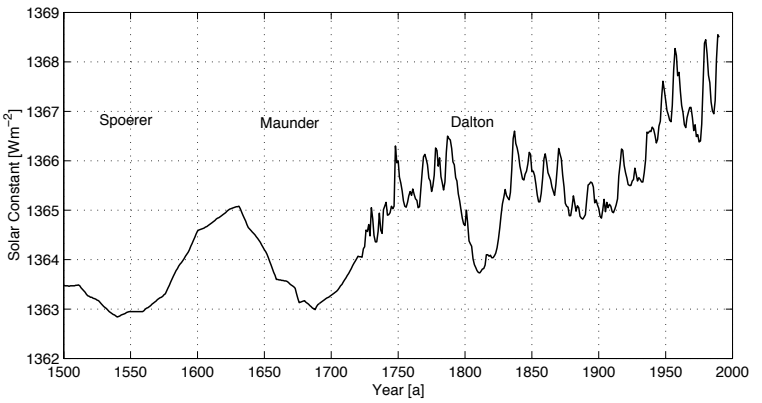


**Figure 2.2:** Evolution of the solar 'constant' since 1500. The most prominent anomalous periods are the Spörer, the Maunder and the Dalton Minima (after Crowley 2000).

Figure 2.2 shows the reconstructed evolution of the solar activity from 1500 onward by Crowley (2000) based on the work of Lean et al. (1995). This reconstruction approach includes a splicing of the Lean et al. (1995) time series into an estimate of the solar variability based on $^{10}$Be. $^{10}$Be is a cosmogenic isotope produced by spallation reactions with oxygen and nitrogen in the upper atmosphere. The connection to the solar output is established by the following mechanism: During periods of higher solar activity, high-density magnetic regions in the solar wind can inhibit the production of $^{10}$Be in the upper atmosphere. This results in an inverse relationship between the $^{10}$Be concentration and the solar radiative flux (Robertson et al. 2001) (cf. also Fig. 2.1).
After the splice was obtained the record was scaled to a 0.25% change in solar irradiance on longer time scales. The differences between this new estimate of Crowley (2000) and the estimate by Lean et al. (1995) pertain to the scaling reference period being the 14th

century and the 17th century (Maunder Minimum), respectively. Hence, a direct comparison between the two time series involves a reduction of 0.35% (Crowley 2000) and a reduction of 0.25% (Lean et al. 1995) within the solar irradiance between the Maunder Minimum and present-day values, respectively, which is well within the range of other different solar reconstructions (cf. Bard et al. 2000).
In terms of the evolution of the solar constant, Figure 2.2 clearly shows the solar minima of the Spörer, the Maunder and the DM as well as the strong increase in solar activity during the first half of the 20th century.
A close inspection of the external solar forcing during the 19th century reflects the DM as a minimum, which is flanked by comparably high values at its beginning around 1790 and its end around 1830. The time prior to 1790 shows an increase modulated through the 11-year Schwabe cycle, whereas the time after 1830 shows a modulated decrease of the solar forcing culminating at the end of the 19th century. (In this reconstruction the mean solar forcing of the DM is 1364.56 $W/m^2$, whereas the solar forcing during the 1880s is approximately 1364.9 $W/m^2$.) Hence, the whole 19th century is characterized by a reduced solar insolation with respect to the 20th century.

## 2.2 Volcanic Forcing

Besides the solar forcing, a second forcing mechanism affects Earth's natural climate, the explosive volcanism. An overview about volcanic influences on climate can be found in Robock (2000; 2004).
The physical impact of the explosive volcanism on climate is related to the ejection of huge amounts of ash and sulfur gases into the upper troposphere and lower stratosphere. The sulfuric emissions undergo a gas-particle conversion, giving rise to the formation of aerosols.
To illustrate the effects of the explosive volcanism on climate, Fig. 2.3 shows a schematic diagram. The most important effect is on solar radiation. Since the sulfate aerosols are about the same size as visible light they strongly interact with solar radiation by scattering. Part of the sunlight is backscattered increasing the net planetary albedo and reducing the amount of solar energy that reaches the Earth's surface. This backscattering is the dominant radiative effect at the surface and results in a net cooling. A large portion of the solar radiation is forward scattered, resulting in enhanced downward diffusive radiation compensating for the large reduction in the direct solar beam. However, in the stratosphere the sulfate aerosols also absorb some of the near infrared sunlight. This leads to a net heating of the stratosphere (Robock 2000).

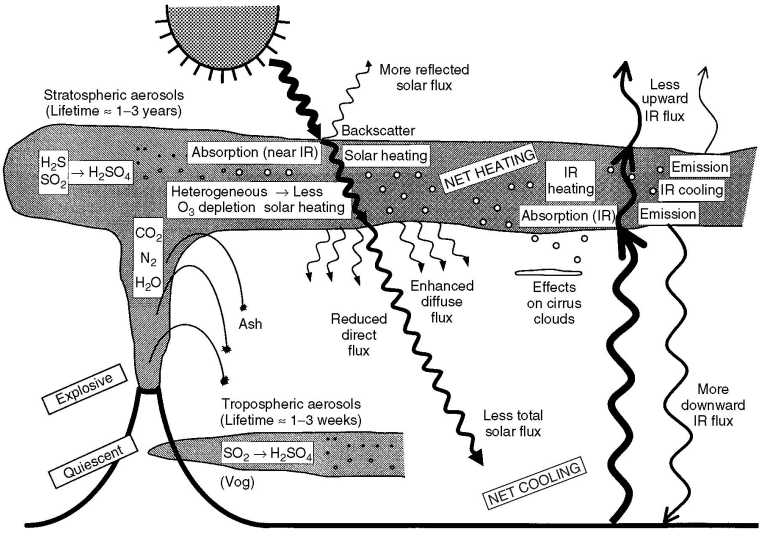


**Figure 2.3:** Schematic diagram of volcanic inputs to the atmosphere and their effects. Note the near-surface cooling and the stratospheric warming (cf. Robock 2000).

The net effect of explosive volcanism is thought to be a cooling of global near surface temperatures (Robock and Mao 1995), but regional deviations might occur, particularly in winter. Graf et al. (1993) analyzed the Pinatubo eruption in 1991 in terms of winter climate effects by means of the global climate model ECHAM2 forced with stratospheric aerosols. Within their perpetual January simulations they find a dynamical atmospheric response with a stronger polar night jet in the Northern Hemisphere extending into the lower troposphere. This results in higher near surface temperatures in northern Eurasia and North America which is consistent with observations. Dynamically this mechanism can possibly be related to the differential heating caused by the stratospheric sulfate aerosols leading to an increased equator-to-pole gradient resulting in an more intense westerly circulation. Usually one speaks of the mild-winter cool-summer phenomena in the aftermath of volcanic events. This implies an influence of the atmospheric dynamics on temperatures in winter, and an influence of the direct radiative forcing in summer (Robock and Free 1996). However, since only the Pinatubo eruption includes satellite measurements it could be questioned if this type of eruption, and hence its climate effects, can be generalized to other volcanic eruptions.
Shindell et al. (2003) conclude in their analysis about volcanic and solar forcing on climate during the pre-industrial era that the volcanic forcing is important for both regional climate change and long-term climate change on global scale. The solar forcing creates a long-term regional climate change that is greater than unforced variability. They use a stratosphere-resolving atmospheric GCM with a mixed layer ocean with a quite coarse resolution (8° lat x 10° lon) for their investigations. Concerning the DM they perform sensitivity studies with eruptions of the Tambora, in terms of a double and triple amount of

sulfuric aerosols as in the Pinatubo eruption (2P and 3P, respectively). For the most probable case of the 3P Tambora event they found a reduction of average surface temperatures of -1.09 °C. An important point connected with the 3P Tambora eruption is the sustained dominance of the radiative cooling over the circulation-induced winter warming, which is described in numerous studies within the first winter after volcanic eruptions (Robock and Mao 1992; Graf et al. 1993; Kirchner et al. 1999).
A further important aspect related to the explosive volcanism is the geographical location of the eruption. The tropical explosive volcanism effects both hemispheres via the atmospheric circulation systems, whereas the extratropical volcanism only effects the according hemisphere.

During the DM a number of volcanic events occurred (cf. Table 2.1), which also seem to have influenced the climate of this time (cf. Robertson et al. 2001). The eruption of the Laki-fissure occurred 1783. Demaree and Ogilvie (2001) describe the 'great dry fog' of the year 1783 which was caused by the *Skaftareldar* eruption in Island. Unlike other volcanic eruptions this one was followed by a very warm European summer and an extreme cold winter. Grattan and Pyatt (1999) analyze the climatic and environmental significance of historical dry fogs. They argue that the Laki fissure eruption failed to have an effective hemispheric climatic impact.
The huge eruption of the year 1809 is only evident in ice-cores (Dai et al. 1991). Observational evidence related to this eruption is found in Lamb (1970). He refers to some evidence of haze occurring over London in early April 1809.

The most prominent eruption is that of the Tambora in 1815 (cf. Stothers 1984). It is the largest of the modern era, more specifically within the last 500 years. There is observational as well as proxy-based evidence of widespread cold conditions, especially in eastern North America and western Europe in 1816. The following years also indicate very low summer temperatures (Briffa et al. 1998). According to Sachs and Graf (2001) the maximum decrease of global surface temperatures after Tambora was 0.7 °C. Sadler and Grattan (1999) examine the linkage between volcanic eruptions and climate change. They claim that the year 1816, the 'year without a summer' after the outbreak of the Tambora, was not exceptional, but that the conditions experienced in some areas in 1816 seem to be the end of a series of cold years that already started in the 1810s. Furthermore they conclude, while referring to Self et al. (1981), that there is little evidence of a cumulative effect of volcanic eruptions, as temperatures did not remain depressed after a series of closely timed eruptions. After the DM, the Babuyan Claro (1831) and the Cosiguina (1835) erupted (Robertson et al. 2001).

| *Volcano* | *Year* | *VEI* | *DVI/$E_{max}$* | *IVI* | *LAT* | *LON* |
|---|---|---|---|---|---|---|
| Grimsvotn [Lakagigar], Island | 1783 | 4 | 2300 | 0.19 | 64.4°N | 17.3°W |
| *unknown* | 1809 | ? | ? | 0.19 | ? | ? |
| Tambora, Sumbawa, Indonesia | 1815 | 7 | 3000 | 0.50 | 8.3°S | 118.0°E |
| Babuyan Claro, Philippines | 1831 | 4 | ? | 0.09 | 19.5°N | 121.9°E |
| Cosinguina, Nicaragua | 1835 | 5 | 4000 | 0.11 | 13.0°N | 87.6°W |

**Table 2.1:** Major volcanic eruptions around and during the Dalton Minimum. Compiled after Robock (2000) and Robertson et al. (2001).

In order to assess the degree of intensity of a volcanic eruption, several indices have been proposed, especially within studies on the influence of the paleovolcanism on climate. The most widespread indices are the dust veil index (DVI) (Lamb 1970), the volcanic explosivity index (VEI) (Newhall and Self 1982) and the ice-core volcanic index (IVI) introduced by Robock and Free (1996). Concerning the climatic-relevant impacts the VEI seems to be most suited.

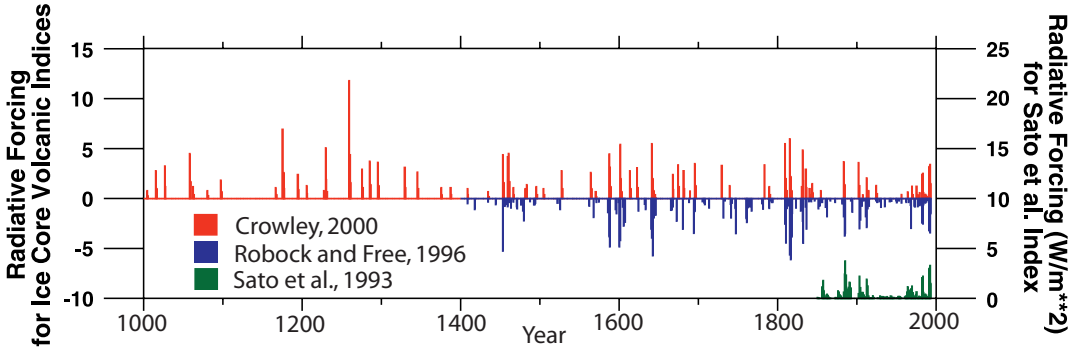


**Figure 2.4:** Ice core time series from Crowley (2000) (multiplied by -1 for display purposes), ice-core index (IVI) from Robock and Free (1996) converted to short-wave radiation forcing by Crowley 2000 and Sato et al. (1993) Northern Hemisphere radiative forcing (multiplied by -1). Note the similarity of the different reconstructions of large eruptions concerning both the intensity and timing. (after Crowley 2000).

The forcing caused by volcanic aerosols used in this study was assessed from concentrations of sulfuric compounds in ice cores also provided by Crowley (2000). He uses two records from Crete and the Greenland Ice Sheet Project2 (GISP2) on Greenland. The volcanism record is based on electrical conductivity or sulfate measurements. The relative amplitude of volcanic peaks was converted to sulfate concentration by scaling the peaks to the 1883

Krakatoa peak in ice cores. Eruptions greater than about 15Mt stratospheric sulfate loading were not accounted for linearly. They were corrected by an exponent of 2/3. This was done to account for the increase of the size of the aerosols through coagulation. Hence, the amount of scattered radiation is proportional to the cross-sectional area, and thus to the 2/3 power of volume. The aerosol optical depth was eventually converted to changes in downward short-wave radiative forcing at the tropopause using satellite data (Sato et al. 1993).
Figure 2.4 shows the volcanic time series by Crowley (2000) (red bars) and another reconstruction by Robock and Free (1996) (blue bars multiplied by -1). Additionally the Northern Hemisphere radiative forcing of Sato et al. (1993) (green bars) is also displayed. The main eruptions (e.g. Tambora, 1815; Krakatoa, 1883) are captured by both curves concerning the intensity and the timing. However, the Robock and Free (1996) time series also includes a variety of smaller eruptions not included within the Crowley (2000) reconstruction. According to Hegerl et al. (2003), the volcanic forcing time series of Crowley (2000) has an estimated uncertainty of approximately 50%.

A third external forcing on climate is the vegetation and land-use change, which is not discussed in detail here. However, findings of Bauer et al. (2003) from the Earth system model of intermediate complexity CLIMBER-2, suggest that the relatively cool climate in the second half of the 19th century is likely due to a cooling from deforestation.

# Chapter 3

# The climate of the Dalton Minimum

The next chapter characterizes the main climatic features of the DM for the different spatial scales concerning the global and hemispheric scale, the North Atlantic-European sector and the Central England temperatures.

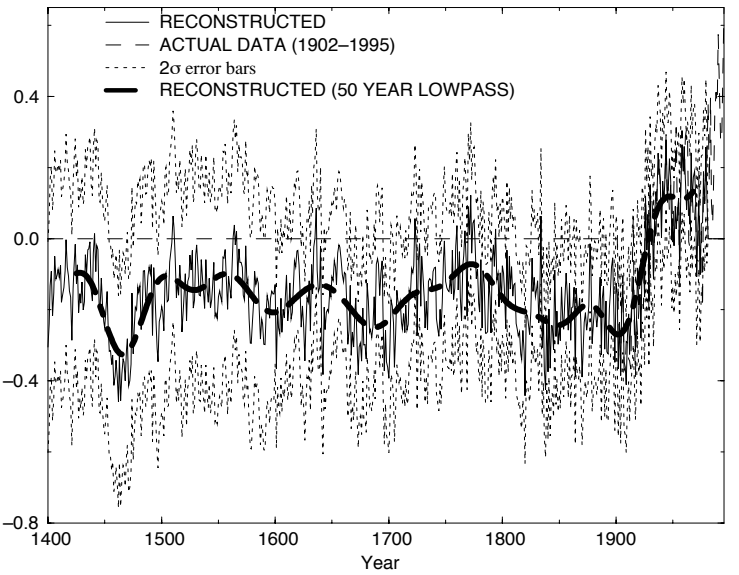


**Figure 3.1:** Northern Hemisphere temperature (°C) reconstructed from multi-proxy network (Mann et al. 1999a). Deviations from the mean 1902–80. Note the below normal temperatures throughout the whole 19th century.

In terms of the global and hemispheric scale temperature evolution the work of Mann et al. (1999a) is presented here including reconstructed global-scale temperature patterns for the

past six centuries by means of a multi-proxy network. Within their study the authors also present a reconstructed temperature time series from 1400 to 1995 for the Northern Hemisphere (cf. Fig. 3.1). The time series shows a clear drop in global temperatures, which is already evident within the 2nd half of the 18th century. The DM is not reflected as clear-cut

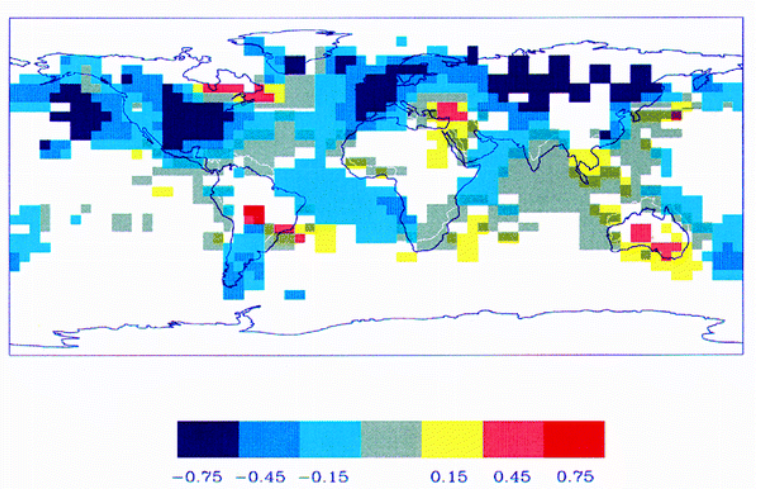


**Figure 3.2:** Reconstructed annual temperature anomaly pattern (°C) for 1816 (Mann et al. 1999a). The zero deviation is defined by the 1902–80 climatological mean for each grid point. Note the prevailing below-normal temperatures over large parts of the globe.

as could be inferred from the anomalous low solar forcing. The temperature anomaly at the end of the 19th century is even more pronounced than during the DM. This phenomenon could possibly be related to the sustained decrease within the external solar forcing from the middle of the 19th century onward (cf. Fig. 2.2) or to a cooling due to deforestation (Bauer et al. 2003). However, besides the reconstruction of Mann et al. (1999a) other reconstruction of the Northern hemispheric temperatures show partly deviating behavior concerning both, the evolution and the amplitude of the temperature anomalies. These reconstructions will be discussed in more detail within chapter 5.1.5.

As an example for an extraordinary year in the course of the DM Figure 3.2 shows a temperature reconstruction for the year 1816, the 'year without a summer' which was possibly caused by the outbreak of Tambora in 1815. In general reduced temperatures over large parts of the globe are evident. However, especially Eastern North America, the Near East, parts of central South America and Australia denote only slightly decreased or even above-normal temperatures with respect to the period 1902–1980. The temperature pattern within the the Atlantic possibly reflects an anomalous circulation pattern related to post-volcanic climate effects after strong volcanic eruptions as e.g. modelled by Shindell et al. (2003). It becomes evident that over Europe the radiative temperature decrease cannot be compensated by the dynamical winter warming.

The climatic conditions during the DM on the continental scale are discussed for the Northeast Atlantic-European area. Luterbacher et al. (2004) reconstructed a high-resolution Northeast Atlantic-European gridded temperature and precipitation data set back to 1500. It has a horizontal resolution of 0.5° lat x 0.5° lon (30° W to 40° E; 30° N to 70° N) and is therefore well suited to get an impression of spatial differences within the temperature patterns. The statistical method applied is based on an Empirical Orthogonal Function (EOF) analysis of the predictor field (here the proxy climate indicators) and of the predictand field (the gridded instrumental air temperature). The corresponding Principal components of the EOFs are used to set up standard statistical regression models linking both sets. These statistical relations are calibrated in the period 1901–1960 and validated in the period 1961–1990. In order to assess the reliability of the reconstructed data, the strength of the linear statistical relationship between reconstruction and observation is measured by the Reduction of Error (RE) in each grid point. This is a quantitative measure of the reconstruction quality and ranges between $-\infty$ and 1 (the case for a perfect reconstruction). Positive values of the RE indicate some skill in the reconstruction. Luterbacher et al. (2002; 2004) present a detailed mathematical treatment of the reconstruction method.

Fig. 3.3 shows the temperature differences between the DM and the period before (1756–1789) and after (1831–1900) the DM for the different seasons. The reason for taking the period 1756–1900 as reference is due to the start of the simulations in the year 1756. The end of the reference period in 1900 was chosen to factor out the bulk of the anthropogenic climate impact. In general, most seasons show positive temperature anomalies mainly over eastern Europe. Temperature anomalies along the Atlantic coast and western Europe are weak. However, the winters (a) have been reconstructed to be colder than the pre-industrial mean over northern and mid Europe. The Mediterranean and Black Sea area has been slightly warmer. The best quality results can be expected for central Europe according to the RE-values (not shown).

During spring time (b) positive temperature anomalies are mainly evident over central and eastern Europe. The quality in terms of RE-values is satisfactory over the whole area. The summer (c) tend also not to have been extraordinary cool. Western and central Europe show values around zero with slightly reduced temperatures over mid Europe. For eastern Europe, above normal temperatures are reconstructed. The RE-values show good quality of the reconstructions for nearly the whole European area with the exception of Southeast Europe, where the highest temperature differences are found. Thus, the trustworthiness of the reconstruction is this region is questionable. The autumn situation (d) in general reflects the spring time pattern with above normal temperatures over central and eastern Europe. The RE-values also show good quality for the whole area.

Hence, according to these reconstructions the DM is not reflected within the European temperatures. Opposed to that, large parts of Europe show positive temperature anomalies with respect to the pre-industrial mean. However, when subjecting the data to a Student's $t$ test

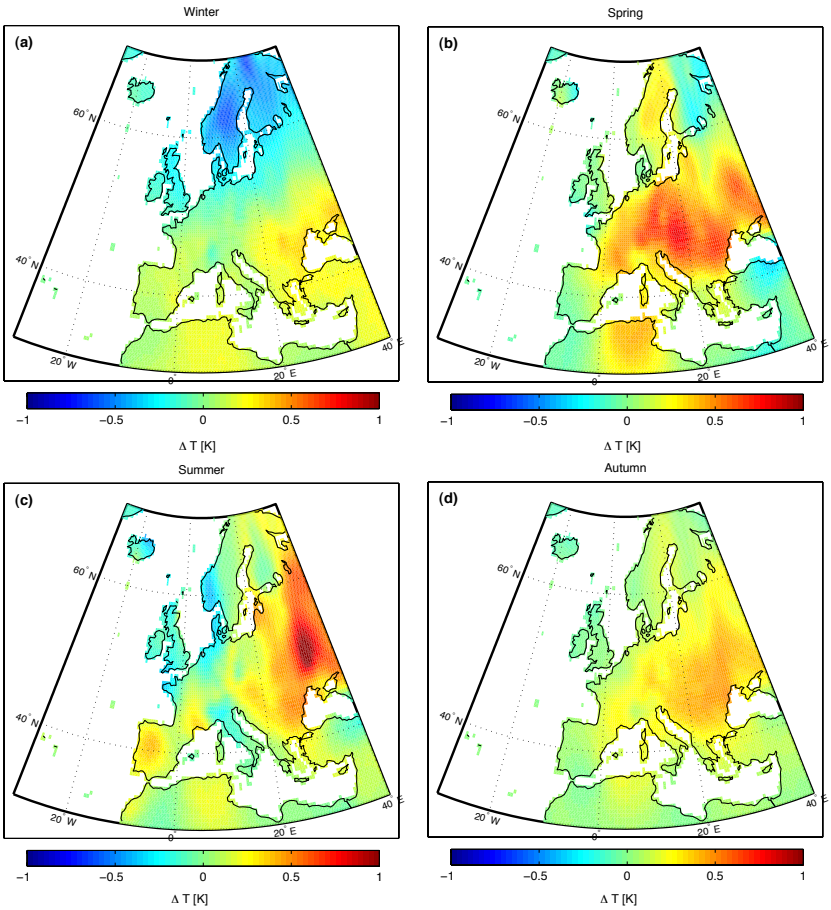


**Figure 3.3:** Reconstructed temperature differences between the DM and the period before (1756–1789) and after (1831–1900) the DM for the different seasons according to Luterbacher et al. (2004). Note the prevailing positive temperature anomalies over large parts of Europe.

almost all regions show statistically non-significant temperature differences. Accordingly, the European area has not been as largely influenced by the anomalous solar and volcanic forcing during the DM as e.g. during the Late Maunder Minimum.

As an example for the local climate during the time of the DM, Figures 3.4 and 3.5, respectively, show the temperature reconstruction for Central England back to 1659 deduced from instrumental observations (Manley 1974). During the DM a slight decrease of winter temperatures can be seen. Within summer time the DM is divided into two parts, one with above normal temperatures until 1810 followed by a sharp decrease in temperatures around 1815. This phenomenon is likely due to the volcanic impacts. The amount of temperature decrease with respect to the times prior (1756–1790) and after (1831–1900) the DM is +0.06 °C for winter time and for -0.06 °C for summer time, respectively.

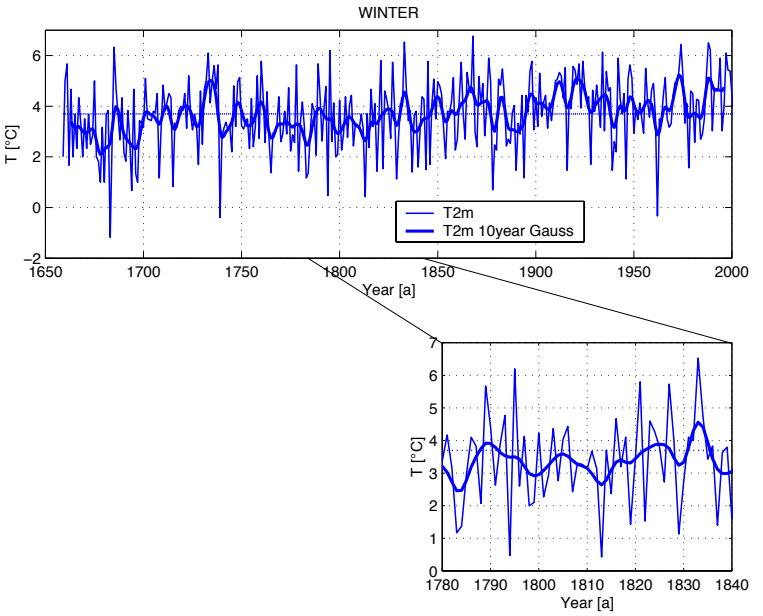


**Figure 3.4:** Central England temperature time series back to 1659 for winter.

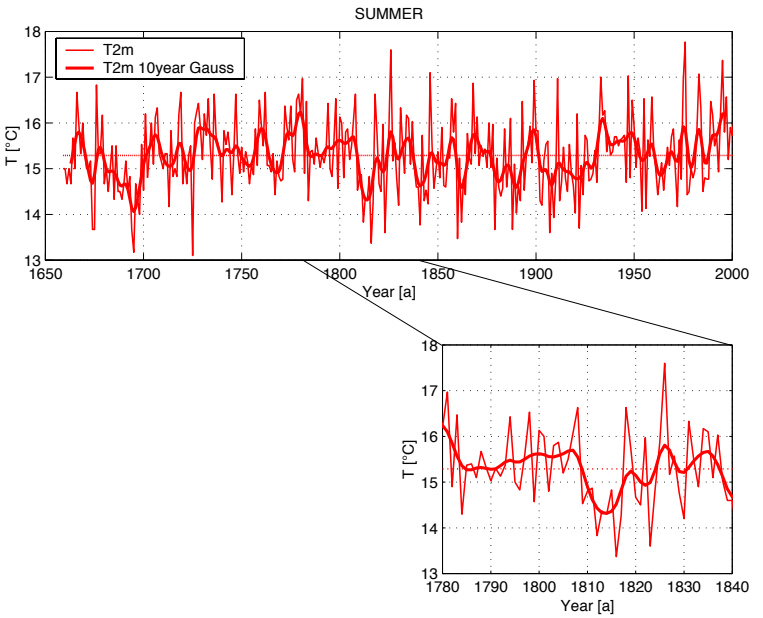


**Figure 3.5:** Central England temperature time series back to 1659 for summer. The Dalton Minimum is split-up into two parts, the latter characterized by a sharp decrease of temperatures.

Taking into account the different climate periods within the DM during summer time, the deviations are +0.20 °C and -0.33 °C for the period 1790–1809 and 1810–1830, respectively. The temperature difference during spring time and autumn is +O.14 °C and

+0.16 °C, respectively.
Thus, there is no clear evidence for a prominent cooling in Central England during the DM, except for the period 1810 to 1830 during summer time. These finding deviates markedly with respect to the Late Maunder Minimum, when all seasons show reduced temperatures with respect to the times prior and after.

Accordingly, there is no clear-cut evidence for a pronounced thermal anomaly during the DM on all spatial scales, especially on the regional. A possible explanation for the lack of a prominent cooling during the DM is related to its comparably short duration. Another reason could be due to the cool climate within the second half of the 19th century characterizing the time of the DM not as an outstanding climatic period. A third argument related to the local scale is concerned with the high interannual variability of the European climate possibly masking the externally induced signals.

Due to the comparatively good data coverage of the North-Atlantic European sector not only in terms of temperature but also in terms of sea level pressure data the following paragraph will shortly put some emphasis on the atmospheric circulation during the time of the DM. In this regard, Jacobeit et al. (2001a) analyses the circulation changes in Europe since the 1780s based on gridded SLP of Jones et al. (1999a). Accordingly, the winters of the first half of the 19th century are characterized by mainly negative indices of the North Atlantic Oscillation (NAO) which implies a weakening of the westerlies. The situation for the summer time in terms of the atmospheric circulation seems to be different as zonal circulation with positive NAO prevails in the first half of the 19th century.
A subsequent study carried out by Jacobeit et al. (2002) focuses on the changes within major European circulation modes based on reconstructions of Luterbacher et al. (2002a). Accordingly, in January during the time of the DM a westerly flow circulation pattern prevails, whereas the extended Russian High pattern is only of minor importance. This result seems to be inconsistent with the negative indices within the NAO in winter reconstructed by Jones et al. (1999a). A reason possibly explaining this difference is that the January situation need not necessarily reflect the conditions for the whole winter time. Furthermore, besides the NAO-reconstruction of Jones et al. (1999a), reconstructions for the NAO have also been undertaken by several other authors (Glueck and Stockton 2001; Luterbacher et al. 2002b; Cook et al. 2002). A common feature of these reconstructions is the deviation among them in the time before the instrumental period. Hence, there is no clear agreement among the reconstructions about the state of the NAO in the pre-industrial era (Schmutz et al. 2000).
In the study of Jacobeit et al. (2002) also internal changes of circulation patterns and their connection to e.g. temperature are described. Accordingly, during the first half of the 19th

century the January westerly flow pattern is related to an anticyclonic mode with below-average temperatures in Central Europe. This relation is opposite during the 20th century. Internal changes are also found for the extended Russian High concerning a maximum of cyclonic subtypes with below-average temperatures in Central Europe. However, this result is put into perspective due to the simultaneous frequency minimum of the extended Russian High pattern at the beginning of the 19th century.
The July situation is characterized by an outstanding importance of the westerly flow pattern at the end of the 18th century. However, this did not coincide with below-normal temperatures, but with a period of marked summer warmth in Central Europe. This internal change within the circulation-temperature connection is possibly related to an anticyclonic mode of the westerly flow pattern.
Thus, in terms of the atmospheric circulation there is some evidence for changes with respect to mean conditions. However, the question remains whether those circulation anomalies can be attributed to changes within the external forcing or whether they are due to natural climate variability.

# Chapter 4

# Model description and Experiment setup

The following section briefly describes the climate model ECHO-G used within the investigations. The setup of the different experiments follows.

## 4.1 Model description

The climate model ECHO-G (Legutke and Voss 1999) is a coupled climate model consisting of the atmospheric model ECHAM4 (Roeckner et al. 1996) and the ocean model HOPE (Wolff et al. 1997). A main difference between ECHO-G and ECHO is the inclusion of a thermodynamic-dynamic sea ice model from Hibler (1979) (Marsland et al. 2003).
The 4th generation atmospheric general circulation model (ECHAM4) was developed at the Max Planck Institute for Meteorology (MPI) in Hamburg. It is one in a series of models originally evolving from the spectral weather prediction model of the European Center for Medium Weather Forecasts (ECWMF). This version has still many features in common with the current ECWMF model. However, to apply the model to climatic issues some of the physical parameterizations have either been replaced or modified.
The ECHAM4-model is based on primitive equations. The prognostic variables are vorticity, divergence, logarithm of surface pressure, temperature, specific humidity, mixing ratio of total cloud water and optionally a number of trace gases and aerosols. The vertical extension is up to a pressure level of 10 hPa, which corresponds to a height of approximately 30 km. A hybrid sigma-pressure coordinate system is used with 19 irregularly ordered levels and with highest resolution in the atmospheric boundary layer. The bottom level is placed at a height of about 30 m above the surface corresponding approximately to the surface layer. In

this study the ECHAM4 model has a horizontal resolution of about 3.75° lat x 3.75° lon. The ocean model HOPE (Hamburg Ocean Primitive Equation) is an ocean general circulation model (OGCM) based on primitive equations with the representation of thermodynamic processes. It is a non-eddy resolving circulation model. HOPE-G has a horizontal resolution of approximately 2.8° lat x 2.8° lon with a grid refinement in the tropical regions over a band from 10° N to 10° S. This meridional grid refinement reaches a value of 0.5° at the equator allowing for a more realistic representation of ENSO variability in the tropical Pacific Ocean (Marsland et al. 2003). The ocean model has 20 vertical, irregularly ordered layers. To get an impression of the model resolution, Fig. 4.1 shows the land-sea mask of the ECHAM4 (a) and the interpolated HOPE-G (b) model.

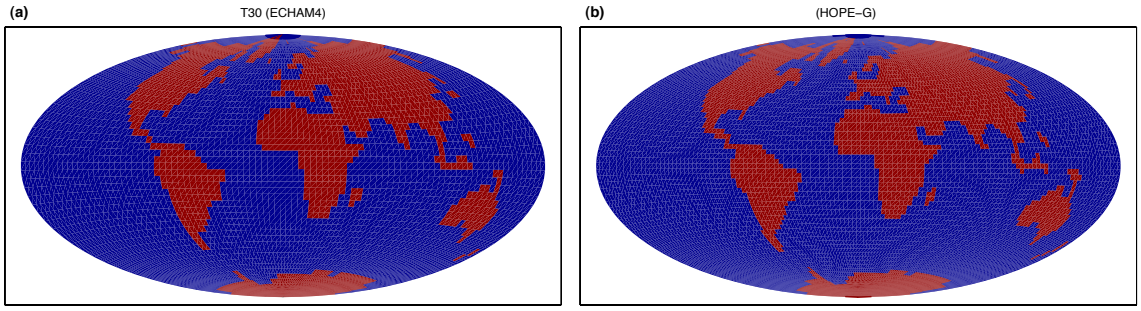


**Figure 4.1:** Land-sea mask of the atmosphere model ECHAM4 (a) and the ocean model HOPE-G (b). Note the coarse resolution e.g. for the European continent.

The coupling as well as the interpolation between the atmosphere and the ocean model is controlled by the coupling software OASIS (Terray et al. 1998). Concerning the coupling dynamics, at a distinct frequency the atmospheric component of the model passes heat, fresh water and momentum to the ocean and gets information about surface conditions of the ocean. This frequency is equal for all exchange fields and describes a 'coupled time step'. The fields that are exchanged are averaged over the last coupled time step.
Further aspects of the exchange processes are flux corrections due to the interactive coupling between ocean and atmosphere in order to prevent climate drift. These heat- and freshwater fluxes were diagnosed in a coupled spin-up integration. Accordingly, the sea-surface-temperature and sea-surface salinity were restored to their climatological observed values. This flux adjustment is constant in time and its global average is zero (Zorita et al. 2004).
A critical issue concerning climate drift is the amount of flux corrections applied in climate models, often taking in the order of the fluxes itself. Flux corrections are especially high at the sea-ice water boundary as well as in regions of vertical convection. Thus, flux corrections are leading to new uncertainties (Cubasch et al. 1995).

An important point related to climate model experiments is the sensitivity of the climate model, e.g. how strong does the model react to changes of the forcing. The sensitivity of the ECHO-G model is located in the middle of the range of the IPCC simulations with a 1% annual increase of atmospheric greenhouse gases. Within these climate change experiments the sensitivity of the ECHO-G model is 1.70 K at the doubling of the present $CO_2$ concentrations. Accordingly, the sensitivity of the ECHO-G model to changes in the radiative forcing is consistent with that of other models (Zorita et al. 2004).
The above mentioned sensitivity is not related to the equilibrium temperature. The estimation of the equilibrium temperature after the work by Tahvonen et al. (1994) for doubled $CO_2$ (equivalent) concentrations yields 2.88 K with upper and lower 95% confidence intervals of 1.14 K and 4.61 K, respectively. This result compares even better to the sensitivity range suggested by the IPCC which is located between 1.5 K and 4.5 K with a 'best guess' sensitivity of 2.5 K (Houghton et al. 2001).

## 4.2 Experimental setup

In order to prove the influence of different external forcings on climate with respect to the DM, three different experiments with the climate model ECHO-G were undertaken. The basis of all experiments is a historical simulation with the same climate model, starting in the year 1000 (González-Rouco et al. 2003), hereafter being called 'HIST'. This simulation is forced with variable solar and volcanic output as well as with changes of greenhouse gas concentrations concerning $CO_2$ and $CH_4$. The $CO_2$ and $CH_4$ concentrations were derived from air which was trapped in Antarctic ice cores (Etheridge et al. 1996).
In this study the volcanic forcing is not directly introduced into the climate model. The major reason for this is the poorly represented stratosphere within this version of the climate model. However, in order to account for the volcanic activity, the optical depth of the sulfuric aerosols is translated into a so called 'effective solar constant'. The rationale behind this approach is the already mentioned net-cooling effect of volcanic aerosols illustrated within Fig. 2.3. Accordingly, the peaks within the curve in the upper right panel of Fig. 4.2 represent the effect of the volcanic eruptions, while the slow variations are reflecting the changes in the solar output. A close inspection of the solar curve also resolves the 11-year solar Schwabe cycle.
One of the greatest shortcomings of this approach is the disregard of the latitude-specific impact and influence of the volcanic aerosols. Thus, the whole globe receives a reduced amount of solar insolation independent of the latitude of eruption. Another shortcoming is the unresolved temporal eruption date within the annual cycle.
During the course of the work a new volcanic data set from Robertson et al. (2001) became

available including a latitude-specific resolution. Despite the different reconstruction approaches the globally averaged aerosol optical depths coincide quite well. However, different results can be obtained through the conversion into a short-wave radiation forcing, depending on the treatment of large eruptions.

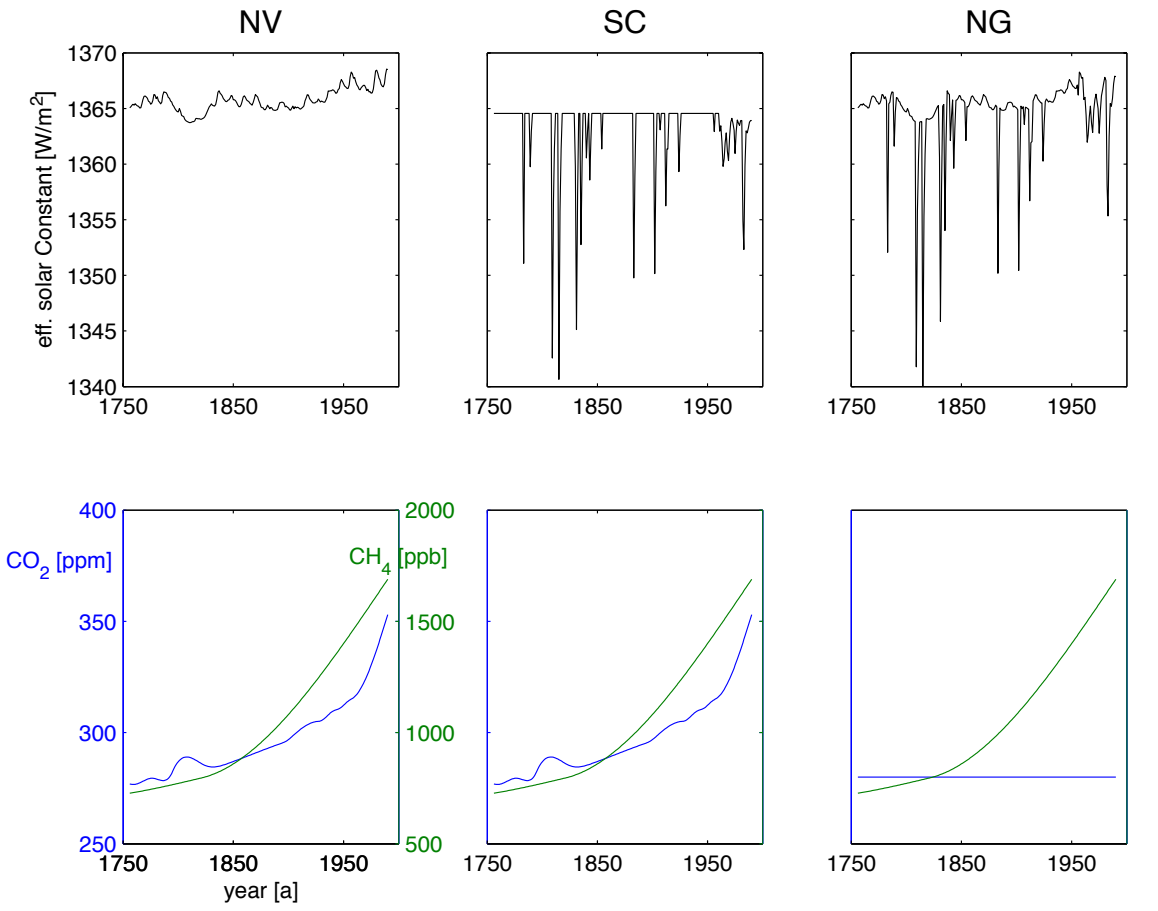


**Figure 4.2:** Different forcings applied on ECHO-G. The NV experiment is only forced with solar variability (left column). The SC experiment is forced with volcanic influence and the mean solar constant of the Dalton Minimum (middle column). The NG experiment is forced with both solar and volcanic variability but with constant $CO_2$ concentrations at 280 ppm (right panel).

The first experiment, denoted 'NV' (no volcanoes), is forced without any volcanic influence, only with the solar forcing and a variable $CO_2$ and $CH_4$ forcing (cf. Fig. 4.2, left column). This experiment is most similar to that of Cubasch et al. (1997) but with another version of the atmospheric and oceanic climate model.
In the second experiment, denoted 'SC' (sun constant), the model is only forced with the

volcanic influence and the mean solar constant of the DM. The greenhouse gas forcing is the same as in the NV experiment (cf. Fig. 4.2, middle column).
The third experiment, denoted 'NG' (no greenhouse gas $CO_2$ increase), addresses on the rising $CO_2$concentrations at the beginning of the 19th century. The $CO_2$concentrations remain at a constant pre-industrial level of 280 ppm throughout the whole integration. Furthermore, the $CH_4$ concentrations were not kept constant, as the emphasis was on the effect of $CO_2$. This experiment is externally forced with the variable output of solar and volcanic activity (cf. Fig. 4.2, right column).

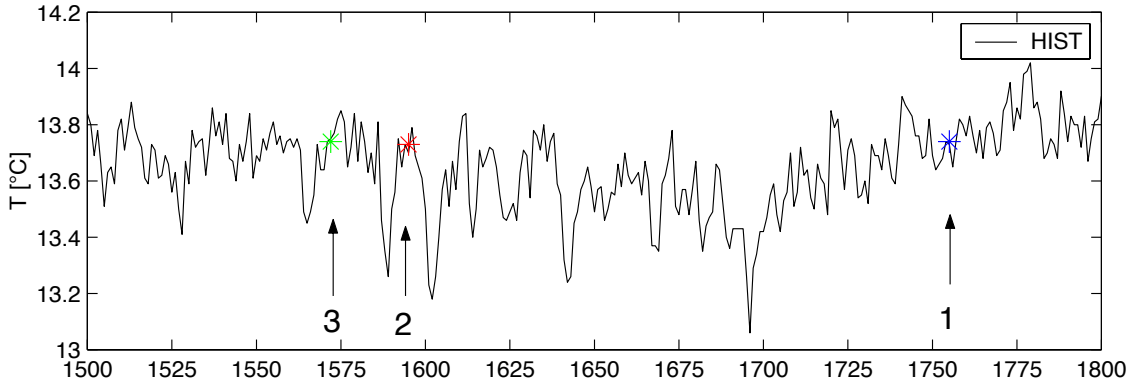


**Figure 4.3:** Mean global near surface air-temperatures for the HIST experiment. The start dates for the ensembles 2 and 3 were selected in terms of the mean global near surface temperature being closest to 1755.

In order to assess the possible bandwidth of the model climate, each experiment has been conducted 3 times. The initial conditions have been selected in terms of global mean temperature being closest to temperatures in 1755 of the HIST simulation (cf. Fig. 4.3). Accordingly, the first ensemble members are simply a continuation of the HIST simulation. The second and third ensemble members are initialized with oceanic and atmospheric conditions during the second half of the 16th century.

# Chapter 5

# Atmospheric and Oceanic Variability

The following forms the main part of the study, namely the analysis of the atmospheric and oceanic variability within the different experiments with respect to the DM and beyond. The next paragraph deals with the temperature evolution within the different experiments. One of the main hypothesis to be tested is whether the volcanoes exert any significant influence on the temperatures of the DM on different spatial scales. The subsequent section analysis the extratropical circulation variability in terms of the Arctic and Antarctic circulation. A question is here to be discussed is to what extent the circulation is influenced by the external forcing. The last subsection deals with the oceanic variability in terms of ocean temperatures, ocean circulation and oceanic heat transport within the North Atlantic Ocean. Besides the behavior of the ocean dynamics during the DM, the question of whether the initial oceanic conditions are able to determine the long term evolution of the ocean will be discussed.

## 5.1 Evolution of temperatures

This section analyses the reaction of the temperatures to the external forcing. This implies not only global mean temperatures but also regional considerations (at scales of 1000-10000 km) and spatially resolved temperature patterns. Another issue addresses the intra-ensemble temperature variability.

### 5.1.1 Global mean temperatures

The evolution of the yearly mean ensemble global near-surface air temperatures for the different experiments is displayed in Figure 5.1 in units of °C. The reason for using absolute temperatures in favor of temperature anomalies is due to the better illustration of the different effects of the different forcings on absolute temperature levels.

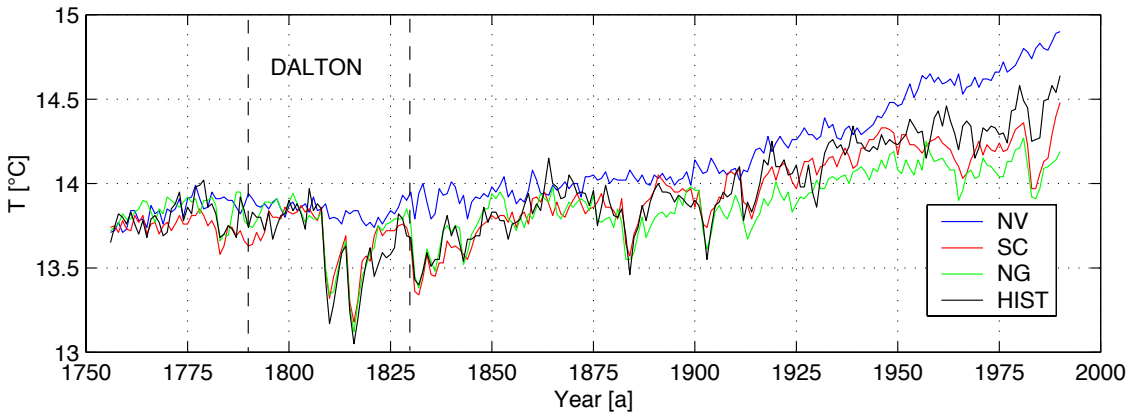


**Figure 5.1:** Yearly mean ensemble near-surface air temperatures for the NV, SC, NG, and the HIST experiments. Note the increased temperature level within the NV experiment and the lack of a clear-cut temperature minimum during the DM.

Within Fig. 5.1 all experiments show the same temperature level prior to 1800. With the incipient volcanic influence in the 1810s the experiments SC and NG as well as HIST show a pronounced decrease in global temperatures. The NV experiment however shows only a weak cooling in the order of 0.1 °C. Accordingly, the temperatures of the volcanic-influenced simulations show a split-up of the DM: The first half of the DM does not show reduced temperatures, opposed to the second half after 1810, when a pronounced temperature depression is evident. Until the mid 19th century further volcanic impacts reduce temperatures within the SC, NG and HIST experiments. Around 1870 all curves reach similar temperature levels again. The eruption of volcanoes during the second half of the 19th century (Krakatoa, 1883) and the beginning of the 20th century again cause a decrease of global temperatures within the experiments SC, NG and HIST. As the NV experiment does not experience the volcanic eruptions, a further increase in global temperatures can be seen.
Within the 20th century, and especially within its second half, the NV experiment shows a tremendous increase in global temperatures opposed to the other experiments, which are influenced by the cooling volcanic effects. The NG experiment with constant $CO_2$ concentrations shows in general the lowest temperature levels, indicating a very prominent

influence of the $CO_2$ within the other experiments. The influence of i) the $CO_2$ and ii) the volcanoes can further be seen within the SC experiment, where despite the lack of solar variability i) an increase in temperatures can be seen and ii) the temperature variability coincides quite well with the other experiments.

In order to emphasize the temperature differences with respect to the reference simulation HIST, Figure 5.2 shows the temperature difference between the ensemble mean of the NV, SC, and NG experiments and the HIST experiment.
Fig. 5.2a shows the temperature differences for the NV experiment. The most striking feature is an abrupt onset of prevailing positive temperature anomalies after 1810, which are evident until the end of the simulation. This strong positive anomalies are dampened within the second half of the 18th century and during the 1940s, when only few volcanic eruptions occurred. The volcanic imprint becomes especially clear for the high positive peaks (e.g. around 1815, 1885, 1900). The second half of the DM shows the highest temperature differences emphasizing the strong volcanic influence during this time. Accordingly, the volcanic activity seems to have a strong impact in reducing the near-surface temperatures.

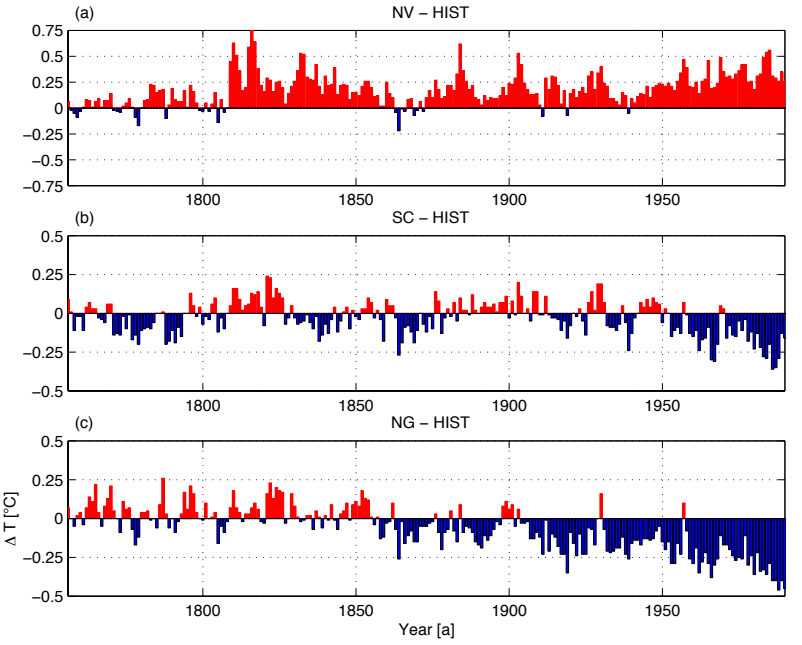


**Figure 5.2:** Temperature difference between the NV(a), SC(b), NG(c), and the HIST experiment. Note the prominent role of the volcanoes after 1810 within the upper panel and the impact of $CO_2$ during the 20th century within the lower panel.

Fig. 5.2b shows the temperature difference between the SC experiment, forced with constant solar activity and variable volcanic and greenhouse gas forcing and the HIST experiment, respectively. In general the differences are not extraordinary until the second half of the 20th century. Slight positive, as well as slight negative, temperature differences can be seen. They are likely related to the variable solar forcing within the HIST simulation. In general the DM shows higher temperatures. This is possibly due to the forcing with the *mean* solar constant of the DM. Accordingly, the solar radiation in the SC experiment does not reach as low values as the variable solar forcing within to the HIST experiment (cf. Fig. 4.2). The second half of the 18th century is mainly characterized by negative temperature differences. These are also possibly related to the lower solar radiation within the HIST experiment. The increasing temperature differences during the second half of the 20th century are possibly due to the lack of increasing solar activity.
Figure 5.2c shows the temperature differences between the NG experiment, forced with constant pre-industrial $CO_2$ concentrations but variable solar and volcanic output and the HIST experiment, respectively. Accordingly, prior to the increase within the $CO_2$ concentrations the NG and HIST experiments are very close to each other in terms of external solar and volcanic forcing. The most prominent feature is the strong increase in negative temperature differences from the mid 19th century on. This might be attributed to a high degree to the constant pre-industrial $CO_2$ concentrations within the NG experiment. The period prior to this $CO_2$ increase exhibits positive temperature differences, especially during the times of the DM. This is somewhat surprising, as here a strong increase within the $CO_2$ concentrations is already evident, but apparently does not force an increase in global temperatures in the HIST experiment. The second half of the 18th century also shows positive temperature differences.

In order to make a closer investigation of the hemispheric-scale temperature evolution, Fig. 5.3 shows the yearly mean ensemble temperatures of the extratropical Northern Hemisphere (a), the tropics (b) and the extratropical Southern Hemisphere (c), respectively. (In this study the term 'extratropical' refers to latitudes north and south of 30° N and 30° S, respectively). In general, in the extratropical Northern Hemisphere (Fig. 5.3a) the evolution of the different experiments is quite similar to the global temperatures. The higher degree of temporal variability is likely due to the high amount of continental areas. Interestingly, the sharp volcanic imprints, evident in the global and tropical temperatures are temporally blurred. This is somewhat surprisingly as one might expect a sharp volcanic signal due to the large continental influence which is supposed to reflect the external volcanic forcing as more pronounced. However, the NV experiment does not show any reduction of the Northern hemispheric temperatures during the DM at all.

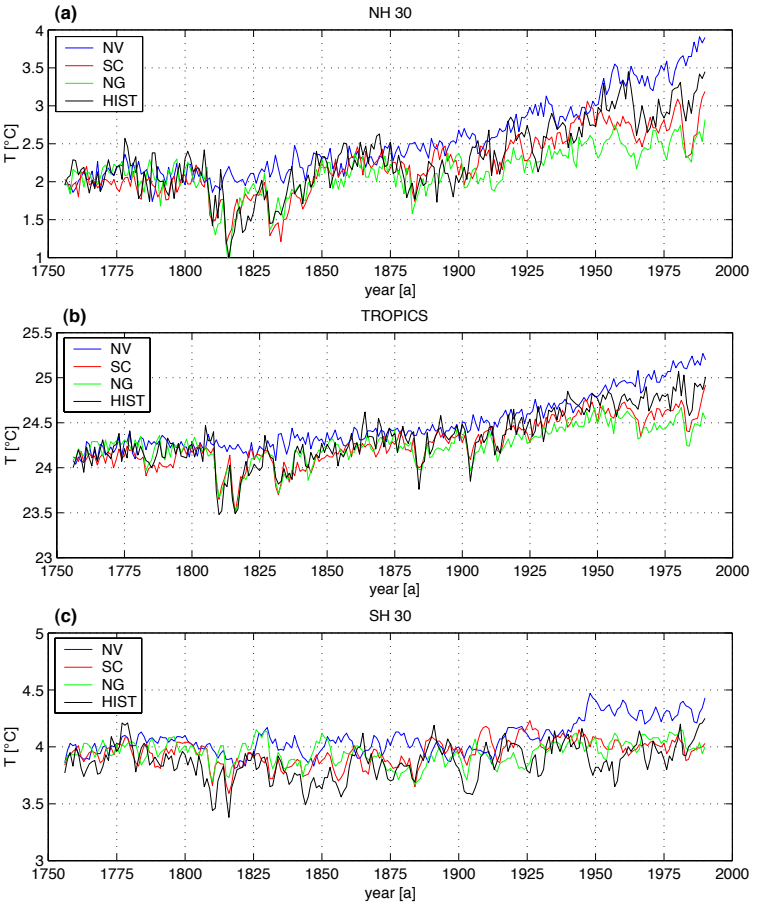


**Figure 5.3:** Temperatures for the NV, SC, NG and HIST experiments for the extratropical Northern Hemisphere (a), the tropics (30° N–30° S) (b) and the extratropical Southern Hemisphere (c). Note the increased variability of the Northern Hemisphere due to the large continental influence compared to the Southern Hemisphere.

The tropical temperatures (Fig. 5.3b) approximate the global temperature the best. This is true for both the increased temperature level within the NV experiment and the pronounced imprint of the volcanic activity within the SC, NG, and HIST experiments, respectively. The increased interannual variability evident in all experiments is possibly due to the El-Niño-Southern Oscillation within the tropical Pacific.

The Southern Hemisphere temperatures (Fig. 5.3c) show marked deviations with respect to the global and Northern hemispheric temperatures. Within the NV experiment a moderate temperature decrease of 0.25 °C can be seen during the DM. During the whole 19th and within the first half of the 20th century no clear temperature trend with respect to the global or Northern hemispheric temperatures is discernible. The lagged response of temperature decrease to the external forcing is possibly due to the large amount of oceanic areas in the Southern Hemisphere. Around 1950 a jump of +0.25 °C occurs within the NV experiment,

which stabilizes until 1990. The SC and NG experiments show quite similar evolutions. During the second half of the DM the two prominent volcanic eruptions are reflected. After the DM only a small increase in temperatures can be seen.
Thus, with respect to the evolution of global mean temperatures the extratropical Northern hemispheric and tropical temperature time series show similar behavior in terms of the reaction to the external forcing. The extratropical Southern hemispheric temperatures do not show this clear reaction e.g. in terms of a sustained temperature increase within the different experiments during the 20th century. Accordingly, the mechanisms governing the temperature evolution over the extratropical Southern Hemisphere must be different. A candidate possibly accounting for the discrepancies might be the large oceanic area covering large parts of the Southern Hemisphere.

### 5.1.2 Regional temperatures

The following section discusses selected extratropical Northern hemispheric regional temperature times series and the temperatures for the high latitude Southern Hemisphere. The motivation of this section is to get insight into the regional temperature variability at scales of 1000-10000 km.

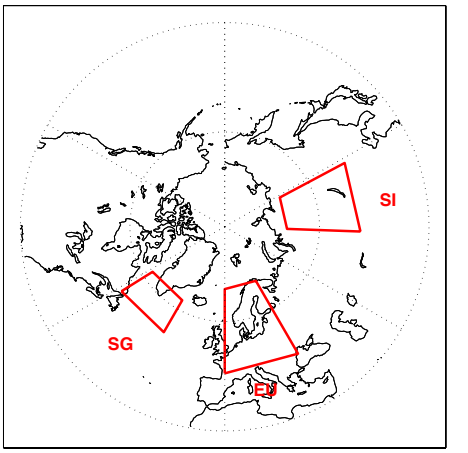


**Figure 5.4:** Geographical locations of selected temperature regions south of Greenland (SG), Europe (EU) and Siberia (SI).

This implies the degree to which the regional temperatures reflect changes within the external forcing and how much they differ with respect to global or hemispheric temperatures. Another issue related to regional temperatures is the possibility to compare their

evolution with reconstructed temperatures by means of proxy or historical data. Here the North Atlantic European sector, especially, deserves attention concerning the availability and quality of historical climate observations (cf. Luterbacher et al. 2004). A comparison between the reconstructed and modelled temperatures during the time of the DM for the North Atlantic European will be given in section 5.1.5.

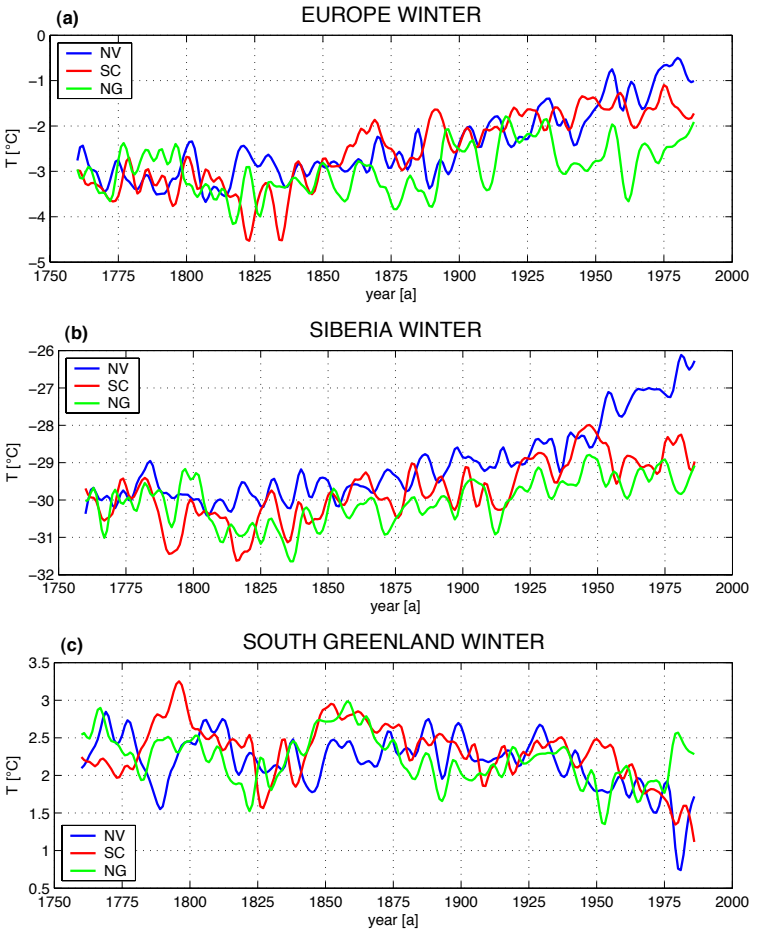


**Figure 5.5:** Regional winter temperature time series for the extratropical Northern Hemisphere for central Europe (a), Siberia (b) and South Greenland (c) for the different experiments. Note the reduction of temperatures during the 20th century over South Greenland. The time series have been smoothed with a 10-years Gaussian low pass filter.

The evolution of the winter temperatures over Europe, Siberia and South Greenland is displayed in Fig. 5.5. The geographical location of the regions is shown within Fig. 5.4. For clarity, the reference simulation HIST has been omitted. The winter time was chosen because at this time the influence of the atmospheric circulation is most pronounced and possible differences between the regional and hemispheric temperatures may be due to

circulation anomalies.
In general, the European temperatures (Fig. 5.5a) do not show a clear-cut picture concerning the reaction on the external forcing with respect to the global temperatures. A result which can be deduced from the unfiltered time series (not shown) is that during the DM the volcanic impacts seen in the Northern hemispheric temperatures in the SC and NG experiments are not as clear-cut reflected in the European winter temperatures. The NV experiment does not show the pronounced increase within the temperature level during the whole period. The NG experiment in general shows the lowest temperatures, but in the early 20th century it reaches the temperature levels of the NV and SC experiments. Around 1930 a separation between the temperatures of the NV and SC experiments and the NG experiment is evident. Interestingly, the SC experiment coincides with the NV experiment over most of the time, although the volcanic impacts are not applied in the NV experiment. Accordingly, on this regional scale the volcanic impacts seem not to exert that climatic relevance as on hemispheric or global scales.
The Siberian temperatures (Fig. 5.5b) show an increased temperature level for the NV experiment during the DM. The temperatures within the SC and NG experiments coincide over large periods. Here, temperatures during the DM are lower than normal but the single volcanic peaks are not clearly separated. This phenomenon was already demonstrated for the European temperatures. Within the second half of the 20th century an accelerated increase of temperatures can be seen for the NV experiment. For the SC experiment the large volcanic influence since 1950 can be ruled out in view of the lack of temperature increase. The overall temperature range is enlarged with respect to the European temperatures by a factor of 2, which can likely be attributed to the high continental influence.
The temperatures for South Greenland (Fig. 5.5c) show a completely different picture with respect to the European and Siberian temperatures. The increased temperature level for NV experiment is not evident. Contrarily, the NV time series in general coincides with the SC and NG experiments. During the DM all experiments show a negative temperature trend. The second half of the 20th century is, as opposed to the European and Siberian temperatures, characterized by decreasing temperatures for the NV and SC experiments. Only the NG experiment shows a moderate increase. This peculiarity of the South Greenland region temperatures in terms of temperatures evolving asynchronous with respect to the global or hemispheric temperatures is possibly due to atmospheric circulation anomalies in terms of the North Atlantic Oscillation (cf. section 5.2.4). Furthermore oceanic sea ice plays a crucial role for the liberation of latent and sensible heat to the atmosphere in this region. Thus, an increased sea ice cover within this region effectively reduces near-surface air temperatures. Another explanation for the decrease in the Greenland temperatures during the 20th century may be attributed to a decline in the meridional overturning resulting in a reduced northward heat transport (cf. section 5.3.3).

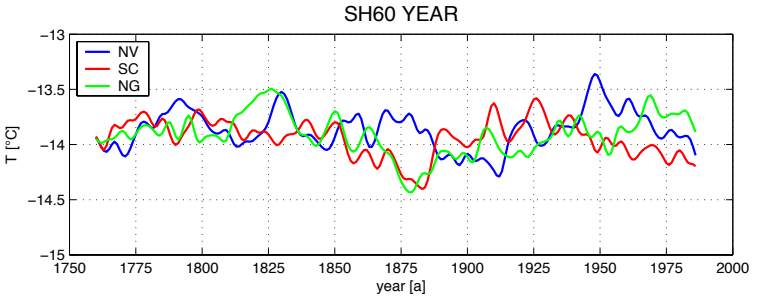


**Figure 5.6:** High latitude Southern hemispheric temperatures south of 60° S for the different experiments. Note the decrease of temperatures within the second half of the 20th century. The time series have been smoothed with a 10-years Gaussian low pass filter.

For the Southern Hemisphere, temperatures are averaged south of 60° S (Fig. 5.6). In general, there are also clear discrepancies with respect to the global or Northern hemispheric temperatures in terms of variability. The temperature range is quite small. Prominent features are the temperature increase within the NG experiment at the main part of the DM and the temperature decrease within NV and SC experiments within the second half of the 20th century. The NV experiment does not show the outstanding increased temperature levels of the Northern hemispheric temperatures. Furthermore the volcanic impacts within the SC and NG experiments are not reflected. Possible reasons for the deviating behavior of Southern Hemisphere high-latitude temperatures can be partly explained by an anomalous atmospheric circulation, which is discussed in section 5.2.4.

### 5.1.3 Spatially resolved temperature deviations

As previously discussed, not all regions show the same temperature evolution. In order to get a spatially differentiated picture, especially during the DM, the temperature difference between the different experiments and the HIST simulation have been calculated. A Student's *t* test accounting for serial correlated data (cf. Zwiers and von Storch 1995 and von Storch and Zwiers 1999) has been performed to determine an explanation. Within the following paragraph the main ideas of the *t* test are introduced and the need for the attention of serial correlated data will be given.
The Student's *t* test aims to test the hypothesis of equality of means. Thus the Null Hypothesis reads as follows:

$$H_0 : \mu_X = \mu_Y \tag{5.1}$$

The according test statistic is given by

$$t_{obs} = \frac{\hat{\mu}_X - \hat{\mu}_Y}{S_p \sqrt{\frac{1}{n_X} + \frac{1}{n_Y}}}, \tag{5.2}$$

with $n_X$ and $n_Y$ being the size of $X$ and $Y$, respectively, $\hat{\mu}_X$ and $\hat{\mu}_Y$ being the means of $X$ and $Y$, respectively. $S_p$ is the pooled estimate of the common standard deviation which reads as follows:

$$S_P^2 = \frac{\sum_{i=1}^{n_X}(\mathbf{x}_i - \hat{\mu}_X)^2 + \sum_{i=1}^{n_Y}(\mathbf{y}_i - \hat{\mu}_Y)^2}{n_X + n_Y - 2} \tag{5.3}$$

The test of the Null hypothesis is carried out against the following alternative hypothesis:

$H_1 : \mu_X \neq \mu_Y$;
with the significance level, $p = P(t \geq |t_{obs}|$.

The upper and lower confidence limits $100(1 - \alpha/2)\%$ for $\hat{\mu}_X - \hat{\mu}_Y$ are calculated after

$$(\hat{\mu}_X - \hat{\mu}_Y) \pm t_{1-\alpha/2} S_p \sqrt{(1/n_X) + (1/n_Y)} \tag{5.4}$$

with $t_{1-\alpha/2}$ being the $100(1 - \alpha/2)$ percentage value of the *t* distribution with $n_X + n_Y - 2$ degrees of freedom. Thus, if $t_{obs}$ lies within the confidence limits $100(1 - \alpha/2)\%$ the Null hypothesis cannot be rejected.
The above procedure for calculating the test statistic *t* is only valid under specific assumptions. It often happens, especially when dealing with meteorological data, that some of the basic assumptions allowing for the application of the test are violated. Two of them are briefly discussed within the next two paragraphs:
**1.** the variances of the samples $X$ and $Y$ are unequal;
**2.** the sample(s) are *auto-correlated* (serial correlation);

**1.**
In order to account for the inequality of the variances of $X$ and $Y$, the *t* statistic changes to

$$t'_{obs} = \frac{\hat{\mu}_X - \hat{\mu}_Y}{\sqrt{\frac{S_X^2}{n_X} + \frac{S_Y^2}{n_Y}}} \tag{5.5}$$

with $S_X^2 = \frac{1}{n_X - 1} \sum_{i=1}^{n_X} (\mathbf{x}_i - \hat{\mu}_X)^2$.
Eq. 5.5 no longer has a *t* distribution under the Null hypothesis. In order to overcome this, the *Behrens-Fischer* problem, one estimates the statistic with a $t$-distribution whose degrees of freedom are calculated from the data after

$$df = \frac{(S_X^2/n_X + S_Y^2/n_Y)^2}{\frac{(S_X^2/n_X)^2}{n_X - 1} + \frac{(S_Y^2/n_Y)^2}{n_Y - 1}} \tag{5.6}$$

Again $t'_{obs}$ is compared to the critical values of the *t* statistic but with the degrees of freedom according to eq. 5.6.

**2.**
Another typical problem with meteorological data is the serial autocorrelation of data. This implies the memory-effect of the data under investigation. For certain purposes this autocorrelation of climate data is quite acceptable, e.g. for the test of the performance of state-of-the art global climate models (cf. Bunde et al. 2003) and climate prediction (cf. Blender and Fraedrich 2003). In terms of testing differences of mean, auto-correlated data can influence the *t* test in such a way that it rejects the Null hypothesis when it is true more frequently than indicated by the significance level.
A means to deal with this problem is to introduce the *equivalent sample size* $n'$. $n'_X$ is defined as the number of independent variables that are needed to receive the same amount of information about $\mu_X$ as the sample of the depended variables $X$. Hence, the original sample size $n$ is replaced by the equivalent sample size $n'$. The estimation of the equivalent sample size $n'$ is calculated by using the auto-correlation function:

$$n'_X = \frac{n_X}{1 + \sum_{k=1}^{n_X - 1} (1 - \frac{k}{n_X}) \rho_X(k)} \tag{5.7}$$

with

$$\rho_X(k) = \frac{1}{\sigma^2} Cov(\mathbf{X}_i, \mathbf{X}_{i+k}) \tag{5.8}$$

Usually only $\rho_X(1)$ is used for the estimation of the equivalent sample size $n'$.
One remaining problem occurs at small $n'$ ($n'_X \leq 30$ and $n'_Y \leq 30$). When the statistic is

calculated with $t'$, the $t$ distribution $t'$ deviates markedly from any $t$ distribution and the test cannot formally be used with small $n'$. In the following analysis there are some regions showing only very few equivalent sample size $n'_X$ and $n'_Y$. According to von Storch and Navarra (1999) the $t$ test operating with the true equivalent sample size is conservative and thus incorrect. The alternative is to use a look up table. This alternative has not been employed here. Thus, for regions with very small equivalent sample sizes the results are biased toward a rejection rate of the Null hypothesis that is too low. Another point related to the auto-correlation of data is the spatial auto-correlation of data also modifying the test statistics. This also, is not included within the analysis. Further information on this problem can be found in von Storch and Zwiers (1999).

Within the following paragraph both, the inequality of the variances as well as the serial autocorrelation have been regarded within the analysis. One shortcoming in the application of the *t* test is that the HIST experiment consists only of one realization, whereas the other experiments reflect the mean of 3 ensemble simulations, where the 2nd and 3rd ensemble members are initialized with changed atmospheric and oceanic conditions. Accordingly, only the first member simulations of the experiments are continuation runs of the HIST simulation with different forcings. In order to account for this problem Figure 5.7a,b show, as an example, the temperature differences between the first member simulation of the NV experiment and the HIST simulation for the DM.

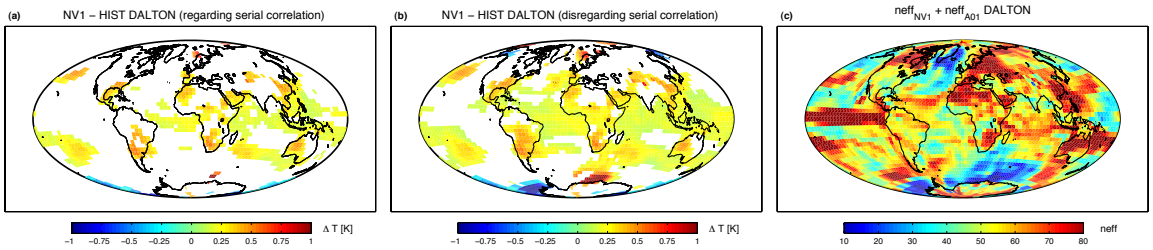


**Figure 5.7:** Temperature difference between the NV1 and HIST simulation for the DM accounting for serial correlation (a) and disregarding serial correlation (b). Only values significant at the 95% level of significance are shown. (c): Sum of effective degrees of freedom for the NV1 and HIST simulation for the DM. Note the differences between (a) and (b) concerning the significance of grid points due to the consideration of serial correlation.

Figure 5.7a shows the temperature differences considering the effect of serial correlation. Figure 5.7b shows the same analysis when disregarding this effect. It becomes evident that many more grid points fail the test. This is especially true for parts of the tropical Atlantic and Indian Ocean as well for some polar oceanic regions over the high latitudes.

In fact, Figure 5.7b shows 38% of all grid points to be statistically significantly different, whereas Figure 5.7a only shows 19% . (In the following the term 'significantly' is related to the statistically significance). Accordingly, when accounting for the serial correlation the Null hypothesis is not rejected for twice as many of the cases. The reasons for this are given in Figure 5.7c. Especially regions, where the $n'$ is low, which is due to a high serial correlation of the data within this region, the grid points turn out to be non-significant. Regions which show very low effective sample sizes are located off the coast of Antarctica and in the northern North Atlantic. These areas are to a large degree influenced by oceanic sea ice, which tends to exhibit a long term memory within the climate. However, as already mentioned, those regions should see more temperature differences to be statistically significant different when accounting for the very low equivalent sample size.

Fig. 5.8 shows the same analysis as Fig. 5.7a, except for the ensemble mean of the experiments. The biggest differences are evident within the experiment without any volcanic influence. The tropical and some extratropical Southern hemispheric regions, especially, exhibit slightly increased temperatures within the NV experiment. No significant differences can be seen for large parts of the Northern hemispheric continents.
The differences within the SC and NG experiments are mostly non-significant on large scales, except some oceanic Southern hemispheric regions. The only region on the Northern Hemisphere indicating significant positive temperature anomalies during the DM is located within the central North Pacific and south of Greenland within the SC experiment. The Labrador region shows lowered temperatures within the SC and NG experiments.

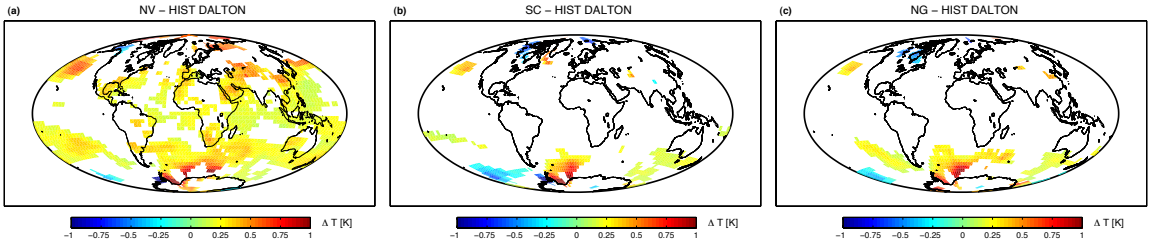


**Figure 5.8:** Temperature difference between the mean of the ensembles NV(a), SC(b), NG(c) and the HIST simulation for the DM. Only values significant at the 95% level of significance are shown, accounting for serial correlated data. Note the pronounced influence of the volcanoes on global and hemispheric scales within (a) and the minor influence of solar and $CO_2$ variability in (b) and (c), respectively.

Accordingly, only the NV experiment shows large scale significant temperature differences, whereas the experiments SC and NG show mostly non-significant differences. Hence, it

could be stated, that the volcanic impact has a strong influence on the temperatures of the DM on global scales, whereas the lack in solar variability (SC) and the constant $CO_2$ concentrations (NG) do not have a significant impact on the temperatures, except in the case of some regional phenomena. However, the volcanic influence over the extratropical latitudes, especially over the Northern Hemisphere, seems not to be able to exert a significant influence on the temperatures (cf. Fig. 5.8a). This phenomenon is likely to be due to the high interannual variability caused by the interplay between the atmospheric and oceanic circulation.

As already seen in Fig. 5.1 the first half of the DM does not show significant temperature differences between the different experiments. The temperature evolution of the NV experiment and the volcanic-forced experiments essentially coincide. In order to account for the split-up of the DM in terms of temperatures, in the following analysis only the second half of the DM (1810–1830) is analyzed.
Fig. 5.9 shows the temperature difference between the mean of the ensemble experiments and the HIST simulation for the second half of the DM. In general the situation is similar to Fig. 5.8 concerning the temperature patterns, especially for the SC and NG experiments. However, the NV experiment shows even more pronounced temperature differences for both the spatial extent and the amount of temperature difference. Hence, large parts of South America, Africa, central Eurasia, the North Atlantic and tropical Pacific, as well as the north polar regions, show significant different temperatures. As already noted, the temperature patterns for the SC and NG experiments are similar to Fig. 5.8b and Fig. 5.8c but with reduced amplitudes. Thus it can be inferred that during the second half of the DM the experiments SC and NG are closer to the HIST simulation, whereas the NV experiment deviates more markedly. Another feature, which can be deduced from Fig. 5.8c, is the – on large scales – non-significant influence of the strong increase of the $CO_2$ concentrations at the beginning of the 19th century. This effect is possibly masked by the large volcanic impacts during that period.

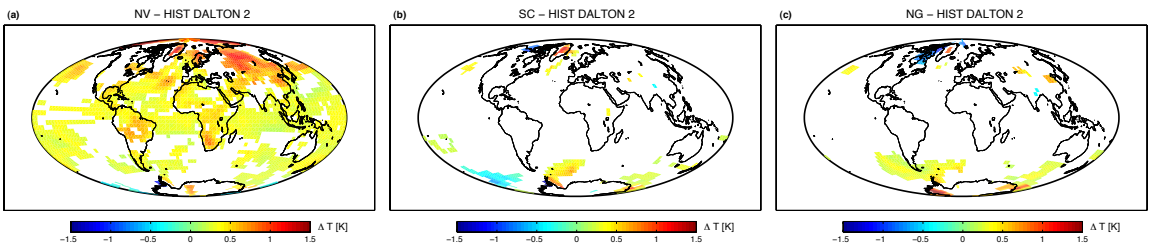


**Figure 5.9:** Temperature difference between the mean of the ensembles NV(a), SC(b), NG(c) and the HIST simulation for the second half of the DM (1810–1830). Only values significant at the 95% level of significance are shown accounting for serial correlated data. Note the even more pronounced influence of the volcanoes within (a).

### 5.1.4 Temperature variability within the NG ensembles

Most of the previous analysis investigated the evolution of the ensemble mean temperatures of the different experiments. As an example, within this section, the intra-ensemble temperature variability will be analyzed for the NG experiment. A virtue of the NG experiment is the variable volcanic forcing possibly allowing for the detection of volcanic imprints within the temperature evolution.
Fig. 5.10 shows the evolution of the yearly mean global temperatures for the 3 simulations of the NG experiment. The temperature evolution of all 3 ensembles is quite similar with a pronounced temperature depression during the second half of the DM and a slight temperature increase within the first half of the 20th century. Thus, on a global scale, the different initial atmospheric and oceanic conditions seem not to influence the temperature evolution to a high degree. Accordingly, changes within the external forcing seem to be the dominant factor for the evolution of the global temperatures.

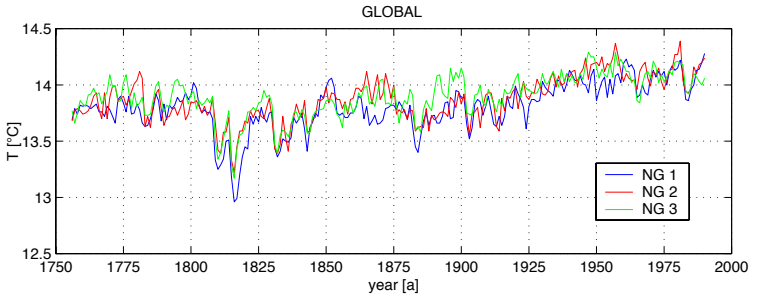


**Figure 5.10:** Yearly mean global temperatures within the NG experiment. Note the similar temperature evolution of the different ensemble simulations on the global scale.

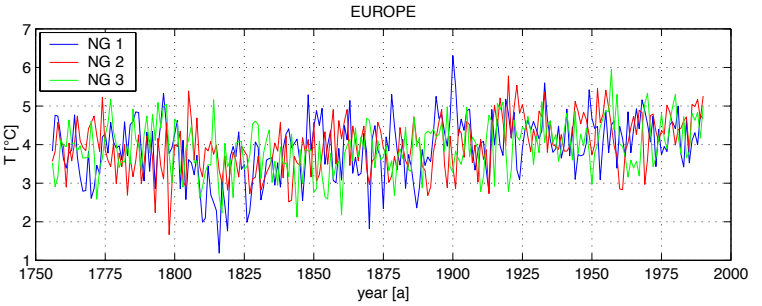


**Figure 5.11:** Yearly mean European temperatures within the NG experiment. Note the strong deviations among the ensemble simulations on this regional scale.

Another picture emerges when investigating regional temperatures. As an example, Fig. 5.11 shows the yearly mean European temperatures for the 3 NG ensembles (for geographical

location see Fig. 5.4). In contrast to the global mean temperatures, no clear agreement among the curves is evident. The volcanic impacts during the second half of the DM are not reflected for the NG2 and NG3 simulations. Only the NG1 simulation shows the volcanic impact. Furthermore, the temperature levels during the 20th century do not show a clear trend towards higher temperatures at the end of the 20th century. Due to the high interannual variability the temperature levels are only slightly increased when compared with the second half of the 18th century. The reasons for the deviating temperature evolution with respect to global temperatures may have different reasons. A selection of them will be discussed in the following paragraph.
The European region is located on the east coast of the North Atlantic. The horizontal resolution of the ECHAM4 model (T30) shows that nearly every land grid point is bordering an oceanic grid point (cf. Fig. 4.1). Accordingly, one reason for the deviations among the temperatures may be due to an oceanic phenomenon. For example, the northward heat transport can be different among the different simulations. Hence, an increased northward heat transport in one simulation can lead to higher European temperatures and vice versa. Another reason for the disagreement among the curves may be simply due to the natural climate variability which might also disguise the external (volcanic) forcing within the NG experiment.

In order to estimate the amount of difference among the members of the NG experiment, a *dissimilarity index* is introduced, so as to possibly assess the influence of the different initial conditions on the evolution of e.g. temperature. The dissimilarity index estimates the distance between the ensemble simulations at a given point in time. In this work, the dissimilarity index $D(t)$ takes the form of the standard deviation (cf. eq. 5.9) of the 3 ensemble simulations at each date $t$:

$$D(t) = \sqrt{\frac{1}{n}\sum_{i=1}^{n}(x_{i,t} - \bar{x}_t)^2} \tag{5.9}$$

Within eq. 5.9, $\bar{x}_t$ denotes the ensemble mean at each date $t$. Here, $n$ becomes 3 and $i$ runs from 1 to 235 (1756 to 1990). A shortcoming with this kind of distance measure in terms of standard deviation is the very small sample size $n$.
In the following the dissimilarity indices based on the global temperatures of Fig. 5.10 and the regional European temperatures of Fig. 5.11 are presented. Figure 5.12 shows the dissimilarity indices after equation 5.9 for the NG ensembles for the yearly mean global and European temperatures. The global dissimilarity index (Fig. 5.12a) shows mean temperature

dissimilarities in the order of 0.04 °C. The highest dissimilarities are evident at the end of the 19th century with a magnitude of 0.1 °C. Until the end of the simulations the index varies around the mean state, with the exception of the 1830s, 1840s and the 1970s. During these times the index shows a very low dissimilarity among the simulations.
Figure 5.12b shows the situation for the European temperatures. In this case the dissimilarity is 5 times larger with respect to the global temperatures. The curve shows a very incoherent picture and no clear statements can be made in terms of a reduction or an increase of the dissimilarity with the progress of time. Peak values are also more pronounced and differ up to 1 °C.

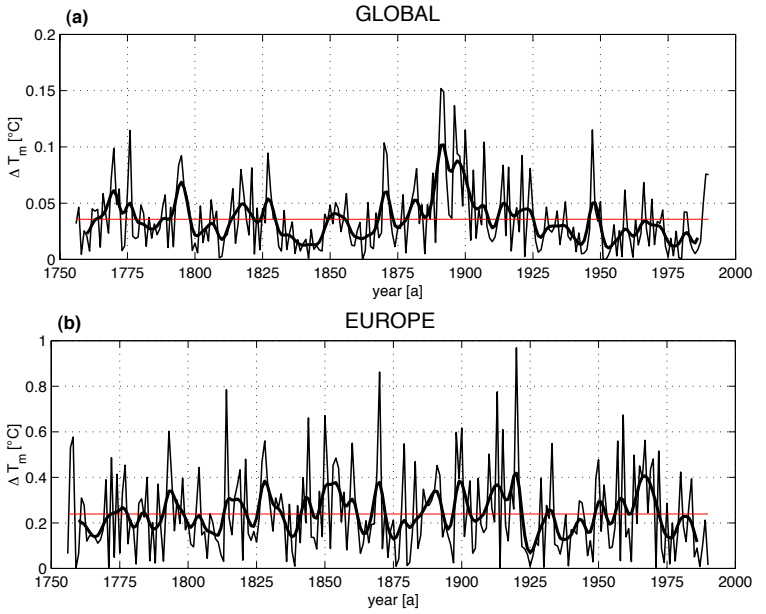


**Figure 5.12:** Dissimilarity index for the NG experiment after eq. 5.9 for the global mean temperatures (a) and the central European temperatures (b). The red line denoted the mean dissimilarity. Note the increased dissimilarity-levels for the central European temperatures ($\Delta T_m$ = mean temperature deviation).

A further feature which can be drawn from Fig. 5.12 is the information about the influence and persistence of the different initial oceanic and atmospheric conditions and/or the influence of the natural climate variability. Given the case that the initial conditions would have a strong impact on the (global or regional) temperatures, this influence should decrease with progress in time, as the ocean adapts more and more to the current external forcing. (It is assumed that the different initial atmospheric conditions virtually play no crucial role in the long-term behavior of the climate system.) This phenomenon should also be reflected within the dissimilarity index in a way that a negative trend within the curve should be seen. As this is not necessarily the case within both, the global and the regional temperature time

series, the initial conditions are possibly not affecting *these* two curves within Fig. 5.12 to a large degree. The situation could be different at other places (e.g. characterized by high autocorrelations) or for other variables.
Another interesting feature within Fig. 5.12a is the increased dissimilarity e.g. around 1900, 150 years after the start of the simulations. This further emphasizes the role of the natural climate variability. Another explanation for the increased dissimilarities at later dates may be due to oceanic phenomena related to the initial conditions but with a long term influence on climate e.g. in terms of the thermohaline circulation.

### 5.1.5 Comparison with reconstructions and observational data

The analysis in the previous sections was completely restricted to the model output. In the following section a comparative analysis between model experiments and empirical reconstructions will be undertaken. This will be done in terms of temperature on the hemispheric scale and for the North-eastern Atlantic-European area, respectively. This analysis will not focus on absolute temperatures but on temperature anomalies with respect to a certain period in order exclude the model bias.
Figure 5.13 shows the reconstructed Northern Hemisphere temperature anomalies with respect to the period 1900–1980 from Mann et al. (1999b), based on a multi-proxy dataset, Esper et al. (2002), based only on dendrochronologies and Jones et al. (1998), based on various normalized paleo-data of various type records together with the climate model experiments.
The combined results of the reconstructed time series show a negative temperature anomaly at the beginning of the 19th century which is possibly related to the DM. This anomaly is mostly pronounced within the Jones et al. (1998) reconstructions, also showing a temperature anomaly at the end of the DM possibly related to the volcanic eruptions during that times. The Esper et al. (2002) reconstructions also show a depression during the first half of the 19th century. This reconstruction in general shows only a weak interannual variability opposed to the other reconstructions, which is related to the reconstruction methodology applied. The Mann et al. (1999b) reconstructions also show a slight decrease in temperatures during the DM. In general Mann's curve exhibits a quite weak decadal climate variability. During the whole 20th century all reconstructions show a quite good agreement including a sustained positive temperature increase at the beginning of the 20th century.

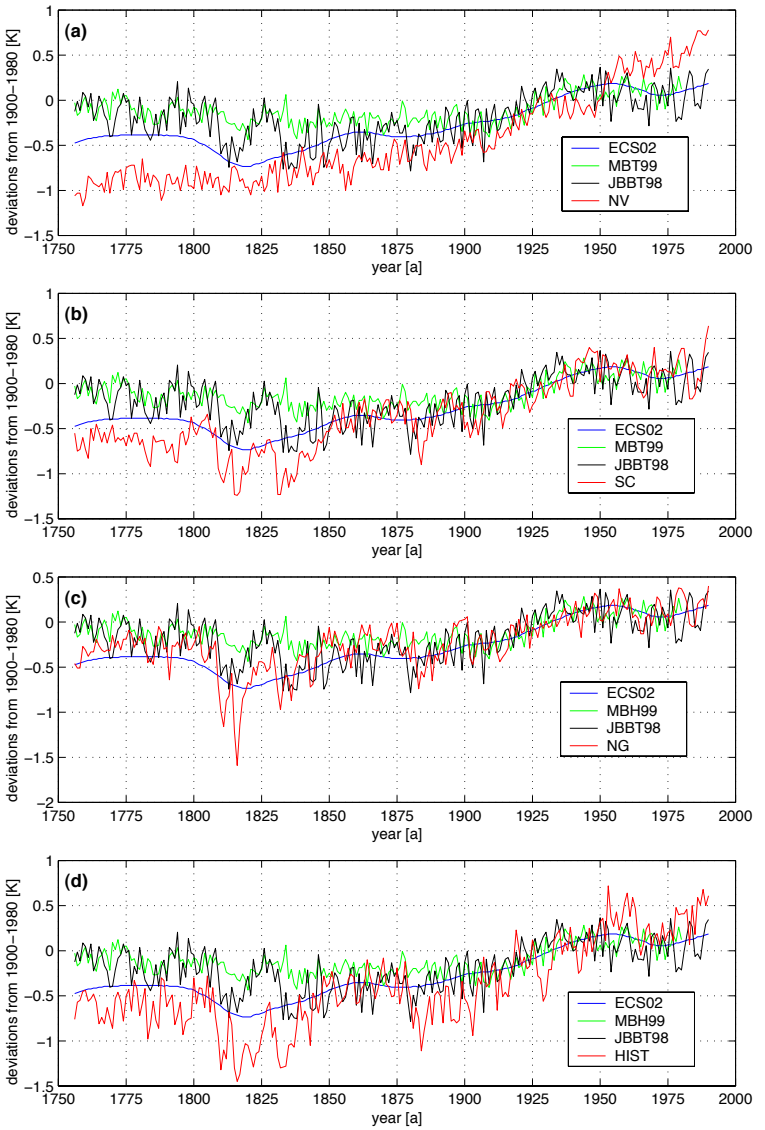


**Figure 5.13:** Northern hemispheric temperature deviations [K] form the period 1900–1980 for different reconstructions and the experiments NV(a), SC(b), NG(c) and HIST(d). Note the good agreement between the reconstructions based on climate proxies and the NG experiment. (ECS02 = Esper et al. 2002; MBT99 = Mann et al. 1999b; JBBT98 = Jones et al. 1998).

Within Figure 5.13a the red line shows the evolution of the Northern hemispheric temperatures with respect to the period 1900–1980 for the NV experiment. The temperature decrease within the reconstructions during the second half of the DM is not captured by this experiment. During the 2nd half of the 20th century temperatures exceed the reconstructions. The SC experiment (Figure 5.13b) also shows a bias toward too low temperatures that until 1850.

However, the temperature decrease during the second half of the DM and around 1830 is captured quite well. After 1850 the temperature evolution coincides quite well with the reconstructions. Also the volcanic impacts and the temperature increase during the first half of the 20th century are reflected within both the reconstructions and the experiment. The NG experiment (Figure 5.13c) coincides with the reconstructions over nearly the whole period. Only the volcanic impacts at the main part of the DM reflect a bias toward temperatures that are too low. This experiment shows even higher agreement with the reconstructions than the HIST experiment (Figure 5.13d), where all possible forcings are included. In the HIST experiment the temperatures, in general, show a negative bias until 1900, whereas the 2nd half of the 20th century shows a bias toward positive temperature anomalies. The increased interannual temperature variability is related to the only-one-member simulation of HIST experiment.
Thus, the experiment with solar and volcanic variable forcing, but with constant pre-industrial $CO_2$ concentrations, is – somewhat surprisingly – the best at reflecting the reconstructed temperatures from 1750 onwards, not only for the decadal variability but also for sub-decadal temperature variations.

There are several possibilities explaining these discrepancies: One might be due to the exaggerated influence of the $CO_2$ within the climate model in terms of feedback loops. A second reason might be due to the lack of industrial aerosols in the model simulations which also dampen the temperature trend possibly caused by greenhouse gases. On the other hand, model studies by Hegerl et al. (2003) by means of an energy balance model, assess the fingerprint of the industrial aerosols in the past as being of only minor importance on global scales. Furthermore, and likely the most important point, is the disregarding of the temperature trend of the period 1980–2000, the time when the temperature trend is mostly pronounced within the instrumental record. According to Houghton et al. (2001), during this period the temperature evolution cannot be explained only by natural climate forcing (solar and volcanic).

As initially mentioned, the representation of the volcanic forcing in the model is admittedly afflicted with a large uncertainty. The volcanic forcing could have been overestimated in these simulations, thus leading to an exaggerated volcanic influence in the DM. However, several considerations still support the implementation of the volcanic forcing as a reduction within the solar radiation. First, the simulated temperature drop after major volcanic eruptions agrees reasonably well with the available empirical evidence. Sachs and Graf (2001) and Rampino and Self (1982) indicate a drop in global temperature of approx. 0.8 °C after the Tambora eruption, whereas the present model results show a temperature decrease of 0.75 °C. For the Krakatoa eruption in 1883, the temperature drop was about

| *Experiment* | NV | SC | NG | HIST | JONES OBS |
|---|---|---|---|---|---|
| *lin. Trend 1900-1980* [°C/decade] | 0.09 | 0.06 | 0.05 | 0.08 | 0.05 |

**Table 5.1:** Northern hemispheric linear temperature trend 1900–1980 for the different experiments and the observations. The NG experiment is closest to instrumental observations during this period.

0.3 to 0.4 °C. Here the model simulates a drop in global temperatures which is approx. 0.6 °C. A second consideration is the clear temperature deviation in the NV experiment compared to the SC and NG experiments. The NV experiment barely shows any drop of global temperatures in the DM and therefore it seems to be quite incompatible with the empirical evidence. Another representation of the volcanic forcing, for instance a multiple of the forcing used here, would probably lead to a linear re-scaling of the volcanic influence on global temperatures, at least to a first approximation. This re-scaling would change the interpretation of the results only in the case that the volcanic forcing were really unrealistic. In view of the simulated temperature drop after the major eruptions, this does not seem to be the case.

As the reconstructed temperatures are not necessarily related to observed instrumental temperatures, Table 5.1 shows the Northern hemispheric linear temperature trend within the different experiments and the instrumental based observations from Jones et al. (1999b). In order to account for the missing values within the observed temperatures, only those grid points co-located with available observations have been used. According to Table 5.1, again there is some evidence that the temperature trend within the NG experiment is closest to observations. Especially the NV experiment without any volcanic influence has a temperature trend which is far too strong. The SC and HIST experiments also show higher temperature trends with respect to the observed trends.

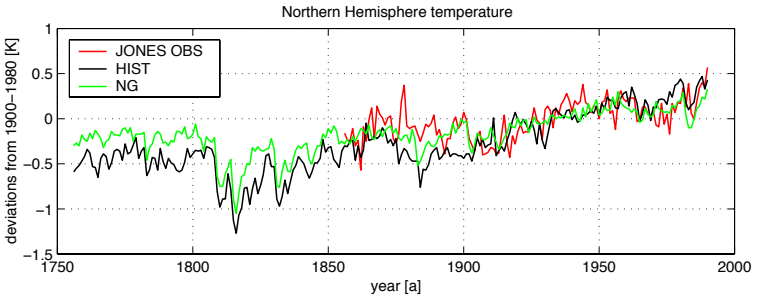


**Figure 5.14:** Northern hemispheric temperature deviations [°C] form the period 1900-1980 for the Jones et al. (1999b) observational data and the HIST and NG experiments. Note the coincidence of the curves during the 20th century but with a temperature trend within the HIST experiment which is too strong.

Additionally, Fig. 5.14 shows the temperature anomalies of the Jones et al. (1999b) Northern hemispheric observational data and the experiments NG and HIST with respect to the period 1900–1980. Accordingly, during the 20th century both experiments coincide with the observations. Just before 1900 some deviations among the curves are evident. However, there is also evidence within the time series that the temperature trend of the HIST experiment is more pronounced during the 20th century with respect to the Jones et al. (1999b) data and the NG experiment.

The next paragraph compares the modelled temperatures with reconstructed temperature data for the North-eastern Atlantic-European area from Luterbacher et al. 2004 (hereafter LUTER). Figure 5.15a shows the yearly temperature difference between the DM and the times prior (1755–1789) and after (1831–1900) for the reconstructions of LUTER. Additionally the HIST simulation is shown (Figure 5.15b). In order to account for the low resolution of the climate model, the high-resolution LUTER data have been interpolated upon the grid of the atmospheric part of the climate model. As the LUTER data do not include oceanic grid points they have also been excluded within the modelled data.

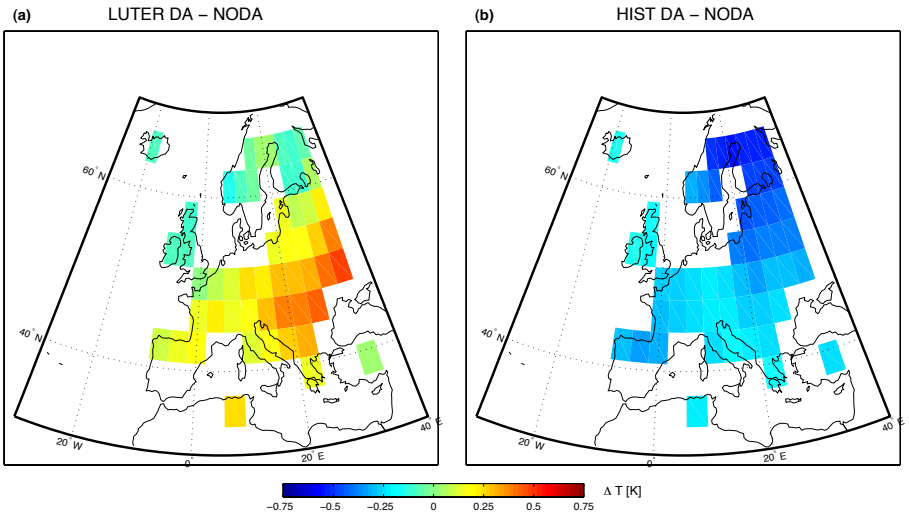


**Figure 5.15:** Yearly temperature difference between the DM and the times prior (1755–1789) and after (1831–1900) the DM for the reconstructed Luterbacher yearly data (a) and the HIST simulation (b). Note the strong discrepancies between model and reconstructions.

A priori the HIST simulation is supposed to reflect the real forcings of climate most adequately, and should be best suited for comparison with observations. Therefore Figure 5.15 shows the temperature difference between the DM and the times before (1755–1789) and after (1831–1900) for the reconstructed LUTER yearly data (a) and the HIST simulation

(b). As already shown within chapter 3, the LUTER reconstruction only shows slightly negative temperature anomalies for the north-western European area. The whole central and south-eastern parts of Europe are characterized by above normal temperatures with respect to the times before and after the DM. In contrast to the reconstructed data the HIST simulation mainly shows below normal temperatures over Europe, especially over the north-eastern parts, as it might be inferred from the external forcing. Accordingly, only the north-western European region shows reduced temperature in both the LUTER data and the climate model. Hence it is difficult to explain the huge differences between the observations and the simulations. For the Late Maunder Minimum (LMM) the temperature anomaly patterns between the LUTER data and the ECHO-G model seem to be quite similar for large parts of Europe (cf. Zorita et al. 2004).
Within the next two paragraphs some arguments are presented which might explain the differences between the reconstructions and the model output. The next paragraph puts emphasis on possible shortcomings of the climate model followed by the discussion of possible shortcomings concerning the empirical reconstructions

A reason that possibly accounts for the differences between the LUTER data and the model is the coarse resolution within the climate model. Müller (2003) has therefore numerically downscaled the large scale information of the HIST experiment for the LMM in order to get a better insight into the specific European climate during the times of the LMM. She concludes that for the regional climate simulation, the general circulation simulations by ECHO-G should exhibit certain circulation features, e.g. in terms of blocking frequencies as well as a minimum resolution. Furthermore, a better representation of marginal seas e.g. the Baltic sea within the general circulation model would be desirable in order to substantially improve the regional climate simulation.
In terms of the atmospheric circulation Müller (2003) investigated the blocking frequencies and intensities. The blocking-index (Tibaldi and Molteni 1990), which incorporates both the strength and frequency of blockings of the westerly circulation within the extratropics, seems to be especially important for the North-eastern Atlantic region. Within the framework of AMIP (Atmospheric Model Intercomparison Project) D'Andrea et al. (1998) analyze 15 atmospheric climate models with respect to the blocking features. Within this paper, the ECHAM4-model is analyzed with a T42 resolution. With this configuration the model performs quite well in terms of the blocking frequencies and strength. The calculations of Müller 2003 for the T30 resolution suggest a very poor representation of the blocking within the eastern North Atlantic. This shortcoming also influences the evolution of temperatures within this region, as the central European region is especially influenced by the allochthonous advection of air masses. The shortcomings of ECHO-G in terms of the atmospheric circulation for the European area are also discussed in Wagner (2000). He

concludes that the zonal circulation is too strong. This possibly prevents the establishment of certain circulation patterns, e.g. in terms of the Russian High in winter time.
Although the above mentioned arguments can explain some of the discrepancies between the climate reconstructions and the model results, the empirical climate reconstructions of LUTER must not necessarily reflect the real climate. The statistical model Luterbacher et al. (2004) uses for the reconstructions of temperatures is calibrated and validated for the climate of the 20th century. Thus, one basic assumption is that the European climate and the processes governing European climate have been constant in the past. One can argue that e.g. oceanic processes in terms of sea surface temperatures (SSTs) or sea ice concentration (SIC) in the Northeast Atlantic have been different in the past. This would possibly affect the reconstructions as the statistical model does not include information of changed oceanic conditions. Thus, if e.g. the Northeast Atlantic SSTs have been lower together with an increased SIC around Greenland, even a westerly circulation could not have advected the mild maritime air masses of modern times.

The following paragraph includes a comparison of the different simulations of the experiments and the reconstructions. This will possibly help to assess the amount of natural climate variability under changed initial conditions and put into perspective the discrepancies between the reconstructions and the reference simulation. Figures 5.16 –5.18 show the temperature differences between the DM and the times prior and after for the 3 ensemble simulations of the different experiments (column 1–3) and the mean of the experiments (column 4). The NV experiment (Fig. 5.16) shows quite different temperature patterns with respect to the different ensembles. Accordingly, the NV1 simulation shows increased temperatures over north-eastern Europe and decreased temperatures over central and south-eastern Europe. The NV2 simulation shows a temperature pattern similar in some respects to the reconstruction, with slightly decreased temperatures over north-western Europe and increased temperatures over eastern Europe. The NV3 simulation shows a temperature pattern which is close to the HIST simulation with mainly negative temperature anomalies over central and eastern Europe, especially in the north-eastern part. Due to the averaging, the mean of the NV ensembles only show very weak temperature anomalies, as the different temperature patterns within the experiment balance each other.

The results obtained for the SC experiments (Fig. 5.17) are quite similar for all simulations. In general there is a moderate cooling over western Europe and a more pronounced cooling over north-eastern (SC2) and south-eastern Europe (SC3). The mean of the ensembles reflects the general temperature pattern with a moderate cooling over western Europe and a more pronounced cooling over eastern Europe.
For the NG simulations (Fig. 5.18) the situation is again somewhat ambiguous. The NG1 simulation shows a strong cooling for the entire Europe, whereas the NG2 simulation shows

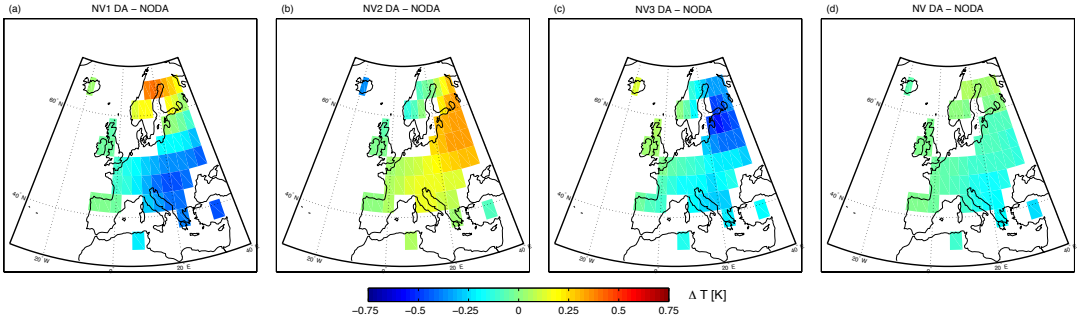


**Figure 5.16:** Yearly temperature difference between the DM and the times prior (1755–1789) and after (1831–1900) the DM for the single member simulations (a-c) and the mean (d) of the NV experiment. Note the NV2 simulation showing positive temperature anomalies over eastern Europe during the DM.

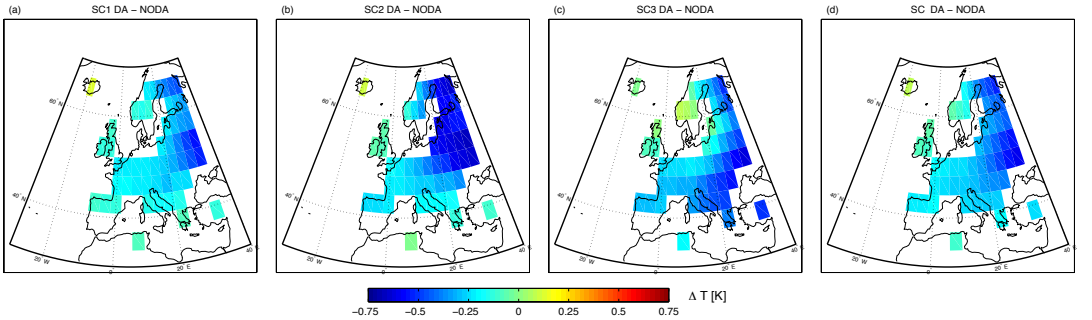


**Figure 5.17:** Same as Fig. 5.16 except for the SC experiment. Opposed to the NV and NG simulations the SC simulations show overall reduced temperatures during the DM.

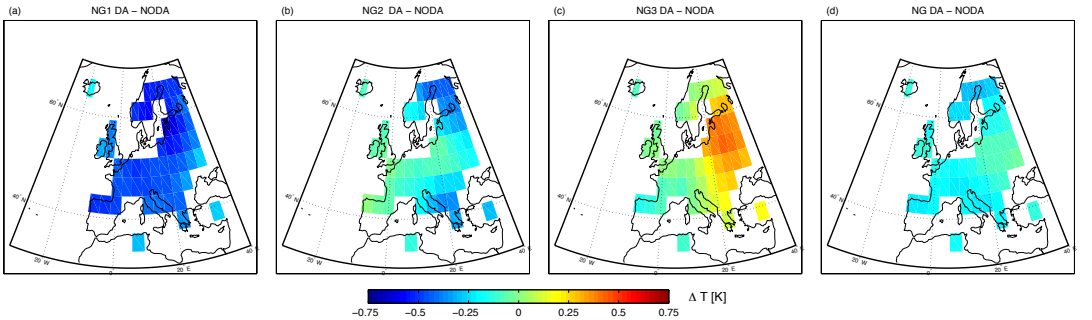


**Figure 5.18:** Same as Fig. 5.16 except for the NG experiment. Note the NG3 simulation showing positive temperature anomalies during the DM over eastern Europe.

only a moderate cooling over north and south-eastern Europe. Within the NG3 simulation a complete different temperature pattern with positive temperature anomalies over eastern Europe and only slightly decreased temperature anomalies over western Europe is evident. The mean of the ensembles again shows a temperature pattern with only small negative tem-

perature anomalies over large parts of Europe.
Thus, the temperature patterns of the NV2 and NG3 simulations demonstrate that within a period of globally reduced temperatures, regional temperatures not might be only moderately reduced, but can even show inverse temperature signals compared to global or hemispheric temperatures. The results for the NG3 experiment are especially interesting in this respect, as the external forcing is the most similar to the real world, and, as it has been shown, the increase in $CO_2$ concentrations does not have any significant impact on the (European) temperatures during the DM.
This result emphasizes, on the one hand, the need for ensemble simulations in order to assess the amount of internal climate variability, and, on the other hand, puts into perspective the shortcomings of the model mentioned above in terms of the representation of circulation features and spatial resolution.
Given the case that only one simulation per experiment had been carried out, one could have easily disqualified the model as being unable to reproduce the past climate on this spatial scale. However, one should bear in mind that the observed past climate is only one realization under myriads of possibilities. Accordingly, when only carrying out one simulation the probability matching the exact trajectory of the past climate is very low. A factor that might be even more important is the unraveling of a variety of trajectories of how climate, especially on regional scales, can look like under the same external forcings. Accordingly, it seems of at least minor importance if the model is really able to reproduce all kinds of peculiarities on the regional scale. In this respect, a highly sophisticated model need not necessarily take *the* trajectory that the real climate took in the past or will take in the future.

### 5.1.6 Summary

Within the previous chapter the temperature evolution of the different experiments was analyzed in terms of:
**1.** the evolution on global and hemispheric scales
**2.** the spatial temperature differences on global scales
**3.** the temperature evolution on hemispheric and regional scales within the NG experiment
**4.** the relation with reconstructions and instrumental data.

Within the analyses carried out under **1.** it was shown that the volcanoes have a significant influence on the global and hemispheric temperatures in terms of a reduction of temperature. The NV experiment shows no clear thermal DM at all, but here the highest temperatures are found at the end of the 20th century. The SC experiment reflects a pronounced temperature

depression during the 2nd half of the DM due to the volcanic influence. Despite the lack of solar variability it greatly resembles the other experiments in terms of temperature variability. The NG experiment also shows pronounced reduced temperatures during the 2nd half of the DM. The temperature increase during the 20th century is quite moderate. This is possibly due to the moderate increase in solar radiation and the $CH_4$ increase. Thus, in terms of the DM, significant differences among the experiments do not appear until the 2nd half of the DM, when the volcanic influence is most pronounced. During the first half of the DM the different experiments coincide quite well and the changes within the external forcing are not apparent. Quite strong discrepancies to this general temperature evolution are evident in the extratropical Southern Hemisphere. Here the impact of the different external forcing becomes unclear. This is possibly due to the large oceanic influence.

Under **2.** the spatial temperature differences between the different experiments and the HIST simulation have been analyzed. Except for the NV experiment most regions of the SC and NG experiments show non-significant temperature anomalies with respect to the HIST experiment, except some oceanic high latitude Southern hemispheric regions. For the NV experiment large parts of the globe show significant increases in temperatures due to the lack of volcanic influence. However, large parts of the continental mid and high latitudes mainly do not show significant temperature differences. This might be due to the large interannual temperature variability. Within the NV experiment the areas of positive temperature differences are larger when only the 2nd part of the DM is taken into account. This emphasizes again the importance of the volcanism during this period. Hence, the volcanoes seem to play a significant role for the formation of a thermal DM on global and hemispheric scales, especially within its 2nd half. The solar forcing (SC) and the $CO_2$ forcing (NG) seem only to play a minor role in terms of temperatures during the DM.

The analysis carried out under **3.** investigates the temperature evolution for the ensemble simulations of the NG experiment. While the different mean global temperatures coincide quite well, the European temperatures show a quite different picture with a strongly increased interannual variability. Within some periods even different temperature levels can be seen. Thus, on a global scale the different simulations converge, which is possibly due to the external forcing, whereas on the European regional scale the different simulations diverge, which might be due to a different evolution within the atmospheric and/or oceanic circulation.

Within the analyses carried out under **4.**, the temperature trend of the different experiments has been compared to instrumental data by Jones et al. (1999b). Accordingly, the NG experiment is closest to instrumental observations in terms of temperature trends in the period 1900–1980. All other experiments over-estimate the observed temperature trend. Furthermore, the Northern Hemisphere temperature time series have been compared to

different reconstructions. Again, the NG experiment seems to agree most favorably with the reconstructions. However, one should be careful in concluding that the NG experiment, forced with constant pre-industrial $CO_2$ concentrations, best resembles the past climate evolution of the Northern Hemisphere since a variety of differently arranged external forcings may lead to a similar temperature evolution. Additionally, the modelled European temperature patterns of the DM have been compared to the Luterbacher et al. (2004) reconstructions. Surprisingly, these reconstructions indicate positive temperature anomalies over much of Europe. Only the northern parts show negative temperature anomalies. Opposed to that, the main part of the model simulations, including the HIST simulation, shows pronounced reduced temperatures over Europe. This does not hold true for NV2 and NG3 simulation. They also show increased temperatures during the DM over much of Europe. This clearly demonstrates i) the virtues of the ensemble approach ii) the importance of natural climate variability under the same forcing and, iii) possible impacts of the oceanic influences on the European temperatures.

## 5.2 The extratropical atmospheric circulation

The following sections discuss the leading modes of the extratropical atmospheric circulation, namely the Arctic (AO) and Antarctic (AAO) Oscillations. Due to the limited space not the full variety of different atmospheric circulation modes has been analyzed. In the following the concepts of the AO and AAO are briefly introduced followed by the presentation of their evolution within the different experiments and their possible connection to the external forcing. The last section puts emphasis on possible relations between the atmospheric circulation and the regional temperature evolution.

The AO was originally introduced by Thompson and Wallace (1998), defining the AO pattern as the first empirical orthogonal function (EOF) of the winter time (DJF) geopotential height field and the corresponding principal component (PC) as the AO index. It characterizes the intensity of the westerlies within the circumpolar vortex over the high-mid latitudes. However, Ambaum et al. (2001) doubt the physical mechanisms the AO suggests. Their results indicate that the North Atlantic Oscillation (NAO) paradigm is possibly more physically relevant and robust for Northern Hemisphere SLP variability than the AO paradigm. However, they admit that this does not necessarily disqualify large parts of the physical mechanisms related with the AO to explain the existence of the NAO. Therefore the NAO may be viewed as the regional expression of the AO. Accordingly, the AO may be thought as the leading winter time *hemispheric* low frequency mode of SLP variability, while the NAO is the leading mode in the *North Atlantic* sector (Marshall et al. 2001). Furthermore the correlation between the winter AO and NAO indices is very strong ($r \sim 0.95$).

The AAO, the Southern hemispheric counterpart of the AO, introduced by Thompson and Wallace (2000) as the Southern Annular Mode, has the same (statistical) definition as the AO. In terms of the AAO several investigations have been undertaken at various atmospheric levels, for example SLP (Gong and Wang 1998), the geopotential height 500 (Mo and White 1985; Rogers and van Loon 1982) as well as for the geopotential height 850 (Thompson and Wallace 2000). The spatial structure of the AAO is more zonal symmetric with respect to the AO. The reasons are mainly due to the lack of large continental areas on the Southern Hemisphere having a strong impact on the high-mid latitudes circulation. Furthermore, over the Antarctic continent, temperatures are much lower than over the North Pole. This leads to an increased mean meridional upper tropospheric temperature gradient inducing a stronger atmospheric vortex-like circulation.

Before analyzing the AO- and AAO indices within the different experiments the concept of the empirical orthogonal functions (EOFs) is briefly described.
The purpose of the EOF analysis is twofold, namely to reduce the amount of information of a random vector $\mathbf{X} = (\mathbf{X_1}, \ldots, \mathbf{X_J})^{\mathbf{T}}$ , with J components from a high- to a low dimensional subspace, and thus to separate the signal form the noise (von Storch and Frankignoul 1998; Müller and von Storch 2003):

$$\vec{\mathbf{X}} = \vec{\mathbf{X}}^s(t) + \vec{\mathbf{X}}^n(t) \tag{5.10}$$

To reduce information one first has to calculate the covariance matrix $C_x$:

$$C_x = \begin{pmatrix} VAR(\mathbf{X_1}) & COV(\mathbf{X_1}, \mathbf{X_2}) & \ldots & COV(\mathbf{X_1}, \mathbf{X_J}) \\ COV(\mathbf{X_2}, \mathbf{X_1}) & VAR(\mathbf{X_2}) & \ldots & COV(\mathbf{X_2}, \mathbf{X_J}) \\ \vdots & \vdots & \vdots & \vdots \\ COV(\mathbf{X_J}, \mathbf{X_1}) & COV(\mathbf{X_J}, \mathbf{X_2}) & \ldots & VAR(\mathbf{X_J}) \end{pmatrix} \tag{5.11}$$

yielding a linear equation system :

$$C\vec{e} = \lambda\vec{e} \tag{5.12}$$

The matrix of eq. 5.11 describes the co-variability of all of its components. The features of $C_x$ are that it is semi-definite and that all its eigenvalues $\lambda_j (j = 1, \ldots, J)$ are real and non-negative. The eigenvectors $\vec{e^j}$ form an orthogonal basis. That means the eigenvectors $\vec{e^j}$ are uncorrelated:

$$\vec{e^j}^T \cdot \vec{e^k} = 0 \mid j \neq k \tag{5.13}$$

After having calculated the eigenvectors $\vec{e^j}$ and eigenvalues $\lambda_j$ one can re-write the random variable $\vec{\mathbf{X}}$:

$$\vec{\mathbf{X}} = \sum_{\mathbf{j=1}}^{\mathbf{J}} \mathbf{c_j}\vec{\mathbf{e}}^{\mathbf{j}} \qquad \mathbf{c_j} = \vec{\mathbf{X}}^{\mathbf{T}} \cdot \vec{\mathbf{e}}^{\mathbf{j}} \tag{5.14}$$

According to eq. 5.14 this is only a coordinate transformation. The state of the system is given by the components $\mathbf{X_j}$ or by the coefficients $c_j$. The vectors $\vec{e^j}$ are called *empirical*

*orthogonal functions*, the coefficients $c_j$ *principal components*. Thus, performing an EOF analysis does not tell anything more about the system than the original data, it is only another, but quite comfortable way, of representing the information of a field. Hence, within the first few EOFs the main amount of variability of $\vec{\mathbf{X}}$ is represented.
The units of the original anomaly fields can be carried by both the EOFs or the PCs. This depends on the so called normalization of the EOFs. In the following sections the EOF patterns are re-normalized according to

$$\vec{e}^{j^+} = \sqrt{\lambda_j}\vec{e}^j \tag{5.15}$$

and

$$c_j^+ = \frac{1}{\sqrt{\lambda_j}}c_j \tag{5.16}$$

whereas $Var(c_j^+) = 1$. In the case of the re-normalized EOFs, the pattern carry the units of $\vec{\mathbf{X}}$ and $\vec{e}^{j^+}$ represents a typical anomaly pattern when $c_j^+$ becomes $\pm 1$ (cf. von Storch and Zwiers 1999).
One problem related to EOFs is that they are not necessarily related to physical processes. Usually only the first EOF, and sometimes the second, can exhibit physically consistent processes. Due to the construction of the EOF in terms of orthogonality the higher indexed EOF often do not show physical processes. This is related to the fact that the processes in the real world are not orthogonal. Dommenget and Latif (2002) demonstrate, that from an artificial example, patterns derived from EOF analysis can sometimes be misleading and be associated with very little climate physics. This becomes especially important when EOF-patterns indicate dipole structures. One way to prove the real bipolarity of the patterns is to isolate one of the maximum values within the dipoles and to calculate the one-point correlation map for the original data field. If the dipole is still evident within the one-point correlation map one can be more confident in the real existence of the dipole structure suggested by the EOF pattern.

### 5.2.1 The Arctic Oscillation (AO)

The Arctic Oscillation (AO) has already be defined in the previous section. The Atlantic counterpart, the North Atlantic Oscillation (NAO), has the same statistical definition as the AO in terms of the leading EOF of the winter time SLP-fields. (Although the original definition of the AO by Thompson and Wallace (1998) is related to the geopotential height fields, the analysis with SLP fields yields very similar results.)

Both modes have gained a lot of importance, as they are possibly influenced by anthropogenic climate change. A change within the intensity and structure of the AO may result in a change of weather patterns e.g. the intensity and pathway of storm tracks within the high-mid latitudes, a change of sea ice and also changes within the spring time Arctic column ozone. Most recent climate models suggest that the AO becomes stronger as a response to greenhouse gases and therefore e.g. Northern hemispheric winter temperatures increase, whereas the Arctic sea ice decreases (Gillett et al. 2002; Shindell et al. 2001a). The last two issues are already evident within the observations. However, Zorita and González-Rouco (2000) conclude, in their analysis with two different climate models, that there are disagreements between different climate models concerning the evolution of the AO for the future.

For the past, especially the LMM, there have been investigations on the intensity of the extratropical westerlies in terms of the AO and NAO as a response to (different) external forcings by Zorita et al. (2004) with the fully coupled atmosphere ocean general circulation model ECHO-G and by Shindell et al. (2001a) with the stratosphere resolving climate model GISS. Zorita et al. (2004) hypothesize that the intensity of the NAO is split into two phases during a period with reduced solar insolation. In the initial phase of the solar minimum the NAO weakens, leading to a reduced advection of maritime air on the European continent. During the second part of the solar minimum the NAO tends towards higher intensities, leading to an increased advection of maritime air over Europe. Further results of this study emphasize the coupling between ocean and atmosphere. The authors propose a mechanism, where the weakening of the Western Boundary currents increases the meridional temperature gradients. This could possibly intensify the atmospheric zonal circulation again. Shindell et al. (2001a) draw attention to the connection between the AO and processes which are related to the stratospheric dynamics. They find a reduced AO/NAO for the LMM and suggest the following mechanism: A cooling of tropical and subtropical SSTs leads to a cooling of the tropical and subtropical upper troposphere due to the reduction of moist convective processes. This results in an weakened latitudinal temperature gradient at around 100 to 200 mb. This reduced temperature gradient leads to decreasing lower stratospheric westerly winds, which fail to refract upward-propagating tropospheric planetary waves towards the equator. The resulting decrease in angular momentum transport to high latitudes and the decrease within the tropospheric westerlies correspond to a low AO/NAO index.

Despite the lack of a fully resolved stratosphere, the reduced upper tropospheric temperature gradients are also evident within the model study of Zorita et al. (2004), possibly leading to the same dynamic processes described by Shindell et al. (2001a). Opposed to Zorita et al. (2004), the model Shindell et al. (2001a) uses lacks an interactive atmosphere-ocean coupling. Hence, the suggested mechanism related to the re-enforcing of the zonal circulation due to oceanic processes is missing.

Within the following section the evolution of the winter time AO for the different experiments will be presented. Figure 5.19 displays the winter time A0 pattern for the HIST experiment. It shows a pressure seesaw between the subpolar and subtropical regions controlling the intensity of the extratropical westerlies. This seesaw is especially pronounced over the oceanic regions. Within the North Atlantic, the centers of action of the Icelandic low and Azores high are reflected. This mode explains 27% of the interannual winter time SLP variance.

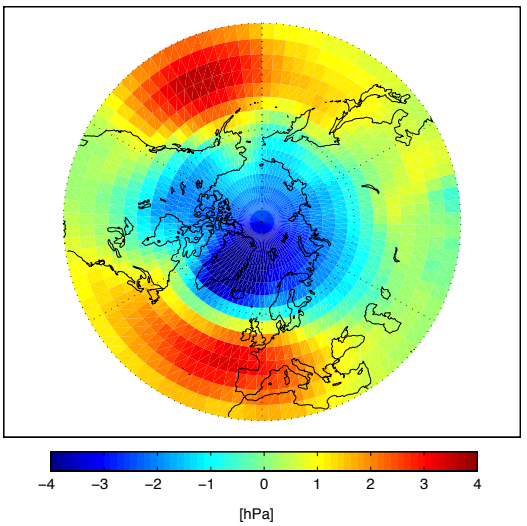


**Figure 5.19:** Arctic Oscillation pattern for the winter season of the HIST simulation. Note the pressure seesaw between subpolar and subtropical latitudes controlling the intensity of the extratropical westerlies.

Figure 5.20a-d shows the evolution of the corresponding winter AO indices for the ensemble mean of the different experiments. The displayed AO indices are not the principal component of the respective experiment. Here the A0 pattern of Fig. 5.19 was projected onto the respective SLP fields. Eventually anomalies have been calculated with respect to the mean of the reference simulation in order to allow for a proper comparison among the different experiments. Hence, positive values of the indices indicate an increased intensity of the westerlies with respect to the reference simulation HIST and vice versa.

Within the NV experiment the period to 1925 is characterized by negative values. Especially the main period of the DM shows a series of negative AO indices. Opposed to that, the period after 1925 shows a strong increase of positive AO indices. This positive culmination is interrupted within the 1970s. This suggests that the external (solar) forcing could have some influence on the low frequency variability, whereas the high frequency variability cannot be explained by the solar forcing. The level of the positive values during

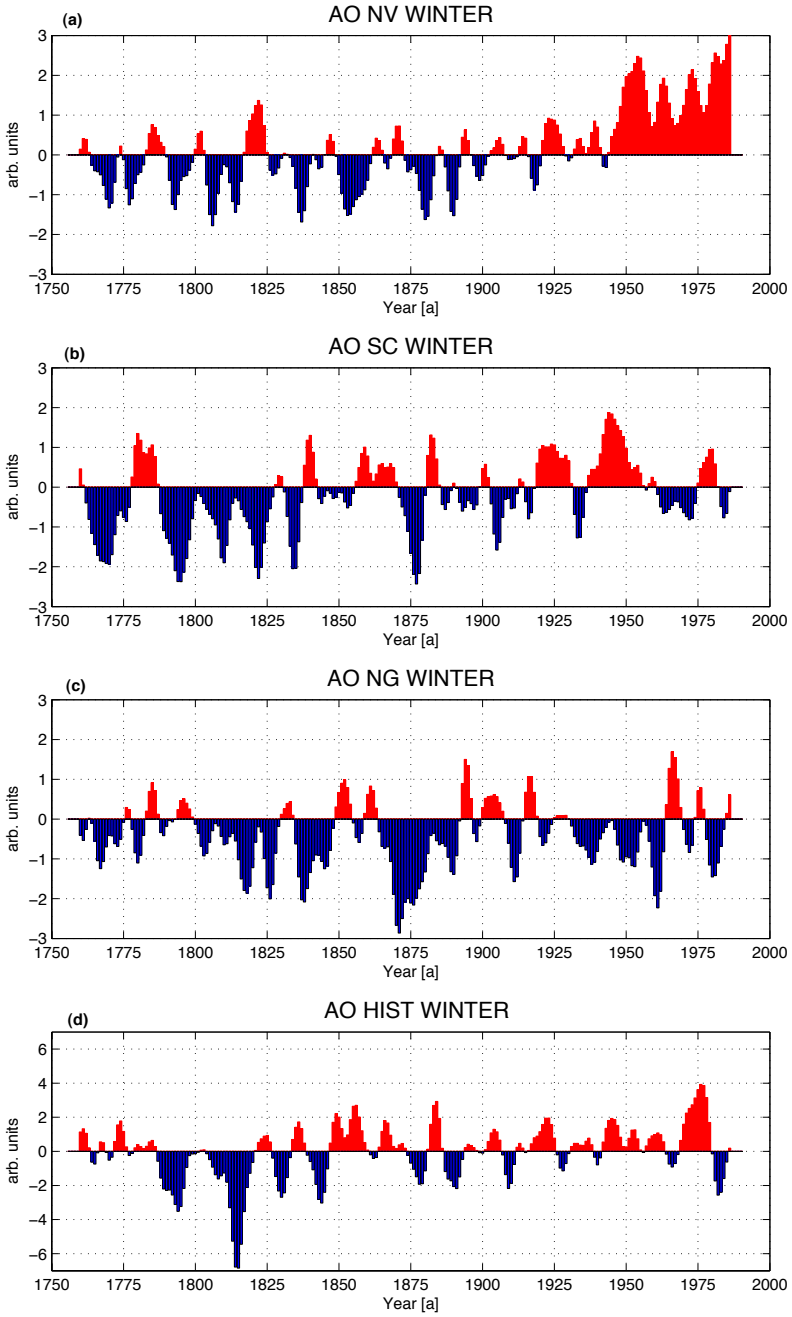


**Figure 5.20:** Winter time Arctic Oscillation index for the NV(a), SC(b), and NG(c) experiments and the HIST simulation (d). The time series have been filtered with a 10-years Gaussian low pass filter. Note the prevailing negative state of the winter time AO during the DM within the different experiments (The zero lines correspond to the mean value of the HIST experiment).

the 20th century seems to be mainly influenced by the greenhouse gas increase, whereas the decrease during the 1960s might be due to the decrease in solar radiation.
The evolution of the AO within the SC experiment also shows periods with prevailing negative AO indices until 1910. The DM is characterized by negative state of the AO. After 1910 there is evidence of a positive state of the AO, which reduces within the 2nd half of the 20th century.
The NG experiment shows a quite different picture with respect to the NV, SC and HIST experiments concerning the state of the AO during the pre-industrial period and during the late 19th and 20th century. During the first half of the DM a positive state of the AO is evident. It is only after large volcanic impacts that a series of negative indices can be seen. The 20th century shows a balanced picture of positive and negative AO periods and no clear trend as e.g. within the NV and HIST experiments can be figured out. The (single member) HIST experiment shows also a more pronounced negative state of the AO during the DM, whereas the 20th century is mainly characterized by positive AO states.
As already mentioned there are some indications of a possible relation between the external solar forcing and the AO. For this reason the following paragraph investigates by means of correlation analysis on possible links between the external solar forcing and the winter time NAO.

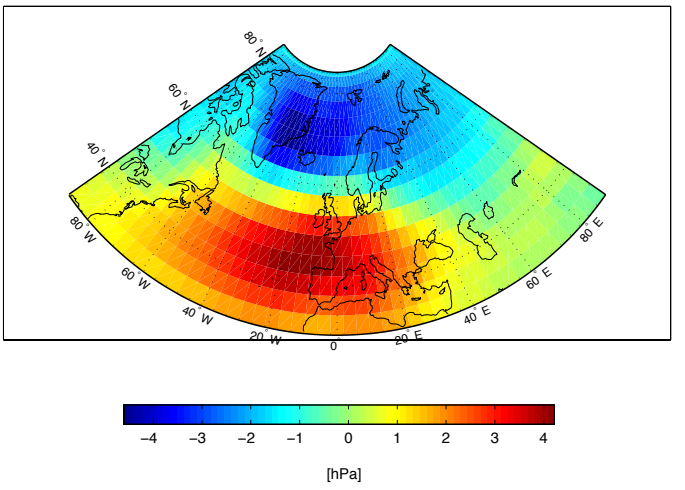


**Figure 5.21:** Winter NAO pattern over the North Atlantic region for the HIST simulation. The pressure seesaw between the subpolar Icelandic low and subtropical Azores high controls the intensity of the westerlies.

Fig. 5.21 shows the winter NAO pattern for the HIST experiment. The NAO paradigm was chosen here in favor of the AO paradigm because there is more observational evidence for the NAO paradigm. The NAO pattern shows a pressure seesaw between the subpolar

| *r(NAO,SF)* | NV | NG | HIST |
|---|---|---|---|
| **1** | 0 (0.21) [0.38*] | 0 (0) [0.14] | 0.1 (0.26) [0.6*] |
| **2** | 0 (0.17) [0.28] | 0 (0) [-0.24] | |
| **3** | 0.12 (0.26) [0.49*] | 0 (0.1) [0.26] | |
| **Mean** | 0.16 (0.37*) [0.55*] | 0 (0) [0] | |

**Table 5.2:** Correlation between the winter time NAO indices and the external solar forcing (SF) of the NV, NG and HIST experiments; unfiltered (10-year Gauss) [30-year Gauss]. The time series have been detrended prior to the analysis. The asterisk denotes significance at the 90% level of significance. Note the high correlations at multi-decadal time scales of the $CO_2$ forced experiments opposed to the zero correlation of the NG experiment.

Icelandic low and the subtropical Azores high, which control the intensity of the westerlies over the Atlantic and the adjacent western parts of the European continent. This pattern explains 37% of the interannual SLP variability within the North Atlantic sector. When comparing the pattern of Fig. 5.21 with the AO pattern within Fig. 5.19 the patterns are very similar within the Atlantic region. As already mentioned the same is true for their indices.
Table 5.2 shows the correlation between the external *solar* forcing and the winter time NAO indices of the different experiments. Accordingly, the highest correlations can be seen for the NV experiment, especially when the time series is filtered with a Gaussian low pass filter. This result suggests that 30% of the ensemble mean winter NAO in the NV experiment can be explained by the external solar forcing. However, the high serial correlation of the external solar forcing reduces the amount of degrees of freedom from 235 to 24 (unfiltered), 22 (10-year Gauss filter) and 19 (30-year Gauss filter).
For the single NG simulations, as well as for their mean, there is virtually no correlation between the external forcing and the NAO index. Within the NG2 simulation there is even a negative (but not significant) correlation between the NAO and the solar forcing. For the HIST experiment again some quite high correlations are found for the low frequencies. This is somewhat surprisingly, as the NG experiment, where solar and volcanic forcing are equal to the HIST experiment, does not show any correlations. Accordingly, for the NV and HIST experiment, some evidence is given for an influence of the external forcing on the winter time NAO in a sense that a reduced solar insolation favors a reduced westerly circulation and vice versa. The NG simulations, which are very close to the HIST simulation, do not show any correlations with the solar forcing, even on a decadal and multi-decadal scales. Thus, there is strong evidence that the correlations between the winter time NAO and the external solar forcing are strongly influenced by the increase of $CO_2$. However, calculating the NAO on a yearly basis (which is quite untypical), yields different results in the NG experiment. Here the correlations between the yearly NAO and the solar forcing show significant correlations on a multi-decadal scale. This phenomenon might be related to the fact that the winter time NAO does not necessarily reflect the variability of the annual NAO.

| | LUTERBACHER | JONES |
|---|---|---|
| **r(NAO,SF)** | 0 (-0.27) [-0.42*] | 0 (-0.29) [-0.46*] |

**Table 5.3:** Correlation of the winter NAO indices from Luterbacher et al. (2002b) and Jones et al. (1999a) with the solar forcing (SF); unfiltered,(10),[30]-year Gauss. All time series have been detrended before the correlations analysis. The asterisk denotes significance at the 90% level of significance. Note the negative correlations obtained for the winter time NAO index.

In order to test whether the model results have something to do with processes in the real climate, the correlation analysis between the winter time NAO and the external solar forcing has been carried out for reconstructions by Luterbacher et al. (2002b) and instrumental observations by Jones et al. (2001a) (cf. Figure 5.22). In general both curves show a similar evolution of the NAO. Within the period 1825 until 1925 there is evidence for a preferred positive state of the NAO with the exception of the period 1875–1900. During the 1950s and 1960s a pronounced negative state of the NAO can be seen. After 1975 there is some evidence for a positive trend within the NAO which is continued in the 1990s (not shown). Table 5.3 shows the results of the correlation analysis between the solar forcing and the winter time NAO for the reconstructions and observations. Surprisingly, the correlations show a negative sign, especially on the multi-decadal basis, indicating that a reduced solar forcing favors positive winter time NAO and vice versa. This result clearly is at odds with the results obtained from most simulations. However, argument putting this results into perspective are as follows: First, as already mentioned, there is a variety of different reconstructions of the NAO possibly leading to different results on the multi-decadal basis. Second, the indices used are possibly too short to obtain trustworthy reliable results at multi-decadal scales. Third, it has been noted that a positive correlation between the NAO index and the external solar forcing in the model exists for the yearly NAO index rather than for the winter time NAO index.

As noted above, the positive correlations between the external solar forcing and the winter time NAO idnices within the NV and HIST experiments are possibly due to the increase of $CO_2$. For the NG experiment there are no (significant) correlations. However, apart from that the NG experiment again shows the most realistic evolution within the winter NAO indices with respect to observations or reconstructions concerning the variability of the NAO index within the 20th century. Again, it should be noted here explicitly that this does not necessarily imply that the forcing within the NG experiment is the only one explaining the past climate by means of a lack of a $CO_2$ increase. There are possibly a huge amount of different combinations concerning the external forcing which lead to the observed historical climate evolution (cf. also Bertrand and van Ypersele 2002).

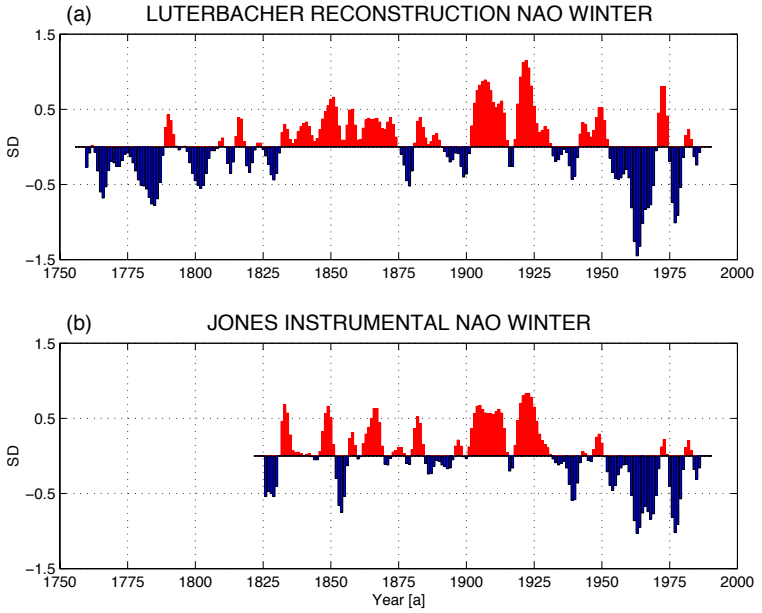


**Figure 5.22:** Evolution of the winter time NAO index for the reconstructions of Luterbacher et al. (2002b) (a) and the instrumental record from Jones et al. (1999a) (b). The time series have been filtered with a 10-years Gaussian low pass filter. Note the disagreements within the evolution during the 19th century (SD = standard deviation).

The next chapter focuses on the Southern hemispheric counterpart of the AO, the Antarctic Oscillation (AAO). After a short introduction to the AAO the evolution of the different indices is described. Afterwards a correlation analysis between the AAO and the external solar forcing is presented.

### 5.2.2 The Antarctic Oscillation (AAO)

The physical evidence of the AAO, or Southern Annular Mode, is not as controversial as for the AO. To a large degree this might be due to the lack of continents and the exceptional low temperatures over the Antarctic continent. Thus the meridional temperature gradient between the tropics and the polar regions is stronger than in the Northern Hemisphere, which leads to intensified upper tropospheric geostrophic winds.
Concerning the future changes of the AAO, Kushner et al. (2001) investigate the response of the Southern Hemisphere, extratropical, atmospheric general circulation to transient, anthropogenic, greenhouse warming in the coupled GFDL (Geophysical Fluid Dynamics Labora-

tory) climate model. Their results indicate an extratropical circulation response consisting of a Southern Hemisphere summer half-year poleward shift of the westerly jet. The previous results are supported by Thompson and Solomon (2002) who find observational evidence for an intensification of the AAO. Here the authors suggest that these recent trends are influenced by the trends within the lower stratospheric vortex which are due to photochemical ozone losses.
Concerning the past evolution of the AAO Jones and Widmann (2002) reconstructed the NDJ AAO index with the help of instrumental and tree-ring-based data. The reconstructions show that within the first half of the 19th century the AAO-index is characterized by a strong interannual variability with no clear trends, except the times around 1800 when the interannual variability is quite weak.

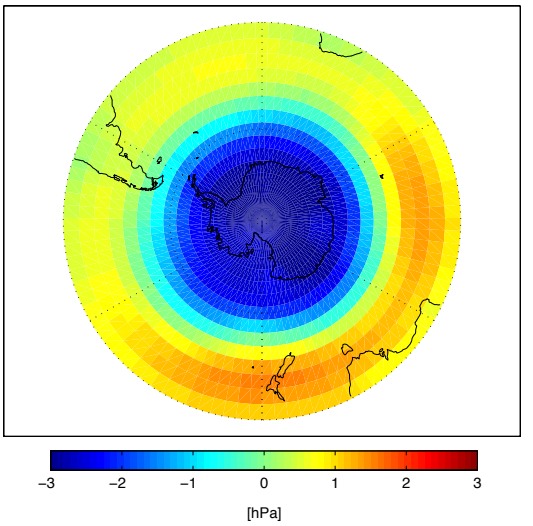


**Figure 5.23:** Antarctic Oscillation pattern (yearly) for the HIST simulation. Note the pressure seesaw between subpolar and subtropical regions with a pronounced vortex-like structure.

The 20th century also is characterized by a strong interannual variability until 1960. Thus, according to this reconstruction, no clear evidence for a reflection of the solar DM is evident within the NDJ-AAO index in terms of preferred positive or negative state.

The AAO-pattern for the HIST simulation is displayed in Fig. 5.23. It shows a pronounced vortex-like pressure seesaw between subtropical and subpolar latitudes. This anomaly pattern explains about 63% of the yearly interannual extratropical Southern hemispheric SLP variance. Opposed to the Northern hemispheric AO pattern, this vortex is zonally symmetric, because of the lack of vast continental land masses within the mid and high latitudes. In order to estimate the associated AAO indices of the different experiments, the

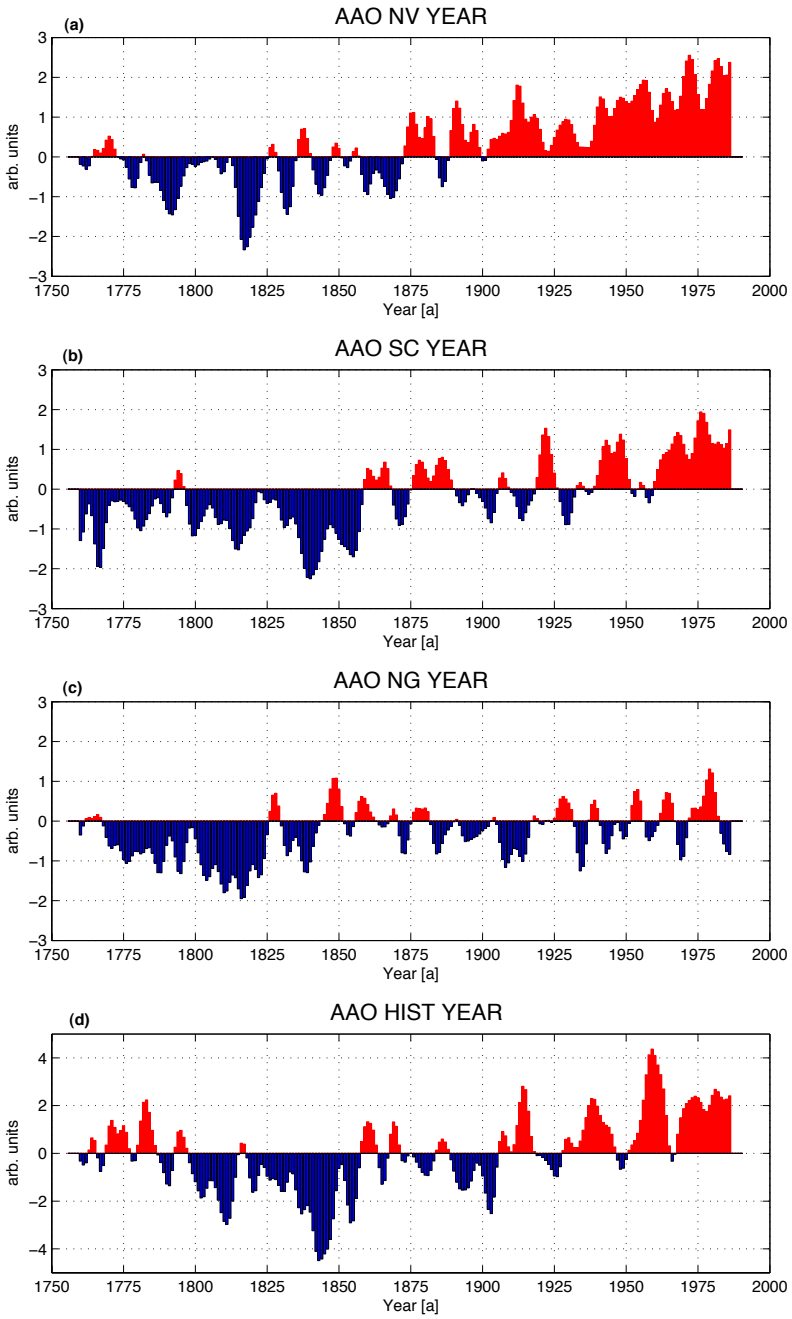


**Figure 5.24:** Antarctic Oscillation index on a yearly basis for the NV(a), SC(b), and NG(c) experiments and the HIST simulation (d). The time series have been filtered with a 10-years Gaussian low pass filter. Note the prevalence of negative AAOIs during the DM and the prevalence of positive AAO indices within the 20th century evident in all experiments (The zero lines correspond to the mean value of the HIST experiment).

| *r(AAO,SF)* | NV | NG | HIST |
|---|---|---|---|
| **1** | 0.17 (0.32) [0.59*] | 0.12 (0.22) [0.38*] | 0.21 (0.39*) [0.49*] |
| **2** | 0.11 (0.22) [0.32] | 0 (0.1) [0.19] | |
| **3** | 0 (0) [0] | 0 (0.13) [0.21] | |
| **Mean** | 0.18 (0.31) [0.46*] | 0.14 (0.27) [0.42*] | |

**Table 5.4:** Correlation between the yearly AAO indices and the external forcing (SF) of the NV, NG and HIST experiments; unfiltered (10-year Gauss) [30-year Gauss]. The time series have been detrended prior to the analysis. The asterisk denotes significance at the 90% level of significance. Note the positive correlations at multi-decadal time scales.

EOF pattern of Fig. 5.23 has been projected onto the yearly mean SLP fields of the ensemble mean of the different experiments. Eventually the mean value of the HIST simulation AAO index has been subtracted from the indices of the other experiments to allow for a proper comparison.
Within Figure 5.24a-d the evolution of the ensemble mean AAO indices of the different experiments is given. All experiments are generally characterized by the prevalence of negative indices during the 18th and 19th century. The 20th century, and here especially its second half, shows a preferred positive state of the AAO.
The evolution of the AAO index within the NV experiment shows mainly negative values until 1875. The DM also shows a series of negative indices. Around 1900 the occurrence of positive AAO indices increases and during the 1930s there is evidence of a strong positive trend which is interrupted during the 1960s. This decrease within the intensity of the westerly circulation was also seen within the winter time AO index.
The SC experiment also shows the prevalence of negative AAO indices in large parts of the 18th and 19th century. The 20th century is also characterized by a strong increase of the AAO index. This phenomenon is possibly due to the increasing greenhouse gas concentrations.
The NG experiment shows again quite a different picture. During the DM a series of very strong negative AAO indices can be seen. The 20th century does not show the high AAO indices of the other experiments. This can possibly be attributed to the lack of the increase of $CO_2$ concentrations. The HIST experiment shows negative AAO indices during the DM and the period until 1850. The 20th century again is dominated by mainly positive AAO indices.

In order to prove whether the AAO is connected to the external solar forcing, Table 5.4 shows the correlations between the AAO indices of the NV, NG and HIST experiment with the external solar forcing. Again, the NV1 simulation shows the highest correlation, especially at longer time scales. Within the NV2 and NV3 simulations correlations gradually

drop. Within the NV3 simulation, no correlations between the AAO and the external solar forcing exists at all. Opposed to the winter NAO index, the yearly AAO index shows some weak correlations with the external forcing for the NG1 experiment. The HIST simulation also shows moderate correlations at lower frequencies. Thus, even within the non-$CO_2$ influenced NG experiment, 18% of the AAO variability can be explained by the external solar forcing at multi-decadal time scales. As the correlations of the 2nd and 3rd ensemble members of the NV and NG experiment are lower than for the NV1 and NG1 experiment, it might be hypothesized that the different initial conditions might also have an impact on the evolution of the AAO. However, in general it can be stated that there is a weak but significant correlation between the external solar forcing and the (mean) AAO, at least at multi-decadal time scales.

As previously noted, the implementation of the volcanic forcing within the experiments is somewhat unrealistic, as during and after a volcanic eruptions the whole globe receives a reduced amount of insolation. In reality the situation is more complex as the climatic effects of volcanism strongly depend e.g. on the latitude and the timing of the eruption within the annual cycle. Thus it comes to a differential heating of different latitudes which possibly exerts an influence on the atmospheric circulation. Accordingly, the atmospheric circulation within the volcanic forced-experiments should be interpreted carefully. As shown within the analysis of Graf et al. (1993), after strong (tropical) volcanic eruptions the winter polar night jet increases due the aerosol heating in the lower tropical stratosphere and the temperature decrease in the polar stratosphere. This increases the meridional temperature gradient. As the present simulation does not include the direct influence of volcanic aerosols within the lower stratosphere this effect cannot be captured. Moreover, as the solar insolation is reduced over the whole globe, the meridional temperature gradients could even decrease. This should lead to a reduced intensity of the westerlies.

In order to assess the influence of the volcanic impact – as modelled within the present study – on the leading modes of the extratropical circulation, Figure 5.25a shows the volcanic events from 1756 to 1990. Accordingly, approximately 50% of the volcanic impacts are evident within the last 30 years of the simulations, when satellite data are available. The DM only includes the two very strong volcanic eruptions previously mentioned. Thus, the volcanic impact is, temporally, weakly pronounced within the DM and the pre-industrial period as a whole. However, volcanic eruptions often are clustered in time (e.g. shortly after the DM a series of strong volcanic eruptions can be seen).

To emphasize the impact of the volcanic eruptions on the AO and AAO, Figure 5.25b shows as an example the AO and AAO indices for the ensemble mean of the NG experiment. The volcanic impacts during the DM in 1809 and 1815 clearly show (strong) negative AO and AAO indices, which can also be seen at the end of the DM, when a series of volcanic

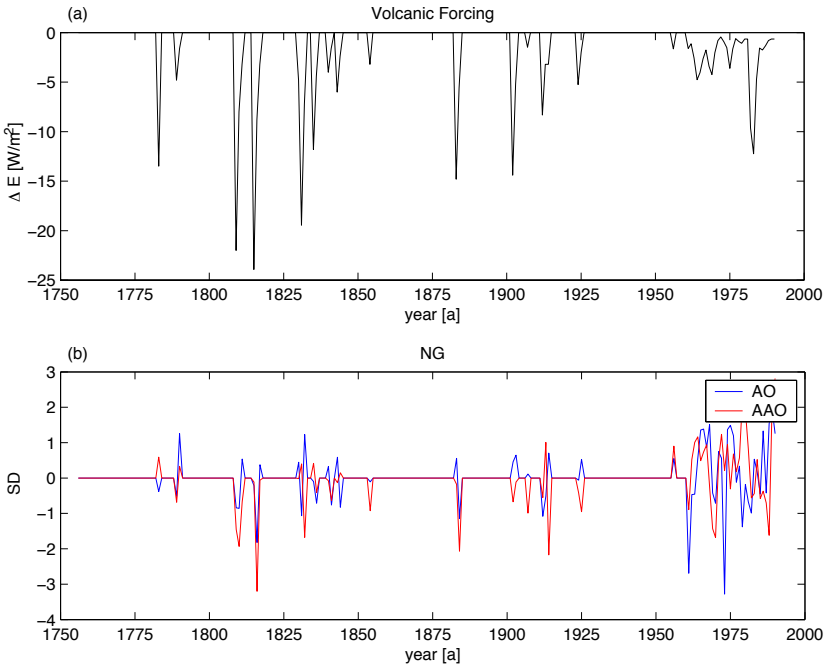


**Figure 5.25:** (a): Change in solar forcing due to volcanic impacts within the volcanic-forced experiments. (b): AO and AAO indices for the mean ensemble NG experiment for years with volcanic impacts. Note the tendency of the indices to become negative after strong volcanic events which is at odds with observational evidence (SD = standard deviation).

eruptions occurs. In this case, the indices do not show the latter negative intensity, which might be due to the weaker eruption intensity. The eruptions within the second half of the 19th and first half of the 20th century also show negative and close to zero indices, especially for the AAO. The last 30 years are characterized by a complex picture. This might be related to the inclusion of all volcanic impacts, and thus also the weak ones. For this period no clear statement can be made in terms of a preferred state of the AO and AAO during volcanic impacts. Accordingly, the influence of the volcanic impact could be misleading, as the circulation tends to reflect the opposite state as it is argued for the real climate system, namely an intensification of the westerlies and not a reduction. An argument which puts these problems into perspective in terms of the implementation of the volcanic impact is that there are quite few volcanic eruptions prior to 1960.

Another question is if the dynamical winter warming due to the positive AO after the Pinatubo eruption, as e.g. analyzed by Graf et al. (1993) can be generalized to other volcanic eruptions. In this respect the study of Shindell et al. (2003) suggests a sustained dominance of the radiative cooling over the circulation-induced winter warming in the case of the Tambora eruption. Thus, the climatic effects related to post-volcanic times could be more diverse and complex concerning the intensity of a volcanic eruption.

### 5.2.3 Circulation-temperature connections

The following section discusses possible links between the temperature evolution of selected regional temperatures, already presented in section 5.1.2, and the atmospheric circulation.

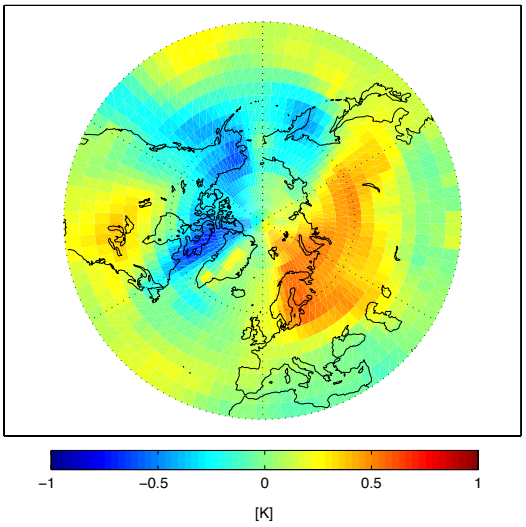


**Figure 5.26:** Regression pattern between the winter AO index and the near surface temperatures on the extratropical Northern Hemisphere within the HIST experiment. Note the positive values over Eurasia accompanied by negative values located mainly over western Greenland.

Figure 5.26 shows the spatial regression pattern of the HIST experiment winter AO index on the respective temperature fields. For the Northern Hemisphere winter situation the well known pattern of above normal temperatures over large parts of Eurasia and south-eastern North America and below normal temperatures mainly over western and southern Greenland can be seen, as e.g. also described in Thompson and Wallace (1998). (The SLP temperature regression patterns of the other experiments are very close to the HIST simulation, except the NV experiment showing higher amplitudes.)
Zorita and González-Rouco (2000) conclude in their analysis over the disagreement in the future predictions of the AO in different climate model simulations, that the spatial mean of the temperature regression patterns are very close to zero. This would imply, that on the Northern hemispheric average, the regional positive and negative temperature anomalies induced by the AO balance each other. The following paragraph will prove this for the NV1

| *Experiment* | NV | SC | NG |
|---|---|---|---|
| **r(AO,EU)** | 0.66* | 0.56* | 0.57* |
| **r(AO,SI)** | 0.64* | 0.57* | 0.59* |
| **r(AO,SG)** | -0.59* | -0.49* | -0.5* |

**Table 5.5:** Correlation of the winter AO index with the European (EU), Siberian (SI) and South Greenland (SG) winter temperatures. All time series have been detrended prior to correlation analysis. The asterisk denotes significance on the 95% level of significance. Note the negative correlations of the South Greenland temperatures and the winter time NAO indices.

and NG1 simulation. These two simulations have been chosen because they differ most pronounced in terms of the external forcing.
The spatial average of the regression coefficients (temperature residual) of the NV1 and NG1 simulation, similar to Fig. 5.26, is +0.09 K and +0.12 K, respectively. The correlation between the winter time AO-index and the extratropical Northern hemispheric winter temperatures is +0.21 for the NV1 simulation and +0.25 for the NG1 simulation. However, the temperature residuals reduce to +0.03 K (+0.04 K) and the correlations to +0.11(+0.09) in the NV1 (NG1) simulation when the analysis is carried out for the whole Northern Hemisphere. Hence, only 6% (NG1) of the mean extratropical Northern hemispheric temperature variability can be explained by the winter time AO. Accordingly, these results do not necessarily support the hypothesis put forward by Wallace et al. (1995) suggesting a (prominent) dynamical influence of the atmospheric circulation on the hemispheric mean temperatures. It is suggested here that the extratropical circulation mainly causes a redistribution of warm and cold air masses over different geographical regions on the extratropical Northern Hemisphere (cf. Fig. 5.26). As the spatial average of the regression coefficients is non-zero, there is a small positive temperature residual, indicating a weak influence of the AO on the hemispheric mean temperatures in a sense that a positive AO leads to a small increase of the hemispheric mean temperatures. However, the analysis presented here and by Zorita and González-Rouco 2000 investigates model results, which might deviate from the observational analysis carried out by Wallace et al. (1995).

As already seen within section 5.1.2, some regional temperature time series deviate markedly from the evolution of global or hemispheric temperatures. This is especially true for the South Greenland temperatures and the temperatures in the Southern Hemisphere south of 60° S.
To get a closer insight into the regional circulation-temperature connection, Table 5.5 shows the correlations between the winter time AO and the regional temperature time series for the different experiments. Concerning the different experiments, the NV experiment generally performs best in terms of the circulation-temperature connection. The European

and Siberian temperatures are positively correlated with the winter time AO indices. Accordingly, the winter time AO is able to explain up to 44% of the European and Siberian temperature variability.
For the South Greenland region the winter time AO can also explain up to a 44% of the temperature variability in the SC experiment. For this regions the correlation between the winter time AO and the temperature is negative.
Physically the following mechanism, explaining the deviations of the South Greenland-temperatures with respect to the European and Siberian temperatures, is suggested: In its high phase the NAO in the North Atlantic region advects cooler polar air masses on the west Greenland coast southward which eventually also reduces temperatures at the southern rim of Greenland. On the other hand, over the Northeast Atlantic mild oceanic air masses are advected eastward on the European continent and lead to a temperature increase (cf. Thompson and Wallace 1998). The Siberian region, on the other hand is not influenced by the mild oceanic air masses, due to its remoteness. The mechanism possibly controlling temperatures in this region is related to the strength of the Siberian high. During positive AO periods the Siberian high is weakened and thus temperatures increase (Gong and Ho 2002).

Besides the AO or NAO, which are defined here as the first EOFs of the winter time SLP field, also the higher order EOFs might explain some of the regional temperature variability. Figure 5.27a shows the second EOF-pattern of the HIST simulation within the North Atlantic region during winter, explaining 15% of the total winter SLP variance in this region. It mainly shows a monopole positive pressure anomaly centered over the Northeast Atlantic and western Europe. Accordingly, in its positive mode, this pattern resembles a blocking like structure preventing the penetration of mild air masses into western Eurasia. In its negative mode a negative pressure anomaly leads to an increased south-(westerly) advection of warm oceanic air into western Eurasia (cf. Fig. 5.27b). Hence, this anomaly pattern should influence the climate of western Eurasia quite strongly, depending on the sign of the associated index. The 'blocking indices' are estimated in the same way as the AO and NAO indices. Fig. 5.28 shows as an example the evolution of both the winter time NAO indices (a-c) and the blocking-indices (d-f) for the different members of the NG experiment. In general there is no clear agreement among the different indices. The different NAO indices and the blocking-indices respectively, indicate again the important influence of i) internal climate variability and ii) the different initial conditions.
However, in terms of the winter time NAOI, only the period around 1875 shows negative NAOI indices within all 3 simulations. During the second half of the DM, only within the NG1 simulation the prevalence of negative NAO indices is evident. The NG2 and NG3 simulations show moderate to low positive values. Concerning the blocking indices during the

| *Experiment* | NV | SC | NG |
|---|---|---|---|
| **r(BLOCK,EU)** | -0.37* | -0.35* | -0.25* |
| **r(BLOCK,SI)** | -0.28* | -0.26* | -0.25* |
| **r(BLOCK,SG)** | 0.22* | 0.18* | 0.16* |

**Table 5.6:** Correlation between the winter time blocking indices (BLOCK) and the European (EU), Siberian (SI) and South Greenland (SG) winter temperatures. All time series have been detrended prior to correlation analysis. The asterisk denotes significance at the 90% level of significance. Note the negative correlations between the blocking indices and the European and Siberian temperatures.

DM, the first and third ensembles show moderate to strong negative indices, whereas the 2nd ensemble shows prevailing moderate to low positive indices. Accordingly, there is no clear-cut prevalence of a preferred circulation state among the different circulation indices for the winter time in the North Atlantic region within the NG experiment during the DM.

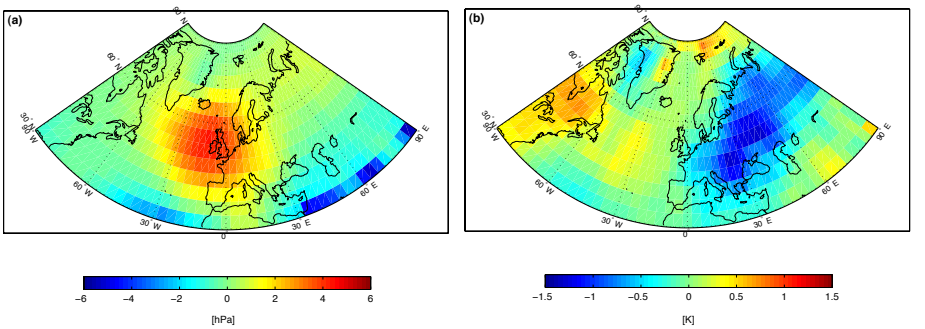


**Figure 5.27:** (a): 2nd EOF of the winter time SLP within the North Atlantic for the HIST experiment. Note the blocking like structure centered over the Northeast Atlantic. (b): Regression pattern between the blocking index (derived from (a)) and the winter temperatures over the North Atlantic region.

Table 5.6 shows the correlation between the blocking indices and the regional temperature time series. The European and Siberian temperatures are negatively correlated with the evolution of the blocking pattern, whereas the South Greenland temperatures are weakly positive correlated. As the EOFs are orthogonal, e.g. statistically uncorrelated, the amount of explained variance by the second EOF is independent to that of the first EOF. Hence, up to 14% of the European temperature variability within the NV experiment can be explained by the 2nd EOF. The blocking index within the NG experiment can only explain around 6% of the European temperature variability. The reasons for the deviating amount of explained variance among the NV, SC and the NG experiment might be again due to the $CO_2$ increase within the NV and SC experiment.

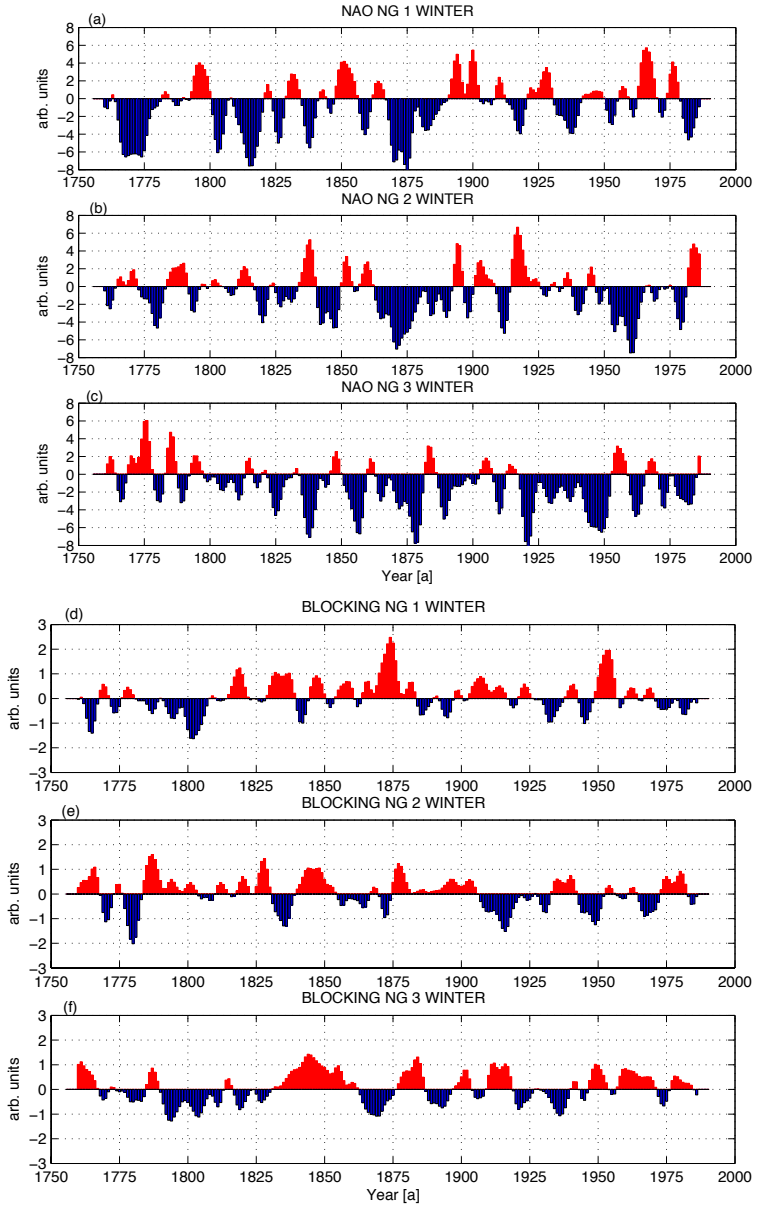


**Figure 5.28:** (a-c): Winter time NAOI indices for the 3 simulations within the NG experiment. (d-f): same as (a-c) except for the blocking indices (for definition see text). The time series have been filtered with a 10-years Gaussian filter. Note the differences among the respective indices concerning their temporal evolution (The zero lines correspond to the mean value of the HIST experiment).

The differences concerning the winter time NAO and the blocking indices between the DM and the times prior and after are given in Table 5.7 (standardized values). Accordingly, the

| *difference(NAOI[DA-NODA]) [SD]* | NV | SC | NG | HIST |
|---|---|---|---|---|
| **1** | -0.04 | -0.05 | -0.04 | -0.54* |
| **2** | +0.13 | -0.05 | +0.09 | |
| **3** | -0.08 | -0.23* | +0.07 | |
| **Mean** | +0.006 | -0.11 | +0.04 | |
| *difference(BLOCK[DA-NODA]) [SD]* | NV | SC | NG | HIST |
| **1** | +0.29 | -0.11 | -0.27 | -0.21 |
| **2** | -0.40* | -0.08 | +0.17 | |
| **3** | +0.06 | +0.52* | -0.48* | |
| **Mean** | -0.15 | +0.11 | -0.19 | |

**Table 5.7:** upper part: Difference of the winter NAO indices between the DM and the times prior (1756–1789) and after (1831–1900). lower part: same as upper, except for the blocking indices. The asterisk denotes significance at the 90% level of significance. Note the non-uniform sign of difference among the different experiments. (SD = standard deviation).

NAO indices only show significant (negative) differences for the SC3 and HIST experiment. This coincides well with the temperature pattern within Figures 5.17c and 5.15. Concerning the blocking indices, the only significant differences are given for the NV2 and NG3 simulation indicating negative deviations during the DM. Dynamically this implies reduced pressure over the Northeast Atlantic leading to a southerly advection of mild air over south-eastern Europe. This also coincides well with the European temperature patterns within Figures 5.16b and 5.18c indicating increased temperatures over large parts of Europe during the DM. (Figures 5.16b and 5.18c show the yearly mean temperature difference. However, the temperature patterns for the respective winter season are quite similar.) Thus there is strong evidence that the atmospheric circulation is able to modify the externally forced climate signals quite profound at the regional scales. Concerning the Southern Greenland temperatures an anomalous atmospheric circulation in terms of the NAO might lead to a reduction of regional temperatures within periods of increasing global temperatures. However, different atmospheric circulation regimes in terms of higher EOFs might also have important impacts on regional temperatures. They will not be discussed here due to the limited space.

Within the previous analysis, only correlations over the whole time period have been analyzed. In order to get a better insight into the stationarity of these correlations Fig. 5.29 shows, as an example, the running correlations between the winter NAO indices and the European and the South Greenland temperature time series for the NV experiment. The running time window is 30 years. A similar analysis has e.g. been carried out by Jacobeit et al. (2001b) demonstrating the instationarities within the circulation-climate relationship based on reconstructed data for the North-eastern Atlantic and Europe.

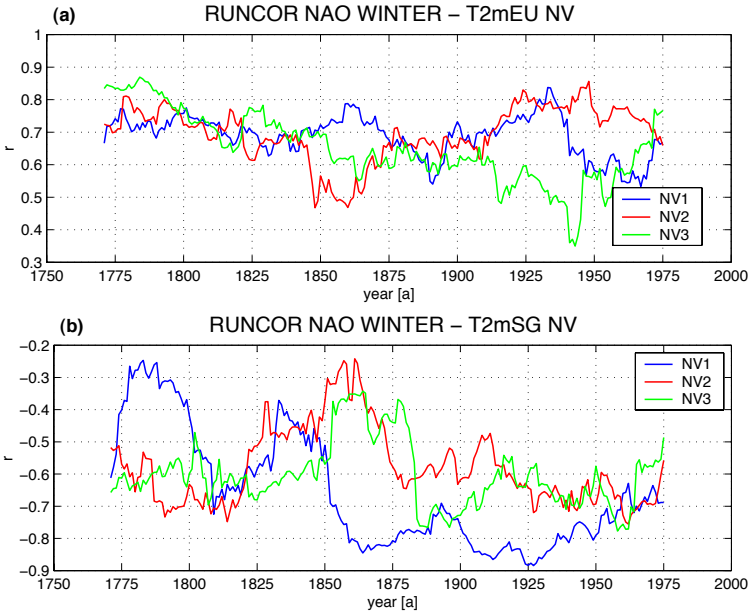


**Figure 5.29:** (a): 30 years running correlations between the winter NAO and the winter temperatures over Europe (EU). (b): same as (a), except for the Southern Greenland (SG) temperatures. The time series have been detrended prior to the analysis. Note the high degree of instationarities, especially within the NAO index-South Greenland temperature correlations.

Within Fig. 5.29a the running correlations between the winter NAO indices and the European temperatures are shown. The different curves coincide quite well at correlations between +0.7 to +0.8 until 1850. Small discrepancies are evident between 1850 and 1875. However, big discrepancies within the correlations of the 20th century are evident. Accordingly, around 1940, more than 60% of the European temperature variability within the NV1 and NV2 simulation, but only 10% within the NV3 simulation, can be explained by the NAO index.

The situation for the South Greenland temperatures (Fig. 5.29b) is even more complex. Only during the DM and within the 2nd half of the 20th century do all simulations show the same correlation levels around -0.7. However, during other periods, e.g. around 1860, the NAO index within the NV1 simulation can explain up to 70% of the South Greenland temperature variability, whereas the NV2 and NV3 simulation only can explain around 15%. As the South Greenland temperature region is located mostly over oceanic areas, the fact that the evolution of the running correlations of the NV2 and NV3 simulations coincide quite well is possibly related to the stronger coherence of their initial oceanic conditions with respect to the NV1 simulation. These results should have – even though based on model results – implications for the reconstruction of the e.g. North Atlantic Oscillation by means of temperature-sensitive proxies. As the NAO always plays an important role

| *Experiment* | NV | SC | NG |
|---|---|---|---|
| **r(AAO,T2mSH60)** | -0.42* | -0.43* | -0.38* |

**Table 5.8:** Correlation of the yearly AAO indices with the yearly mean Southern hemispheric temperatures south of 60° S (T2mSH60). All time series have been detrended prior to correlation analysis. The asterisk denotes significance at the 90% level of significance. Note the negative correlation between the intensity of the westerlies and the polar Southern hemispheric temperatures.

in reconstructing the North Atlantic-European climate one should therefore pay attention to these circulation-temperature instationarities, which would significantly influence the reconstruction of the past climate (cf. also Zorita and González-Rouco 2002). Another implication of these results shows the huge amount of instationarities within the climate system, which might be related to processes between the slowly varying ocean and the fast varying atmosphere.

The next paragraph focuses on the circulation-temperature connections in the high latitude Southern Hemisphere (SH60). The analysis of the correlations between the AAO indices and the SH60 temperatures shows, in general, negative correlations. Thus, up to 18% of the SH60 interannual temperature variability can be explained by means of the AAO for the NV experiment. This amount reduces to 14% for the NG experiment (cf. Table. 5.8).
The same analysis carried out for the correlations between the winter time AO and temperatures north of 60° N shows no correlations at all. In this respect, the Southern Hemisphere deviates markedly from the Northern Hemisphere concerning the connections between the extratropical circulation and the high latitude temperatures. The Southern Hemisphere spatial AAO-temperature regression pattern for the NV1 simulation is displayed in Figure 5.30a. (Again, for the other simulations similar regression patterns are obtained). It shows a more zonally symmetric temperature pattern with respect to the Northern hemispheric AO-temperature pattern. Accordingly, in general, below-normal temperatures mostly over the Antarctic continent and above normal temperatures over the low-mid latitudes are evident. An interesting feature are the re-emerging negative temperature anomalies around 60° S, especially within the Pacific-Indian ocean area. Thus, over the high-mid and high Southern hemispheric latitudes an increased AAO index reduces the near-surface temperatures.
Table 5.9 shows the differences in the near-surface temperatures south of 60° S (upper part) and in the AAO indices (lower part) between the DM and the times prior and after. Accordingly, the prevailing negative AAO indices in all experiments, mostly within the NV experiment, coincide with positive temperature anomalies. Table 5.9 further demonstrates that the stronger the AAO index, the stronger the negative temperature anomaly. As there

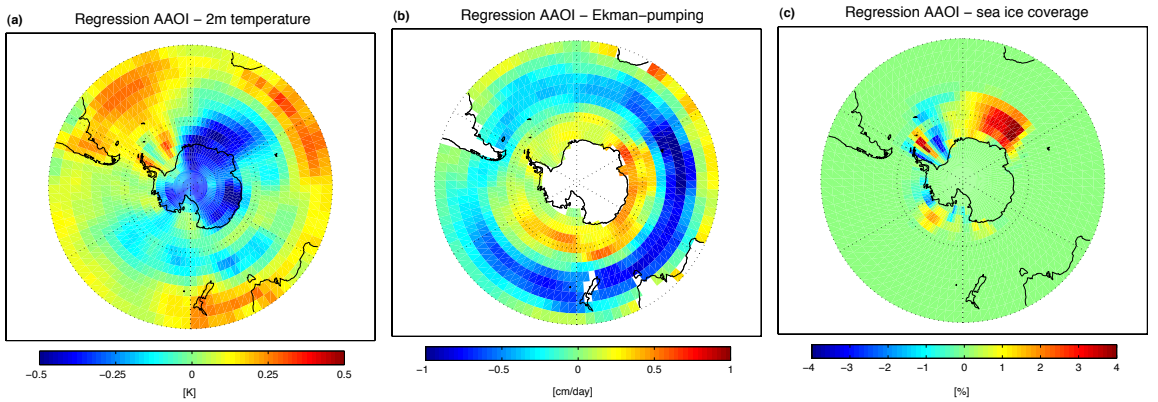


**Figure 5.30:** Regression pattern between the AAO indices and different variables. (a): near surface temperatures. (b): Ekman-pumping (positive=upward). (c): the sea ice coverage. Note the temperature-reducing potential of an increased AAOI on the high latitude Southern Hemisphere by means of an increased Ekman-pumping and sea ice coverage.

are clear differences in terms of strength and the sign of the difference (cf. NV3) within and between the different experiments, again the importance of the internal climate variability and/or the ocean-atmosphere interaction due to the different initial conditions is emphasized. The mechanisms possibly leading to the high latitude Southern hemispheric temperature anomalies can partly be explained by the effects of the AAO on the Southern Ocean in terms of Ekman-pumping and sea ice concentration. Opposed to the Northern Hemisphere, the Southern Hemisphere, as a whole, mainly consists of oceanic areas. Hence, the lack of continents and the inertia of the ocean are important factors controlling the temperature variability. The oceanic coverage of the high-mid and high Southern hemispheric latitudes allows for vertical Ekman-pumping, which itself is related to the intensity of the westerlies and hence the AAO. In this respect according to the Ekman-theory (cf. Peixoto and Oort 1992), a pronounced westerly circulation leads to a divergent northward and southward directed upper oceanic flow, bringing up cooler deep waters to the ocean surface. Figure 5.30b shows the regression pattern between the AAO index and the according Ekman-pumping for the NV1 simulation. This pattern possibly explains part of the increased SH60 temperatures during the DM and can possibly be attributed to the weak westerlies leading to a reduced Ekman-pumping. A modelling study carried out by Hall and Visbeck (2002) also supports the AAO-Ekman-pumping mechanism.

Another mechanism possibly further increasing near-surface temperatures during negative AAO phases is the reduction of oceanic sea ice around the Antarctic continent. Figure 5.30c shows the regression pattern between the AAO index and the oceanic sea ice concentrations. Accordingly, during high AAO phases, an increase within the sea ice coverage is evident, whereas during low AAO phases a reduction of sea ice occurs. This implies a reduction of the albedo and hence a reduction of the backscattering of the incoming short-wave radiation.

| *difference(T2mSH60[DA-NODA]) [K]* | NV | SC | NG | HIST |
|---|---|---|---|---|
| **1** | +0.06 | +0.20* | +0.36* | +0.10 |
| **2** | +0.24* | +0.11* | +0.22* | |
| **3** | -0.05 | +0.03 | +0.06 | |
| **Mean** | +0.09* | +0.12* | +0.22* | |
| *difference(AAOI[DA-NODA]) [SD]* | NV | SC | NG | HIST |
| **1** | -0.26 | -0.16 | -0.33* | -0.17 |
| **2** | -0.57* | -0.08 | -0.25 | |
| **3** | +0.14* | +0.18 | -0.22 | |
| **Mean** | -0.23* | -0.02 | -0.26* | |

**Table 5.9:** upper part: Difference of the near-surface temperatures south of 60° S between the DM and the times prior (1756–1789) and after (1831–1900). lower part: same as the upper part except for the yearly AAO indices. The asterisk denotes significance at the 90% level of significance. Note the prevailing negative AAO indices accompanied by positive temperature anomalies during the DM within most simulations. (SD = standard deviation).

A temperature decrease over much of Antarctica, especially its eastern part, as well as the extension of the sea ice coverage around eastern Antarctica during the recent positive trend within the AAO is also evident within the observations (cf. Thompson and Solomon 2002; Yuan and Martinson 2000).

### 5.2.4 Summary

Within the previous chapter the evolution of the extratropical circulation in terms of the Arctic (AO) and North Atlantic Oscillation (NAO) and the Antarctic Oscillation (AAO) has been analyzed with respect to:
**1.** the mean ensemble evolution
**2.** possible connections with the external solar forcing
**3.** its implications for the regional circulation-temperature relation.

The analysis carried out under **1**. yields a different picture concerning the experiments forced with (NV, SC, HIST) and without (NG) increasing $CO_2$ concentrations. In the $CO_2$ influenced experiments, prevailing negative indices are found for the period until 1900, especially within the DM, whereas a strong positive trend within the circulation indices is evident within the 20th century. This holds true for both, the AO (NAO) and the AAO. The NG experiment does not show this pronounced trend within the 20th century. Another

finding is the influence of the volcanism, implemented here as a reduction of the global insolation, leading, during volcanic events, to prevailing negative circulation states, which is at odds with the observations. Hence, it can be concluded that the $CO_2$ increase has a strong impact on the evolution of the circulation during the 20th century, whereas the volcanic influence could be misleading in terms of circulation states after strong volcanic events.

Within the analysis carried out under **2.** there is evidence of an external forcing of the circulation within the NV and HIST experiments, especially on multi-decadal periods, in terms of a positive correlation. This result is put into perspective by the analysis of the NG simulations, where only insignificant correlations are found. The analysis of reconstructions and instrumental records even shows negative correlations between the solar forcing and the NAO. Hence it can be concluded that again the $CO_2$ increase has a strong impact on the relation between the solar forcing and the circulation, as within the NG experiment no correlation is found at all. However, results based on annual data rather than winter time find correlations between the solar forcing and the NAO also for the NG experiment. For the yearly AAO, the solar forcing is correlated positively within both the NV, NG, and HIST experiments at decadal time scales.

The analysis carried out under **3.** demonstrates the importance of the extratropical circulation on the regional scale. For the relation between the winter time AO and the Northern hemispheric temperatures there is only a small agreement. Only very little of the hemispheric-scale temperature variability can be explained by the AO. The analysis of the evolution of the indices of the first (NAO) and second (BLOCK) winter time EOF-SLP within the North Atlantic region demonstrates a quite different evolution within the different NG simulations. These disagreements between the different simulations within the same experiment are possibly due to i) internal climate variability and ii) the different initial conditions. However, the different evolution of the indices may explain some peculiarities found within the previous chapter in terms of temperature patterns during the DM. For example, a positive temperature pattern over Europe during the DM may be due to a northward advection of air masses according to the 2nd EOF SLP index. For the Southern Hemisphere during the DM, mainly positive temperature anomalies are evident. They can partly be explained by a negative correlation with the AAO indices. The mechanisms explaining this phenomenon are possibly due to an increased high latitude Ekman-pumping and a decreased sea ice coverage around Antarctica during low phase AAO indices.

## 5.3 Oceanic variability within the North Atlantic

The following chapter investigates selected oceanic phenomena within the North Atlantic ocean. Due to the limited space only very few items are investigated concerning the temperature and circulation variability of the Gulf Stream and the northward heat transport in the North Atlantic. Prior to these investigations a short motivation for the importance of the ocean as main climate factor is given.

The oceans plays a prominent role within the global climate. This includes the transport of energy and mass from the tropics and subtropics to the high latitudes. A very important point is related to the different time scales concerning the atmosphere and the oceans. The atmosphere reacts quite fast on changes of e.g. the external forcing in the order of days or weeks. The ocean on the other hand reacts more sluggish. This is due to the physical inertia of large water bodies and the vertical stratification of the world ocean. Only the uppermost 300 m adapt in the order of months or a few years to changes of the overlaying atmosphere. However, the mid ocean beneath the mixed layer needs longer reaction times, in the order of decades.
An important factor at high latitudes is the heat release due to convection, whereby the formation of deep water occurs. This process occurs mainly in the Labrador seas (LabseaGroup 1998) and the Greenland-Norwegian seas (Bonisch and Schlosser 1995). A study carried out by Pickart et al. (2003) also suggests the Imringer sea to be of importance concerning the oceanic convection. The production of deep waters is a key processes in sustaining the so called thermohaline circulation, which is especially important for the North Atlantic region (Broecker 1991). Recently a paper by Wunsch (2002) expresses doubts based on energy-balance considerations about the mechanisms connected to the density-driven theory of the thermohaline circulation.
A climate factor influencing the high latitudes is related to the oceanic sea ice. In the presence of sea ice the atmosphere-ocean heat exchange is suppressed and, via the increased albedo, the incoming short-wave radiation is scattered back. Furthermore the ocean ice modulates the intensity of the thermohaline circulation by means of freshwater release (cf. Holland et al. 2001).

Another point which deserves attention is related to the importance of the atmosphere-ocean interaction. At long time scales it is hypothesized that a collapse of the meridional overturning circulation in the North Atlantic could lead to a cooling of the surrounding continental regions (Rahmstorf and Ganopolski 1999). In contrast it has also been common belief that

the relatively mild winter temperatures in Europe compared to their counterparts in North America are caused by the heat transport due to the Gulf Stream and/or the North Atlantic Meridional Circulation. Recently, some model results indicate that this zonal temperature gradient may be caused by the mean atmospheric circulation (Seager et al. 2003).

The following chapter consists of three main parts. In the first section the evolution and spatial structure of the ocean mixed layer temperatures are analyzed. After the analysis of the Gulf Stream circulation the oceanic northward heat transport within the North Atlantic is discussed. This section includes an investigation of the impact of the different initial oceanic conditions within the simulations on the future behavior of the system.

### 5.3.1 Ocean temperature variability within the mixed layer

This section investigates the ocean temperatures (OT) within the oceanic mixed layer. This layer is represented in this study by the -100 m depth. The statistical analysis applied is again the empirical orthogonal function analysis (EOFs). This strategy allows for the identification of possible multipole structures within the ocean. Averaging of the OT over the whole North Atlantic ocean possibly neglects multipoles and hence the spatial temperature structure gets lost.
Fig. 5.31 shows the leading EOFs of the -100 m OT fields within the North Atlantic ocean based on the diagonalisation of the covariance matrix (a), the covariance matrix with detrended anomaly fields (b) and the correlation matrix with detrended standardized fields (c) of the HIST simulation. The latter analysis does not show anomalies in terms of temperatures anymore, but correlation coefficients between the gridpoint and its respective time series. (This is due to the fact, that the calculation of the covariance matrix with standardized values yields the correlation matrix).

Fig. 5.31a shows negative temperature anomalies within the central North Atlantic. Positive temperature anomalies are found in the subtropical North Atlantic and the Mediterranean sea. This pattern changes dramatically when detrending the weighted anomaly fields prior to EOF analysis (Fig. 5.31b). Accordingly, the negative temperature anomaly pattern within the North Atlantic vanishes completely. However, within this pattern, positive temperature anomalies prevail within the subtropical North Atlantic and negative temperature anomalies are evident in the Labrador seas and off the coast of west Africa. These negative anomaly regions are also evident within Fig. 5.31c, where the (detrended) standardized anomaly fields of the EOF-analysis are displayed. The positive anomaly region is extended with respect to Fig. 5.31b and now covers nearly the whole subtropical North- and Northeast Atlantic.

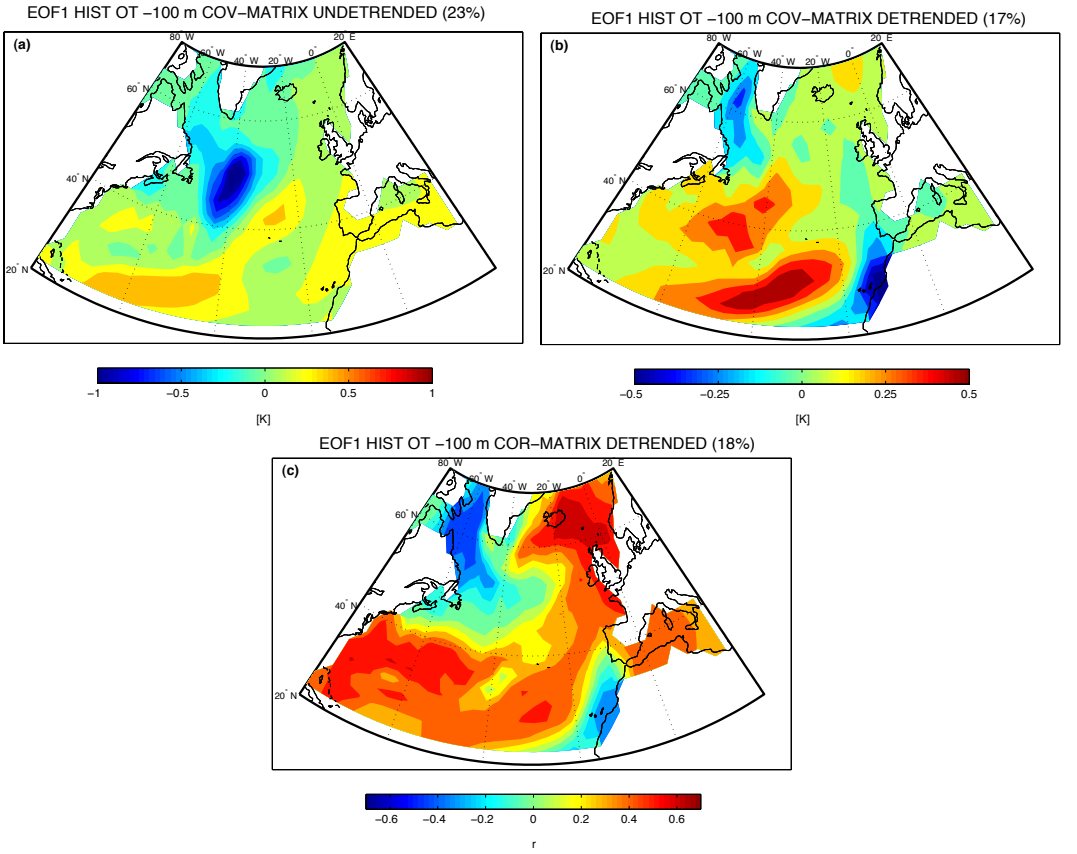


**Figure 5.31:** Leading EOFs of the OT fields within the North Atlantic ocean based on the covariance matrix (a), the covariance matrix with detrended anomaly fields (b) and the correlation matrix with detrended standardized fields (c). Note the pronounced differences within the EOF patterns concerning the non-detrended and detrended data, respectively.

As already mentioned within the introduction to EOFs, the EOF patterns, even the leading ones, do not necessarily reflect real physical processes. In order to test whether the EOF pattern of Fig. 5.31b shows a physical meaningful mode, the time series of the centers with maximum positive and negative values have been correlated with all other gridpoints. Fig. 5.32 shows the so called one-point correlation maps between the *detrended* gridpoints within the central part of the subtropical Atlantic and off the coast of West Africa with all other gridpoints within the North Atlantic.
Fig. 5.32a reflects, in a broad sense, the multipole structure of Fig. 5.31b. Fig. 5.32b, on the other hand, shows a pattern with positive values off the coast of West Africa and negative values along the path of the Gulf Stream and North Atlantic current. (For better illustration, the mean horizontal ocean velocities are additionally plotted). This implies that above normal temperatures off the coast of West Africa coincide with lower than normal temperatures of the Gulf Stream.

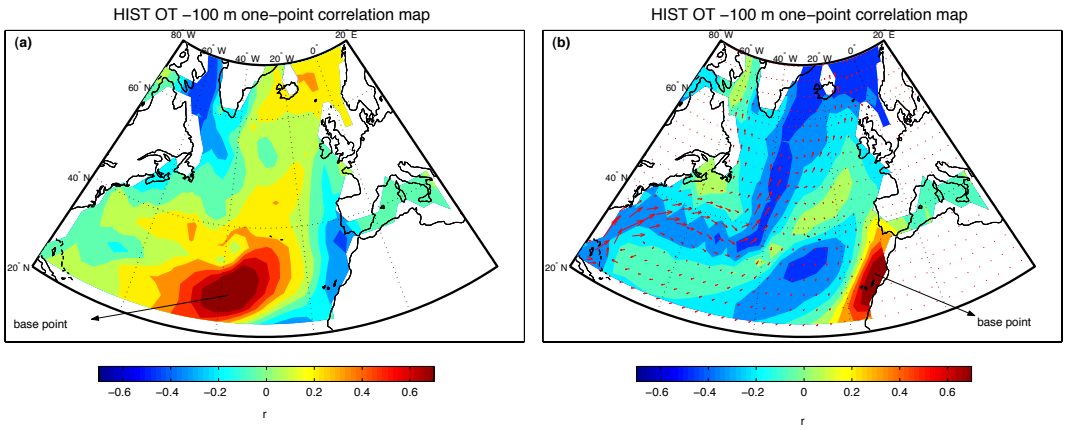


**Figure 5.32:** One point-correlation maps for the highest values within Fig. 5.31b. (a): base point within the central subtropical North Atlantic. (b): base point off the coast of West Africa. Note the lack of multipoles as compared to Fig. 5.31b and the reflection of the Gulf Stream pathway within the right panel.

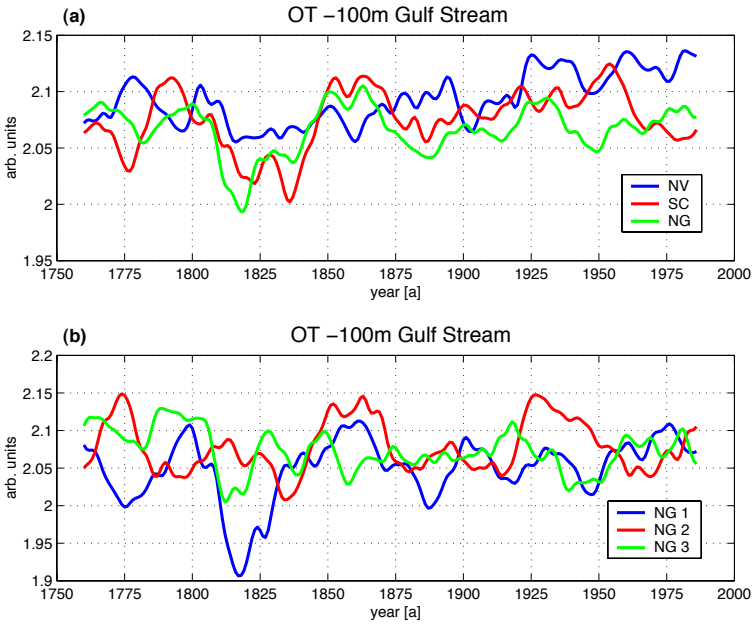


**Figure 5.33:** (a): Oceanic temperature variability of the Gulf Stream (cf. Fig. 5.32b) within the different experiments. (b): same as (a) except for the simulations within the NG experiment. (For calculation of the Gulf Stream OT evolution see text). The time series have been smoothed with a 10-years Gaussian low pass filter. Note the reduction of OT during the DM within (a) in all experiments.

From the pattern shown in Fig. 5.32b, an index of the Gulf Stream temperatures has been defined, as follows. As the negative correlations within Fig. 5.32b reflect the Gulf Stream

| *difference(GS-OT[DA-NODA]) [arb. units*0.01]* | NV | SC | NG | HIST |
|---|---|---|---|---|
| **1** | -0.79 | -1.06 | -4.30* | -4.6* |
| **2** | -1.97* | -0.43 | -1.91* | |
| **3** | -0.23 | -1.13 | +0.13 | |
| **Mean** | -1.0* | -0.87 | -2.0* | |

**Table 5.10:** Difference between the Gulf Stream ocean temperatures (OT) -100 m for the different experiments between the DM and the times prior (1756–1789) and after (1831–1900). The asterisk denotes significance at the 90% level of significance. Note the in general reduction of OT during the DM evident within most simulations

pathway, the negative values have been multiplied by -1 and eventually projected on the respective ocean temperature fields of the different experiments. The resulting Gulf Stream temperature indices for the mean of the different experiments are shown in Fig. 5.33a. The indices for the simulations within the NG experiment are displayed within Fig. 5.33b. However, it should be noted here that due to the dimensions of the Gulf Stream pathway, different temperature regimes may exist (e.g. with above normal temperatures off the coast of Florida and below normal temperatures within the central North Atlantic as e.g. analyzed by Sutton and Allen (1997)).

Within Fig. 5.33a the DM is reflected by a temperature depression, mostly pronounced in the SC and NG experiments. After the DM, the Gulf Stream temperatures of SC and NG experiments are higher than the temperatures of the NV experiment until 1875. Within the 20th century the NV experiment shows a strong positive trend which is accompanied by the SC experiment until 1950. Afterwards the SC experiment shows a negative trend until 1990. The NG experiment does not show this pronounced positive trend within the 20th century and the temperature levels vary around pre-DM conditions. The situation within the NG experiment (Fig. 5.33b) shows a quite different evolution of temperatures during the DM (cf. also Table 5.10). Until the end of the simulation the different curves coincide quite well at a decadal basis, except the period 1900–1925, when the NG2 simulation shows increased temperature levels with respect to NG1 and NG3 simulations.

Table 5.10 shows the differences of the Gulf Stream temperatures indices for the different simulations between the DM and the times prior and after. Accordingly, most of the simulations show a decrease within the temperatures of the Gulf Stream during the DM. This is most pronounced for the NG1 and HIST simulations. The SC experiment on the other hand does not show significantly reduced temperatures at all. Interestingly, the NG3 simulation differs again, as the difference here is slightly increased. However, in terms of the ensemble mean, the NV and NG experiments show significantly reduced temperatures within the Gulf Stream pathway.

The next section analyses the North Atlantic ocean current variability also with respect to the Gulf Stream circulation.

### 5.3.2 The North Atlantic ocean current variability

The oceanic circulation is characterized by velocities $\vec{\mathbf{U}}$ and $\vec{\mathbf{V}}$. This requires analysis tools that are capable of dealing with a two-component field. One way is to extend the above explained EOF analysis to a so called Complex EOF (CEOF) analysis (cf. von Storch and Frankignoul 1998). The other way is to derive scalar fields from the vector fields that preserve the relevant information contained within the vector field. For an almost non-divergent vector field this can be achieved by the calculation of the so called *stream function*. Having calculated the stream function, the (scalar) data fields can be analyzed with the ordinary EOF-analysis.
The stream function of a vector field reads as follows:

$$u = \frac{\partial \Psi}{\partial y} \qquad v = -\frac{\partial \Psi}{\partial x} \tag{5.17}$$

The stream function is a scalar field, where positive values indicate clockwise rotation and vice versa. The gradient of the stream function field is related to the intensity of the current. Thus, the more narrow the stream lines, the stronger the intensity of the flow.
In order to show the similarities between the vector field and the stream function field, Figure 5.34 shows both the horizontal ocean velocities and the stream function of the -100 m layer for the North Atlantic. Within Fig. 5.34a the western boundary current of the Gulf Stream is reflected within the subtropics showing maximum velocities of 20cm/s off the coast of Florida. The North Atlantic current is also discernible. These features are also evident within the horizontal stream function within Fig. 5.34b, where the red areas denote the anticyclonic rotation in the subtropical circulation cell. The strong gradients among the stream lines along the Northeast American coast are related to the high velocities of the Gulf stream.
In order to get insight into the temporal and spatial variability of the stream function fields of the North Atlantic ocean an EOF analysis has been performed. Figure 5.35 shows the leading EOF stream function pattern for the HIST experiment, explaining 45% of the interannual North Atlantic stream function variability. In general the EOF pattern within Fig. 5.35 reflects an anticyclonic velocity anomaly within the western and central subtropical part of the North Atlantic ocean. A weak but discernible cyclonic velocity anomaly can be seen within the central parts of the North Atlantic.
Fig. 5.36 shows the projection of the first EOF of the detrended horizontal stream function fields of the HIST experiment onto the ensemble mean of the NV, SC, and NG experiments (a) and within the NG experiment (b). Here a positive index implies an increased Gulf Stream circulation within the North Atlantic.

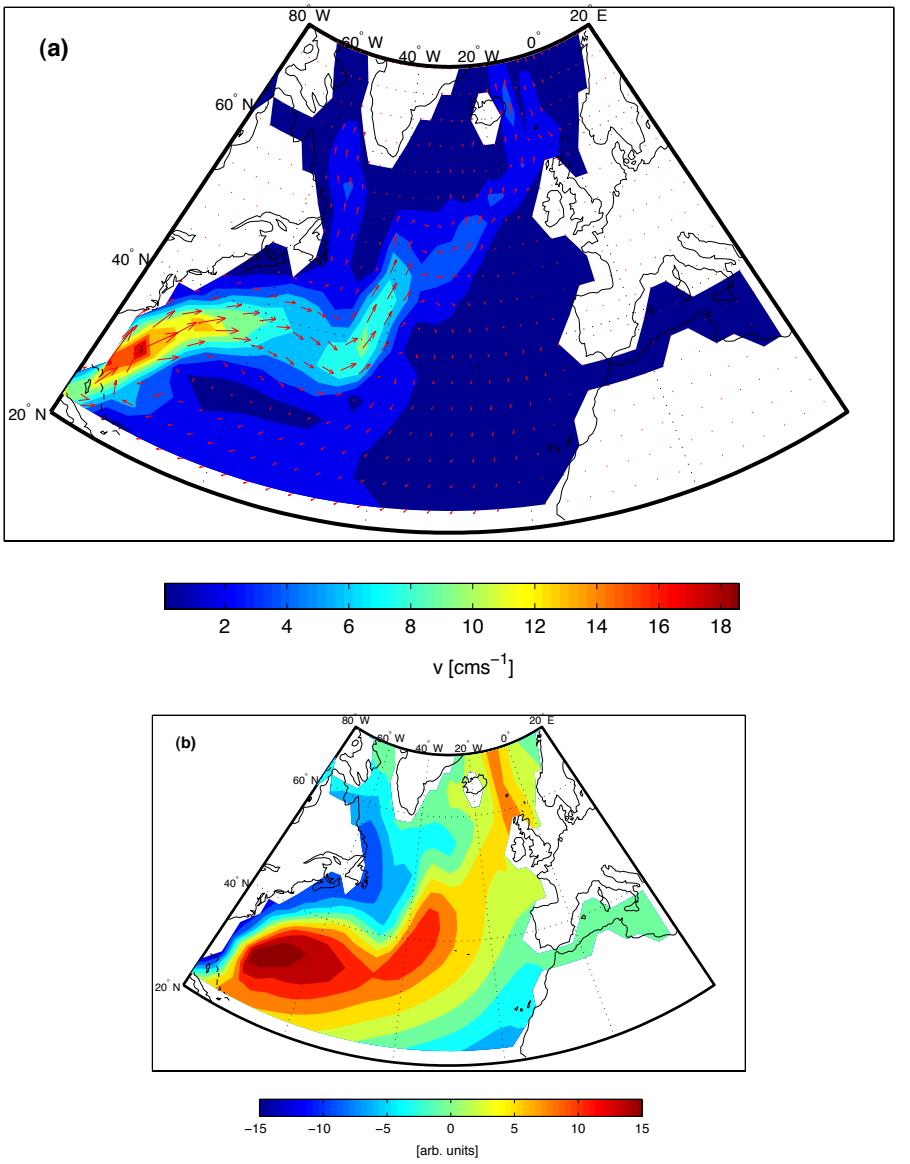


**Figure 5.34:** Mean velocities (a) and horizontal stream function (b) within the -100 m layer in the North Atlantic ocean (red areas denote clockwise rotation). The Western boundary current of the Gulf Stream is evident in both panels.

Accordingly, the projected times series of the SC and NV experiments show, in general, a decline within the circulation over the whole period, mostly pronounced within the NV experiment. The NG experiment, on the other hand, does not reflect a strong negative trend during the 20th century. The NV experiment shows the strongest decrease within the second half of the 20th century. The DM is reflected for the SC and NG experiments, but it is not captured by the NV experiment. As the SC and NG experiments are strongly influenced by

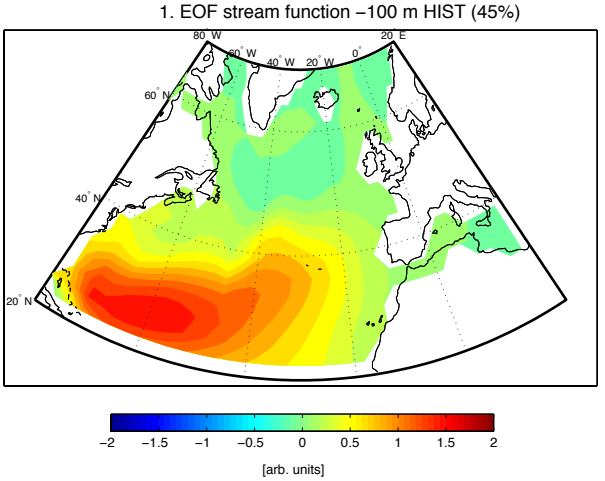


**Figure 5.35:** Leading EOF pattern of the North Atlantic stream function field. The input fields have been detrended prior to analysis. Note the clockwise circulation anomaly within the western subtropical Atlantic.

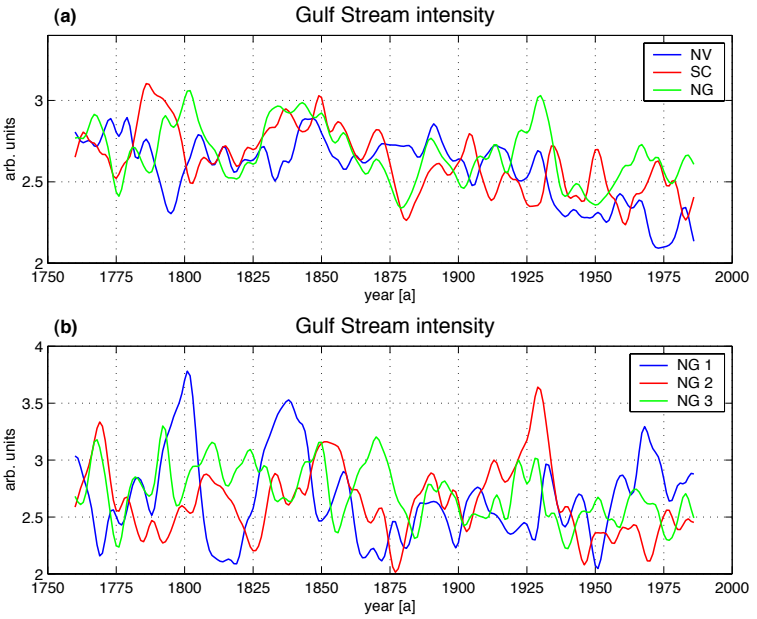


**Figure 5.36:** (a): Projection of the leading stream function EOF pattern of Fig. 5.35 onto the fields of the different experiments. (b): same as (a) except for the simulations within the NG experiment. The time series have been smoothed with a 10-years Gaussian low pass filter. Note the ambiguous evolution of the indices among the NG simulations within (b) during the DM.

increasing $CO_2$ concentrations during the 20th century, the most probable reason for the decrease within the Gulf Stream circulation may be due to this. Accordingly, the evolution

| *difference(GS[DA-NODA]) [arb. units]* | NV | SC | NG | HIST |
|---|---|---|---|---|
| **1** | -0.20* | -0.02 | +0.12 | -0.06 |
| **2** | -0.01 | +0.03 | -0.19* | |
| **3** | -0.17* | +0.01 | +0.21* | |
| **Mean** | -0.12* | +0.007 | +0.046 | |

**Table 5.11:** Difference between the Gulf Stream for the different experiments between the DM and the times prior (1756–1789) and after (1831–1900). The asterisk denotes significance on the 90% level of significance. Note the different Gulf Stream intensity anomalies within the NG experiment.

of the Gulf Stream intensity is opposite to the evolution of the Gulf Stream temperatures, especially during the 20th century.

Figure 5.36b shows the situation for the different ensemble simulations carried out in the NG experiment. Above all, the curves differ markedly, especially during the DM. This phenomenon is also reflected within Table 5.11 showing the differences within the intensity of the Gulf Stream circulation between the DM and times prior and after. Hence, the NV experiment is the only one showing a significant reduction within the ocean circulation during the DM, even if the curve within Fig. 5.36a does not suggest this. For the SC experiment there are virtually no differences, whereas the NG experiment shows an increase within the circulation for the NG1 and NG3 simulations and a decrease for the NG2 simulation. The HIST experiment also shows a small, but insignificantly reduced Gulf Stream circulation.

These results, especially those for the NG3 simulation, demonstrate again that the Gulf Stream circulation need not necessarily reduce during a period with reduced solar insolation, as e.g. indicated by Zorita et al. (2004). However, it could be heavily influenced by the internal climate variability and the initial conditions. On the other hand Zorita et al. (2004) derive their results by analyzing the Late Maunder Minimum, which is by far more pronounced than the DM. Hence the anomalous solar forcing during the DM is possibly too weak to exert a significant impact on the Gulf Stream circulation.

In the following section a synthesis between the thermal characteristics and the dynamical characteristics within the North Atlantic ocean in terms of the oceanic northward heat transport will be presented.

### 5.3.3 Northward heat transport

The northward heat transport (NHT) with respect to latitude $\phi$ reads as follows (cf. Klinger and Marotzke 2000):

$$H(\phi) = \int_{-D}^{0} \int_{W}^{E} (c_p \rho) v \Theta R \cos(\phi) d\lambda dz \tag{5.18}$$

In equation 5.18, $c_p$ denotes the specific heat, $\rho$ is the density of water, $v$ the meridional ocean velocity, $\Theta$ is the potential temperature, $R$ is the radius of the Earth, $z$ is the depth, $\lambda$ is the longitude, $D$ is the depth of the deepest oceanic layer, and $W$ and $E$ are the western and eastern boundaries.

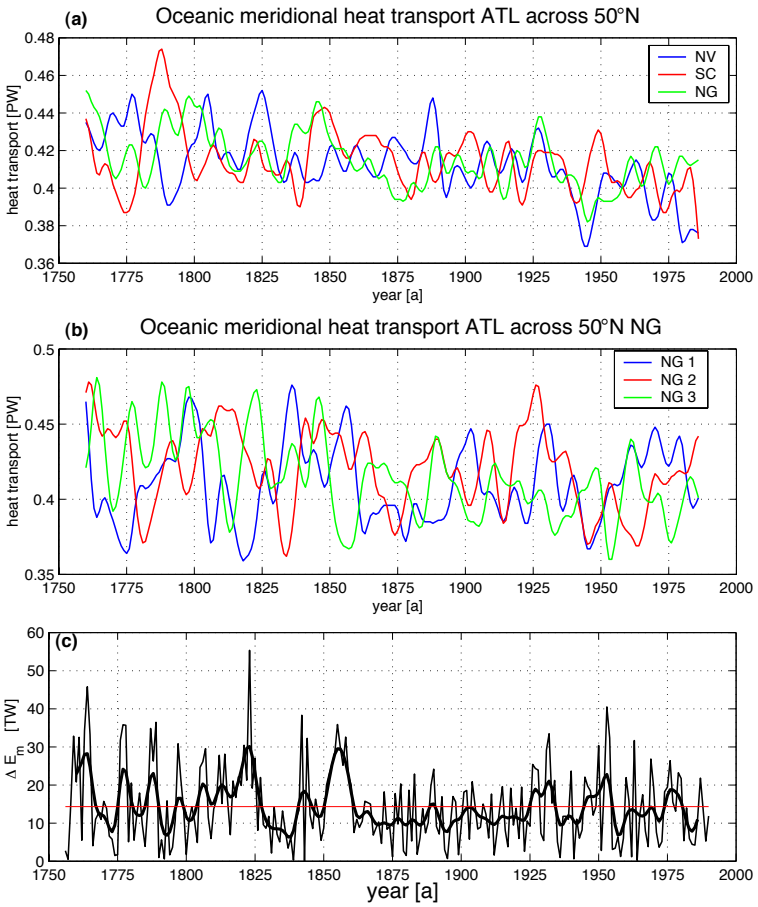


**Figure 5.37:** Mean ensemble meridional heat transport across 50° N within the North Atlantic for the different experiments (a) and within the NG experiment (c). The time series have been smoothed with a 10-years Gaussian low pass filter. (c): Dissimilarity index of the NG experiment. Note the strong decrease within the heat transport in experiments NV and SC within the North Atlantic. (PW = $10^{15}$W; TW = $10^{12}$W).

| *difference(NHT[DA-NODA]) [TW]* | NV | SC | NG | HIST |
|---|---|---|---|---|
| **1** | -20.3* | -0.53 | -2.37 | -14.15* |
| **2** | +21.57* | -0.10 | +12.23* | |
| **3** | +8.85 | -2.4 | +14.06* | |
| **Mean** | +3.37 | -1.01 | +7.97* | |

**Table 5.12:** Difference between the northward meridional heat transport (MHT) across 50° N for the different experiments between the DM and the times prior (1756–1789) and after (1831–1900). The asterisk denotes significance at the 90% level of significance. Note the positive NHT anomaly during the DM for the 2nd and 3rd ensemble members of the NV and NG experiment.

The oceanic northward heat transport is used here in favor of the meridional overturning as it combines both dynamical and thermal characteristics. However, the oceanic northward heat transport and the meridional overturning are correlated with r=0.76.
Figure 5.37 shows the evolution of the NHT across 50° N within the North Atlantic for the ensemble mean of the different experiments (a) and the simulations within the NG experiment (b). In general, within Figure 5.37a, all experiments, except the NG experiment, show a general decline within the NHT from the 19th to the 20th century. The DM is not reflected as might be suggested by the external forcing. Again, especially the NV experiment, shows the strongest decline within the NHT during the 20th century. This decrease of the NHT seems to be due to the strong $CO_2$ increase during the 20th century. Figure 5.37b shows a very incoherent evolution of the NHT among the ensembles of the NG experiment. Within the first 100 years there is virtually no period when the curves meet at the same level.
This phenomenon is also evident within Table 5.12 where the differences of the NHT between the DM and the times prior and after are displayed. Except the SC experiment all other experiments show strong differences concerning the DM. Thus, there is evidence for a significantly reduced NHT within the NV1 simulation, whereas the NV2 simulation shows a significantly increased NHT during the DM. The SC experiment shows no clear-cut differences among the different simulations. In general, the first ensemble members of the experiments, especially those of the NV1 and HIST experiments, show a significantly reduced NHT. Interestingly, the NG1 experiment, which is very close to the HIST experiment concerning the external forcing, does not show this pronounced difference. Hence, as the external forcing is the same, the constant $CO_2$ concentrations within the NG1 experiment could be the reason for those differences.
In order to test this hypothesis, Fig. 5.38 shows the evolution of the NHT for the NV1, NG1, and HIST experiments. Concerning the NV1 and HIST experiments the curves coincide perfectly until 1783, when the Laki eruption occurs. The NG1 experiment, on the other hand, deviates markedly from the other two curves from the very beginning. Hence, it can

| *difference(Experiment-HIST)[TW]* | NV | SC | NG |
|---|---|---|---|
| **1** | -3.96 | +0.9 | -2.99 |
| **2** | +27.1* | +11.0* | +23.2* |
| **3** | +12.5* | +8.01 | +23.7* |

**Table 5.13:** Difference between the northward meridional heat transport (MHT) across 50° N between the single members of the different experiments and the HIST simulation for the DM. The asterisk denotes significance at the 90% level of significance. Note the positive NHT anomaly during the DM for the 2nd and 3rd ensemble members opposed to the first member simulations.

be concluded that even small disturbances within the forcing, in this case in terms of $CO_2$, may lead to significant changes in the evolution of the NHT.

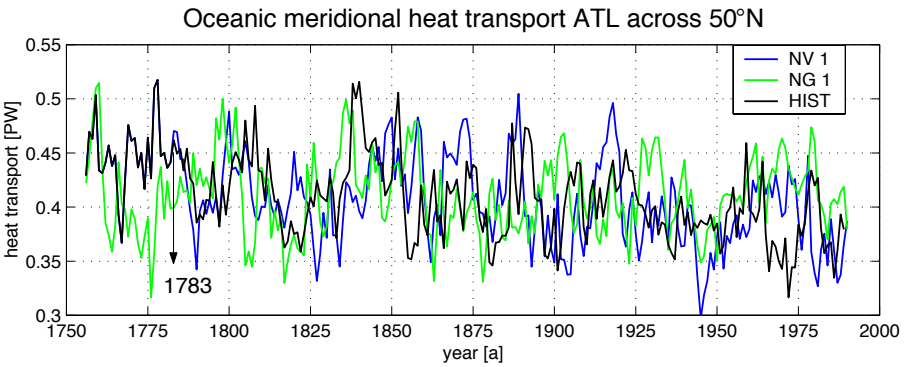


**Figure 5.38:** Oceanic meridional heat transport across 50° N within the North Atlantic for the NV1, NG1 and HIST simulation. Note the coincidence of the NG1 and NV1 simulation until 1783, when the external forcing differs for the first time.

In order to further investigate the initial oceanic influence on the evolution of the NHT, Table 5.13 shows the differences between the different simulations and the HIST simulation for the DM. Accordingly, for the first ensembles the differences remain insignificant. The 2nd and 3rd ensemble members, on the other hand, show a significantly increased NHT within the DM with respect to the HIST experiment. Thus, opposed to the near-surface temperatures on global and hemispheric scales, the initial oceanic conditions seem to control the future behavior of the oceanic variability, e.g. in terms of the NHT. Another result, which may be drawn from Table 5.13 is related to the adaptation of the ocean to the external forcing. In this analysis the ocean within the 2nd and 3rd ensemble has virtually no time to adapt to the changed external forcing. The change of the external solar forcing within the 2nd and 3rd simulations (e.g. the difference between the conditions in 1755 and 1594(a) and 1571(b), respectively) is -0.88 $Wm^2$(a) and -2.67 $Wm^2$(b). This change in solar forcing

should be a minor cause, as a volcanic eruption can disrupt the solar forcing even more strongly. What seems to be more important is the oceanic history over the past decades or centuries representing the integral of the external and internal climate variability. It is quite unlikely that the ocean, including the ocean interior, adapts to the external forcing within a few decades (in this case within 35 years until the beginning of the DM). According to the dissimilarity index within Figure 5.37c, there is some evidence that the different NG simulations converge within the second half of the 19th century as the dissimilarity during and after that period is apparently reduced with respect to the period 1755–1860. Thus, at least 100 years are necessary until the ocean, in terms of the NHT, adapts to the changed external forcing.

### 5.3.4 Summary

Within the previous chapter the North Atlantic ocean variability has been investigated in terms of:
**1.** the spatial ocean temperature variability within the ocean mixed layer
**2.** the variability of the Gulf Stream circulation
**3.** the variability of the northward heat transport, and
**4.** the persistence and influence of the initial oceanic conditions.

The investigations under **1.** result in a spatially differentiated temperature pattern in the North Atlantic ocean. This includes the emergence of a temperature quadrupole when detrending the data prior to the EOF analysis. Accordingly, positive temperature anomalies in the subtropical and north-eastern North Atlantic are accompanied by negative temperature anomalies in the Labrador Sea and off the coast of West Africa. The one-point correlation maps with the base point off the coast of West Africa identifies the Gulf Stream pathway being negatively correlated with the West African coast upwelling region. The projection of this pattern on the respective oceanic fields yields time series of the temperature variability of the Gulf Stream. Here the DM is reflected in the ensemble mean of all experiments, whereas the simulations among the NG experiment show marked deviations. Concerning the long term evolution, a positive trend is evident for the NV and SC experiment, especially pronounced within the 20th century. This trend is not reflected within the NG experiment and is possibly due to the influence of the $CO_2$ increase.

The analyses carried out under **2.** investigate the Gulf Stream circulation variability. It is defined here as the projection of the leading stream function EOF pattern of the HIST experiment onto the -100 m stream function fields of the different simulations. The results show a pronounced negative trend of the NV and SC experiment during the 20th century. The DM is well reflected within the SC and NG experiment in terms of a reduction of the Gulf Stream circulation. However, this result is put into perspective when looking at differences between the DM and the times prior and after. Accordingly, a disagreement within the Gulf Stream intensity concerning the different simulations becomes evident. Thus, the circulation is only significantly reduced for the ensemble mean of the NV experiment, whereas for the other experiments no clear-cut statements concerning a reduction of the intensity of the Gulf Stream can be made.

The analysis carried out under **3.** investigates the variability of the oceanic northward heat transport (NHT) within the North Atlantic basin across 50° N. The analysis results, in general, in a reduced NHT within the 20th century for the NV and SC experiments which is possibly due to the reduction within the Gulf Stream circulation. The DM is not as clear-cut reflected within the ensemble mean as might be inferred in terms of the external forcing. The differences within the NHT concerning the DM and the times prior and after as well as the differences with respect to the HIST simulation are very sensitive to the initial oceanic conditions. Thus, e.g. the first ensemble members show a reduction in the NHT for the NV1 and HIST simulations, whereas the NV2 simulation shows an increase.

The analysis of the initial oceanic conditions carried out under **4.** shows i) a pronounced impact of slight changes within the external forcing concerning the $CO_2$ variability and ii) a very strong impact of the initial oceanic conditions on the future behavior of the NHT. In this respect the constant $CO_2$ levels of the NG1 experiment lead to a disagreement in the evolution of the NHT with respect to the HIST simulation, although the external solar and volcanic forcing are the same. The NV1 simulation agrees completely with the HIST experiment until 1783, when the first volcanic eruption occurs. The impact of the initial oceanic conditions seems to be crucial for the future evolution of the NHT. Hence, the first ensemble members only show slight differences with the HIST simulation during the DM, whereas the 2nd and 3rd ensemble members show pronounced differences. This result is put into perspective due to the fact that the NHT of the different simulations within the NG experiment converge after approximately 100 years. Accordingly, there was possibly too little time for the ocean to adapt to the change within the external forcing and hence part of the previous disagreements within the evolution of e.g. the Gulf Stream circulation and the NHT are due to this fact.

# Chapter 6

# Conclusions and Outlook

In the last chapter the main results of the previous thesis are discussed in terms of the working hypothesis formulated within the introduction. The overall goal was to examine the reaction of different climate variables and processes under changed external forcings and initial conditions with special consideration of the Dalton Minimum (DM).
In order to analyze the effects of the different external forcings a special experiment setup was designed, including different ensemble simulations with the climate model ECHO-G, with the simulations starting in 1755. The reference simulation, from which different initial conditions were derived, is a 1000 year integration, forced with variable solar and volcanic output and a variable amount of selected greenhouse gases ($CO_2$, $CH_4$). The different experiments were forced 1) without volcanic forcing, 2) with only volcanic forcing and 3) with solar and volcanic variable forcing but with constant pre-industrial $CO_2$ concentrations.

The most important finding is that without any volcanic influence there is no pronounced reduction within the mean global and hemispheric temperatures during the DM, more specifically after 1810. This result is also supported by reconstructions for the Northern hemispheric temperatures indicating a temperature drop in the period after 1810. However, on the extratropical regional scales there is only little evidence for a pronounced volcanic signal. This result is also supported by empirical reconstructions. A comparison of the temperature effect of single volcanic eruptions with the historical evidence on hemispheric scales shows a reasonable level of agreement and thus gives some confidence with respect to the volcanic forcing used in this study.
The change within the solar variability seems to be of minor importance on global scales. This is supported by the fact that there are no distinct differences between the experiments

with constant solar forcing and variable solar forcing before 1810. Furthermore, the strong $CO_2$ increase in the course of the DM seems to have no significant impact on the temperatures of the DM. Contrarily, the reference simulation including the increase within $CO_2$ even shows negative temperature anomalies at the beginning of the 19th century.
Thus, the evolution of temperatures on the global and Northern hemispheric scales are supposed to be driven by changes within the external forcing, whereas the temperature evolution on regional scales is influenced and modified by the variability of the atmospheric and/or oceanic circulation.
The comparison of the different experiments with reconstructions and the instrumental record for the whole time period 1755–1990 shows the best agreements with the experiment forced with constant pre-industrial $CO_2$ concentrations. This is evident in both the reconstructions and the instrumental record. However, this result should hinder the conclusion that the $CO_2$ increase does not affect the climate evolution, as there are possibly many constellations concerning the external forcing leading to this result. Thus, e.g. the introduction of industrial aerosols could alter those results in a way that the reference experiment, including all forcings, eventually agrees best with reconstructions and observations.
On the European regional scale the reconstructions suggest mostly positive temperature anomalies during the DM with respect to the times prior and after. The different model experiments in general show negative temperatures during the DM, except two simulations where positive temperature anomaly patterns emerge. In this respect, this result emphasizes: i) the virtue of the ensemble approach for the assessment of the regional climate variability, ii) the importance of natural climate variability and iii) the possible impact of the initial conditions.

The influence of the external forcing on the Arctic Oscillation (AO) shows statistically significant results only on a multi-decadal basis for the only solar forced and reference experiments in terms of a positive correlation. The experiment with constant pre-industrial $CO_2$ concentrations virtually shows no correlation with the external forcing. In this respect it can be concluded that the $CO_2$ increase should be the major reason for establishing this connection, which does not exist for the winter time. Opposed to that results obtained on a yearly basis show significant positive correlations for all solar forced experiments. The Antarctic Oscillation (AAO) also shows positive correlations for the solar forced experiments.
Thus it can be concluded that there is some evidence for a connection between the solar variability and the leading modes of circulation on a yearly basis on a multi-decadal time scale. The physical mechanisms establishing this connection could possibly be related to an increase within the upper-tropospheric equator-to-pole temperature gradient in times of increased solar insolation leading to a more pronounced westerly flow within the extratropics.

However, a fact that might put into perspective the model results is the comparison between reconstructions and observations concerning the solar forcing-winter time North Atlantic Oscillation (NAO) showing significant negative correlations with the external forcing at decadal time scales.
The analysis of the circulation-temperature connection demonstrates that not all regions experienced negative temperature anomalies during the DM. Especially South Greenland as well as the high latitude Southern Hemisphere are characterized by only moderately reduced or even increased temperatures during the DM. The reason for this deviations with respect to the global or hemispheric temperatures are possibly due to the state of the circulation mode in terms of the AO and AAO, respectively. Accordingly, the South Greenland temperatures are likely influenced by the winter time AO/NAO, whereas the high latitude Southern Hemisphere temperatures are possibly influenced by the variability of the AAO and related phenomena concerning anomalies within the Ekman-pumping and the sea ice coverage around Antarctica.

Concerning the oceanic variability within the North Atlantic basin the evolution of the mixed layer Gulf stream/North Atlantic current temperatures show a decrease within most experiments during the DM and a temperature increase during the 20th century for the experiment without any volcanic forcing. However, in terms of the oceanic northward heat transport (NHT) within the North Atlantic basin across 50° N a reduction within the 20th century for the $CO_2$ forced experiments is evident possibly due to the reduction within the Gulf Stream circulation. A physical mechanism which might explain this reduction within the respective experiments is a slow-down within the thermohaline circulation caused by a temperature increase within the high latitudes reducing the production of North Atlantic deep waters. The DM is not as clear-cut reflected within the ensemble mean as might be inferred in terms of the external forcing, especially concerning the volcanic forced experiments. The differences within the NHT concerning the DM and the times prior and after as well as the differences with respect to the reference simulation are very sensitive to the initial oceanic conditions.
The analysis of the impact of the initial oceanic conditions eventually showed a pronounced impact of slight changes within the external forcing concerning the $CO_2$ variability and a very strong impact of the initial oceanic conditions on the future behavior e.g. of the NHT. In this respect the first member of the experiment with a constant $CO_2$ level shows a disagreement in the evolution of the NHT with respect to the reference simulation, although the external solar and volcanic forcing are the same. Thus, even slight changes e.g. in terms of $CO_2$ might lead to changes within the future evolution of the NHT within the North Atlantic ocean.

In the course of this work several points were established, which could contribute to improvements of the future work and sharpened the view for the present work. Briefly, these points are:
Concerning the climate model, there are deficiencies concerning the state of various atmospheric and oceanic climate variables. This includes the strength and position of the centers of variability and the their variability in terms e.g. of the blocking intensity and frequency. Within the Pacific ocean the El-Niño-Southern Oscillation is overestimated. Another shortcoming of the model is the applied flux corrections in order to prevent climate drift, and the low atmospheric and oceanic resolution. Hence, in terms of the explicit treatment of volcanic aerosols a higher resolved stratosphere is needed. Accordingly, for future investigations the new generation of climate models developed at the MPI in Hamburg (ECHAM5-HOPE-C) are possibly better performing in this respect.
Arguments against changing the current model are as follows: First, the comparison with existing paleoclimatic runs become more difficult. Second, the findings in this study in terms of the ensemble approach suggest that there is a huge amount of internal climate variability, mostly affecting the regional scales, which would not be absent at all in a more elaborated climate model.
Concerning the external forcing, other reconstructions of the solar forcing could be used in the simulations. Besides the solar forcing reconstructed by Crowley (2000), which is essentially applied here, other reconstructions also could be used, e.g. those by Hoyt and Schatten (1993) or a newer reconstruction by Solanki and Fligge (1999). In terms of the DM, Usoskin et al. (2002) find evidence for a lost sunspot cycle in the beginning of the DM. This new finding also could be included into the solar forcing time series in order to test whether this modification leads to different results.
Concerning the volcanic forcing a better implementation in terms of a latitudinal resolved volcanic impact e.g. after Robertson et al. (2001) would be desirable to overcome the shortcomings of the present simulations related to the winter time atmospheric circulation.
Another point of improvement is concerned with the reaction time of the ocean. This implies a longer time period between the change in the initial conditions and the onset of the period of interest. As the present study suggests, this should be at least 100 years.
Furthermore changes in land-use could be also considered as an additional forcing factor.
A last point within this outlook points to the importance of the ensemble-approach. As the computational power is steadily increasing it should be possible to carry out more than a few simulations with the same external forcing but some dozens in order to i) increase the statistical basis and ii) get further information of how climate can evolve both temporally and spatially under the same external forcings.

# Acknowledgments

First I would like to thank Prof. Dr. H. von Storch for the appraisal of the work. He gave me the opportunity to prepare this thesis at the GKSS Research Centre in Geesthacht. I further have to thank Prof. Dr. J. Jacobeit for the readiness to be the second assessor and to visit Hamburg for the disputation.

Special thanks are due to Dr. E. Zortia (Dr. Z.) who was the actual tutor of the thesis and helped me whenever necessary. Many thanks also to Dr. J. F. González-Rouco who provided a compiled ECHO-G version and helped a lot to keep the model running. Many thanks also to Dr. J. Luterbacher who provided the European temperature data. The work of Dr. D. Bray is much appreciated concerning the improvement of the English.

I am also grateful to Dr. C. Matulla for numerous encouraging discussions. Dr. H. Kuhn is acknowledged here explicitly because of his devotional manner to abide the Computer facilities. Thanks also to Dr. B. Müller and Dr. M. Widmann for fruitful discussions in the course of the work.

Thanks to B. Hünicke, C. Nunneri and A. Schulte-Rentrop for the 'sechzehn null null' coffee sessions.

Last but not least many thanks to Anne and my family for the moral support.

# References


Ambaum, M., B. Hoskins, and D. Stephenson (2001). Arctic Oscillation or North Atlantic Oscillation? *J Climate 14*, 3495–3507.

Bard, E., G. Raisbeck, F. Yiou, and J. Jouzel (2000). Solar irradiance during the last 1200 years based on cosmogenic nuclides. *Tellus 52B*, 985–992.

Bauer, E., M. Claussen, V. Brovkin, and A. Hühnerbein (2003). Assessing climate forcings of the earth system for the past millennium. *Geophys Res Lett 30*, doi:10.1029/2002GL016639.

Beer, J., W. Mende, and R. Stellmacher (2000). The role of the sun in climate forcing. *Quaternary Sci Rev 19*, 403–415.

Bertrand, C. and J.-P. van Ypersele (2002). Transient climate simulation forced by natural and anthropogenic climate forcings. *Int J Climatol 22*, 623–648.

Blender, R. and K. Fraedrich (2003). Long Time Memory in Global Warming Simulations. *Geophys Res Lett 30*, doi:10.1029/2003GL017666.

Bonisch, G. and P. Schlosser (1995). Deep-water formation and exchange-rates in the Greenland Norwegian seas and the Eurasian basin of the Arctic-ocean derived from tracer balances. *Prog Oceanogr 35*, 29–52.

Briffa, K. R., P. Jones, F. Schweingruber, and T. Osborn (1998). Influence of volcanic eruptions on Northern Hemisphere summer temperature over the past 600 years. *Nature 393*, 450–495.

Broecker, W. (1991). The great ocean conveyor. *Oceanography 4*, 79–89.

Bunde, A., J. Eichner, R. Govindan, S. Havlin, E. Koscielny-Bunde, D. Rybski, and D. Yjushin (2003). Power-Law persistence in the atmosphere: Analysis and Applications models. In M. Gell-Mann and C. Tsallis (Eds.), *Nonextensive entropy – Interdisciplinary applications*. Oxford University press.

Cook, E., R. D'Arrigo, and M. Mann (2002). A Well-Verified, Multiproxy Reconstruction of the Winter North Atlantic Oscillation Index since A.D. 1400. *J Climate 15*, 1754–1764.

Crowley, T. (2000). Causes of climate change over the past 1000 years. *Science 289*, 270–277.

Cubasch, U., B. Santer, and G. Hegerl (1995). Klimamodelle - wo stehen wir? *Phys Bl 51*, 269–276.

Cubasch, U., R. Voss, G. Hegerl, J. Waszkewitz, and T. Crowley (1997). Simulation of the influence of solar radiation variations on the global climate with an ocean-atmosphere general circulation model. *Clim Dynam 13*, 757–767.

Cubasch, U. and R. Voss (2000). The influence of total solar irradiance on climate. *Space Sci Rev 94*, 185–198.

Dai, J., E. Mosleythompson, and L. Thompson (1991). Ice core evidence for an explosive tropical volcanic eruption 6 years preceding Tambora. *J Geophys Res 96*(D9), 17361–17366.

D'Andrea, F., S. Tibaldi, M. Blackburn, G. Boer, M. Deque, M. Dix, B. Dugas, L. Ferranti, T. Iwasakia, A. Kitoh, V. Pope, D. Randall, E. Roeckner, D. Strauss, W. Stern, H. van den Dool, and D. Williamson (1998). Northern hemispheric atmospheric blocking as simulated by 15 atmospheric general circulation models in the period 1979-1988. *Clim Dynam 14*, 385–407.

Demaree, G. R. and A. Ogilvie (2001). Bons baiser d'islands: Climatic, environmental, and human dimensions impacts of the lakagigar eruption (1783-1784) in iceland. In *History and Climate: Memories of the Future?*, pp. 219–245. Kluwer Academic Publishers.

Dommenget, D. and M. Latif (2002). A Cautionary Note on the Interpretation of EOFs. *J Climate 15*, 216–225.

Eddy, J. (1976). The Maunder Minimum. *Science 192*, 1189–1202.

Esper, J., E. Cook, and F. Schweingruber (2002). Low-Frequency Signals in Long Tree-Ring Chronologies for Reconstructing Past Temperature Variability. *Science 295*, 2250–2253.

Etheridge, D., L. Steele, R. Langenfelds, R. Francdey, J. Barnola, and V. Morgan (1996). Natural and anthropogenic changes in atmospheric $CO_2$ over the last 1000 years from air in Antarctic ice and firn. *J Geophys Res 101*(D2), 4115–4128.

Friis-Christensen, E. and H. Svensmark (1997). What do we know about the sun-climate connection? *Adv Space Res 20*, 913–921.

Gillett, N., M. Allen, R. McDonald, C. Senior, D. Shindell, and G. Schmidt (2002). How linear is the Arctic Oscillation response to greenhouse gases? *J Geophys Res 107*(D3), doi:10.1029/2001JD000589.

Glaser, R. (1995). Thermische Klimaentwicklung in Mitteleuropa seit dem Jahr 1000. *Geowissenschaften 13*, 302–312.

Glaser, R. (2001). *Klimageschichte Mitteleuropas. 1000 Jahre Wetter, Klima, Katastrophen*. Wissenschaftliche Buchgesellschaft.

Glueck, M. and C. Stockton (2001). Reconstruction of the North Atlantic Oscillation, 1429-1983. *Int J Climatol 12*, 1453–1465.

Gong, D. and S. Wang (1998). Antarctic Oscillation: Concept and applications. *Chinese Sci Bull 43*, 734–738.

Gong, D. and C. Ho (2002). The Siberian High and climate change over middle to high latitude Asia. *Theor Appl Climatol 72*, 1–9.

González-Rouco, J. F., H. von Storch, and E. Zorita (2003). Deep soil temperature as proxy for surface air-temperature in a coupled model simulation of the last thousand years. *Geophys Res Lett 30*, doi:10.1029/2003GL018264.

Graf, H. F., I. Kirchner, A. Robock, and I. Schult (1993). Pinatubo eruption winter climate effects: model versus observations. *Clim Dynam 9*, 81–93.

Grattan, J. and F. Pyatt (1999). Volcanic eruptions dry fogs and the European palaeoenvironment record: localised phenomena or hemispheric impacts? *Global Planet Change 21*, 173–179.

Hall, A. and M. Visbeck (2002). Synchronous Variability in the Southern Hemisphere Atmosphere , Sea Ice and Ocean resulting from the Annular mode. *J Climate 15*, 3043–3057.

Hegerl, G., T. Crowley, S. Baum, K.-Y. Kim, and W. Hyde (2003). Detection of volcanic, solar and greenhouse gas signals in paleo-reconstructions of Northern Hemispheric temperature. *Geophys Res Lett 30*, doi:10.1029/2002GL016635.

Hibler, W. (1979). A dynamic-thermodynamic sea-ice model. *J Phys Oceanogr 9*, 815–846.

Holland, M., C. Bitz, M. Eby, and A. Weaver (2001). The Role of Ice-Ocean Interactions in the Variability of the North Atlantic Thermohaline Circulation. *J Climate 14*, 656–675.

Houghton, J., Y. Ding, D. Griggs, M. Noguer, P. van der Linden, X. Dai, K. Maskell, and C. Johnson (Eds.) (2001). *Intergovernmental Panel on Climate Change Third Assessment Report Climate Change 2001: The Scientific Basis*. Cambridge University Press.

Hoyt, D. and K. Schatten (1993). A discussion of plausible solar-irradiance variations, 1700-1992. *J Geophys Res 98*(A11), 18895–18906.

Jacobeit, J., P. Jones, T. Davies, and C. Beck (2001a). Circulation changes in Europe since the 1790s. In *History and Climate: Memories of the Future?*, pp. 79–99. Kluwer Academic Publishers.

Jacobeit, J., P. Jönsson, L. Bärring, C. Beck, and M. Ekström (2001b). Zonal indices for Europe 1780-1995 and running correlations with temperature. *Climatic Change 48*, 219–241.

Jacobeit, J., H. W., C. B. J. Luterbacher, A. Philipp, and K. Sturm. (2002). Atmospheric circulation variability in the North-Atlantic-European area since the mid-seventeenth century. *Clim Dynam 55*, 341–352.

Jones, J. and M. Widmann (2002). Instrumental and Tree-Ring-Based Estimates of the Antarctic Oscillation. *J Climate 16*, 3511–3524.

Jones, P., K. Briffa, T. Barnett, and S. Tett (1998). High-resolution palaeoclimatic records fot the last millennium: interpretation, integration and comparision with General Circulation Model control-run temperatures. *The Holocene 8*, 455–471.

Jones, P., T. Davies, D. Lister, V. Solonosky, T. Jonsson, L. Bärring, P. Jönsson, P. Maheras, F. Kolyva-Machera, M. Barriendos, J. Martin-Vide, M. Alcoforado, H. Wanner, C. Pfister, E. Schuepbach, E. Kaas, T. Schmith, J. Jacobeit, and C. Beck (1999a). Monthly mean pressure reconstructions for Europe for the 1780-1995 period. *Int J Climatol 18*, 23–36.

Jones, P., M. New, D. Parker, S. Martin, and I. Rigor (1999b). Surface air temperature and its changes over the past 150 years. *Rev Geophys 37*, 173–199.

Jones, P., T. Osborn, and K. Briffa (2001). The Evolution of Climate Over the Last Millennium. *Science 292*, 662–667.

Kirchner, I., G. Stenchikov, H.-F. Graf, A. Robock, and J. Antua (1999). Climate model simulation of winter warming and summer cooling following the 1991 Mount Pinatubo volcanic eruption. *J Geophys Res 104*(D16), 19039–19055.

Klinger, B. and J. Marotzke (2000). Meridional Heat Transport by the Subtropical Cell. *J Phys Oceanogr 30*, 696–705.

Kushner, P., I. Held, and T. Delworth (2001). Southern Hemisphere Atmospheric Circulation Response to Global Warming. *J Climate 14*, 2238–2249.

LabseaGroup (1998). The Labrador Sea deep convection experiment. *B Am Meteorol Soc 79*, 2033–2058.

Lamb, H. (1970). Volcanic dust in the atmosphere; with a chronology and assessment of its meteorlogical significance. *Phil Trans Roy Soc 266*, 425–553.

Lean, J., J. Beer, and R. Bradley (1995). Reconstructions of solar irradiance since 1610 - implications for climate change. *Geophys Res Lett 22*, 3195–3198.

Lean, J. and D. Rind (1998). Climate Forcing by Changing Solar Radiation. *J Clim 11*, 3069–3094.

Lean, J. and D. Rind (1999). Evaluating sun-climate relationships since the Little Ice Age. *J Atmos Sol-Terr Phy 61*, 25–36.

Legutke, S. and R. Voss (1999). The Hamburg atmosphere-ocean coupled model ECHO-G. Technical Report 18, German Climate Computer Center (DKRZ).

Luterbacher, J., R. Rickli, E. Xoplaki, C. Tinguely, C. Beck, C. Pfister, and H. Wanner (2001). The Late Maunder Minimum (1675-1715) A Key Period for Studying Decadal Scale Climatic Change in Europe. *Climatic Change 49*, 441–462.

Luterbacher, J., E. Xoplaki, D. Dietrich, R. Rickli, J. Jacobeit, C. Beck, D. Gyalistras, C. Schmutz, and H. Wanner (2002a). Reconstruction of sea level pressue fields over the Eastern North Atlantic and Europe back to 1500. *Clim Dynam 18*, 545–561.

Luterbacher, J., E. Xoplaki, D. Dietrich, P. Jones, T. Davies, D. Portis, J. Gonzalez-Rouco, H. von Storch, D. Gyalistras, C. Casty, and H. Wanner (2002b). Extending North Atlantic Oscillation Reconstructions Back to 1500. *Atmos Sci Lett 2*, 114–124.

Luterbacher, J., D. Dietrich, E. Xoplaki, M. Grosjean, and H. Wanner (2004). European seasonal and annual temperature variability, trends and extremes since 1500 A.D. *Science*. *303*, 1499–1503.

Manley, G. (1974). Central England temperatures - monthly means 1659 to 1973. *Q J Roy Meteor Soc 100*, 389–405.

Mann, M., R. Bradley, and M. Hughes (1999a). Global-scale temperature patterns and climate forcing over the past six centuries. *Nature 392*, 779–787.

Mann, M., R. Bradley, and M. Hughes (1999b). Northern Hemisphere temperatures during the past millennium: Inferences, uncertainities, and limitations. *Geophys Res Lett 26*, 759–762.

Marshall, J., Y. Kushnir, D. Battisti, P. Chang, A. Czaja, R. Dickson, J. Hurrell, M. McCartney, R. Saravanan, and M. Visbeck (2001). North Atlantic climate variability: phenomena, impacts and mechanisms. *Int J Climatol 21*, 1863–1898.

Marsland, S., M. Latif, and S. Legutke (2003). Antarctic circumpolar modes in a coupled ocean-atmosphere model. *Ocean Dynamics 53*, 323–331.

Mende, M. and R. Stellmacher (2001). Effect of Earth Orbital and Solar variability on Climate. In Lozán, H. Graßl, and P. Hupfer (Eds.), *Climate of the 21st Century: Changes and Risks*, pp. 27–33. Wissenschaftliche Auswertungen.

Mo, K. and G. White (1985). Teleconnections in the Southern Hemisphere. *Mon Weather Rev 113*, 22–37.

Müller, B. (2003). *Eine regionale Klimasimulation für Europa zur Zeit des späten Maunder Minimums 1675-1705*. Ph. D. thesis, University of Hamburg.

Müller, P. and H. von Storch (2003). *Computer Modelling in Environmental Sciences*. Berlin - Heidelberg - New York: Springer.

Newhall, G. and S. Self (1982). The Volcanic Explosivity Index (VEI): an estimate of explosive magnitude for historical volcanism. *J Geophys Res 82*, 1231–1238.

Oh, H.-S., C. Ammann, P. Naveau, D. Nychka, and B. Otto-Bliesner (2003). Solar forcing and Climate: A multi-resolution analysis. *J. Atmosph. Sol-Terr. Phys. 165*, 191–201.

Peixoto, J. and A. Oort (1992). *Physics in Climate*. American Institue of Physics.

Pickart, R., A. Spall, M. Ribergaard, G. Moore, and R. Milliff (2003). Deep convection in the Irminger Sea forced by the Greenland tip jet. *Nature 424*, 152–156.

Rahmstorf, S. and S. Ganopolski (1999). Long-term global warming scenarios computed with an efficient coupled climate model. *Climatic Change 43*, 353–367.

Rampino, M. and S. Self (1982). Historic Eruptions of Tambora (1815), Krakatau (1883), and Agung (1963), Their Stratospheric Aerosols, and Climatic Impact. *Quat Res 18*, 127–143.

Robertson, A., J. Overpeck, D. Rind, E. Mosley-Thompson, G. Zielinski, J. Lean, D. Koch, J. Penner, I. Tegen, and R. Healy (2001). Hypothesized climate forcing time series for the last 500 years. *J Geophys Res 106*(D14), 14783–14803.

Robock, A. and J. Mao (1992). Winter warming from large volcanic eruptions. *Geophys Res Lett 19*, 2405–2408.

Robock, A. and J. Mao (1995). The volcanic signal in surface-temperature observations. *J Clim 8*, 1086–1103.

Robock, A. and M. Free (1996). The volcanic records in ice cores for the past 2000 years. In *Climatic variations and Forcing Mechanisms of the Last 2000 years*, pp. 533–546. Springer-Verlag.

Robock, A. (2000). Volcanic eruptions and climate. *Rev Geophys 38*, 191–219.

Robock, A. (2004). Climatic impact of volcanic emissions. In S. Sparks and C. Hawkesworth (Eds.), *State of the Planet (in prep.)*.

Roeckner, E., K. Arpe, L. Bengtsson, M. Christoph, M. Claussen, L. Dümenil, M. Esch, M. Giorgetta, U. Schlese, and U. Schulzweida (1996). The atmospheric general circulation model ECHAM4: model description and simulation of present-day climate. Technical Report 218, Max Planck Institut für Meteorologie.

Rogers, J. and H. van Loon (1982). Spatial variability of sea level pressure and 500mb height anomalies over the Southern Hemisphere. *Mon Weather Rev 110*, 1375–1392.

Rozelot, J. (2001). Possible links between the solar radius variations and the Earth's climate evolution over the past four centuries. *J Atm Sol-Terr Physics 63*, 375–386.

Sachs, M. and H.-F. Graf (2001). The Volcanic Impact on Global Atmosphere and Climate. In Lozán, H. Graßl, and P. Hupfer (Eds.), *Climate of the 21st Century: Changes and Risks*, pp. 34–37. Wissenschaftliche Auswertungen.

Sadler, J. and J. Grattan (1999). Volcanoes as agents of past environmental change. *Global Planet Change 21*, 181–196.

Sato, M., J. Hansen, M. McCormick, and J. Pollack (1993). Stratospheric aerosol optical depths, 1850-1990. *J Geophys Res 98*, 22987–22994.

Schmutz, C., J. Luterbacher, D. Gyalistras, E. Xoplaki, and H. Wanner (2000). Can we trust proxy-based NAO index reconstructions? *Geophys Res Lett 27*, 1135–1138.

Seager, R., D. Battisti, J. Yin, N. Gordon, N. Naik, A. Clement, and M. Cane (2003). Is the Gulf Stream responsible for Europe's mild winters? *Q J Roy Meteor Soc 128*, 2563–2586.

Self, S., M. Rampino, and J. Barbera (1981). The possible effects of the large 19th and 20th century volcanic eruptions on zonal and hemispheric surface temperatures. *J Volcanol Geoth Res 11*, 41–60.

Shindell, D., G. Schmidt, M. Mann, D. Rind, and A. Waple (2001a). Solar climate of regional climate change during the Maunder Minimum. *Science 294*, 2149–2152.

Shindell, D., G. Schmidt, R. Miller, and D. Rind (2001b). Northern Hemisphere winter climate response to greenhouse gas, ozone, solar, and volcanic forcing. *J Geophys Res 106*(D7), 7193–7210.

Shindell, D., G. Schmidt, R. Miller, and M. Mann (2003). Volcanic and Solar Forcing of Climate Change during the Preindustrial Era. *J Climate 16*, 4094–4107.

Solanki, S. and M. Fligge (1999). A reconstruction of total solar irradiance since 1700. *Geophys Res Lett 26*, 2465–2468.

Stothers, R. (1984). The great Tambora eruption in 1815 and its aftermath. *Science 224*, 1191–1198.

Sutton, R. and M. Allen (1997). Decadal predictability of North Atlantic sea surface temperature and climate. *Nature 388*, 563–567.

Tahvonen, O., H. von Storch, and J. von Storch (1994). Economic efficiency of $CO_2$ reduction programs. *Clim Res 4*, 127–141.

Terray, L., S. Valcke, and A. Piacentini (1998). The oasis coupler user guide. Version 2.2. Technical Report TR/CMGC/98-05, CERFAS.

Thompson, D. and J. Wallace (1998). The Arctic Oscillation signature in the wintertime geopotential height and temperature fields. *Geophys Res Lett 25*, 1297–1300.

Thompson, D. and J. Wallace (2000). Annular Modes in the Extratropical Circulation. Part I: Month to Month Variability. *J Climate 13*, 1000–1016.

Thompson, D. and S. Solomon (2002). Interpretation of Recent Southern Hemisphere Climate Change. *Science 296*, 895–899.

Tibaldi, S. and F. Molteni (1990). On the operational predictablity of blocking. *Tellus 42*, 343–365.

Usoskin, I., K. Mursula, and G. Kovaltsov (2002). Lost sunspot cycle in the beginning of Dalton minimum: New evidence and consequences. *Geophys Res Lett 29*, doi:10.1029/2002GL015640.

von Storch, H. and C. Frankignoul (1998). Empirical modal decomposition in coastal oceanography. In H. Kenneth and A. Robinson (Eds.), *The Sea*, Volume 10, pp. 419–455. John Wiley and Sons.

von Storch, H. and A. Navarra (Eds.) (1999). *Analysis of Climate Variability*. Springer.

von Storch, H. and F. Zwiers (1999). *Statistical Analysis in Climate Research*. Cambridge University Press.

Wagner, S. (2000). Dekadische atmosphärische und ozeanische Variabilität in einer Kontrollsimulation mit dem Klimamodell ECHO-G. Diplomarbeit, Universität Würzburg, (unpublished).

Wallace, J., Y. Zhang, and J. R. Renwick (1995). Dynamical contribution to hemispheric temperature trends. *Science 270*, 780–783.

Wolff, J., E. Maier-Reimer, and S. Legutke (1997). The Hamburg Primitive Equation Model HOPE. Technical Report 18, German Climate Computer Center (DKRZ).

Wunsch, C. (2002). What is the Thermohaline Circulation? *Science 298*, 1179–1181.

Yuan, Y. and D. Martinson (2000). Antarctic Sea Ice Extent Variability and Its Global Connectivity. *J Climate 13*, 1697–1717.

Zorita, E. and J. F. González-Rouco (2000). Disagreement between predictions of the future behavior of the Arctic Oscillation as simulated in two different climate models: Implications for global warming. *Geophys Res Lett 27*, 1755–1758.

Zorita, E. and J. F. González-Rouco (2002). Are temperature-sensitive proxies adequate for North Atlantic Oscillation reconstructions. *Geophys Res Lett 29*, doi:10.1029/2002GL015404.

Zorita, E., H. von Storch, J. González-Rouco, U. Cubach, J. Luterbacher, S. Legutke, I. Fischer-Bruns, and U. Schlese (2004). Transient simulation of the climate of the last five centuries with an atmosphere-ocean coupled model: Late Maunder Minimum and the Little Ice Age. *Met Zet*. *13*, 271–289.

Zwiers, F. W. and H. von Storch (1995). Taking Serial Correlation into Account in Tests of the Mean. *J Climate 8*, 336–351.